

**MONITORING THE TEMPORAL VARIATION OF
FORMALDEHYDE EMISSIONS OVER
ISLAMABAD, PAKISTAN USING MINI MAX-
DOAS, NASA PANDORA SPECTROMETER, AND
SATELLITE OBSERVATIONS**



**By
Abeer Salman
Registration No. 00000361408**

**Supervisor
Prof. Dr. Muhammad Fahim Khokhar**

**A thesis submitted in partial fulfillment of the requirement for the
degree of Master of Science in Environmental Science**

**Institute of Environmental Science & Engineering
School of Civil & Environmental Engineering
National University of Sciences & Technology
Islamabad, Pakistan
2023**

MONITORING THE TEMPORAL VARIATION OF
FORMALDEHYDE EMISSIONS OVER
ISLAMABAD, PAKISTAN USING MINI MAX-
DOAS, NASA PANDORA SPECTROMETER, AND
SATELLITE OBSERVATIONS

Submitted by
Abeer Salman
00000361408

**A thesis submitted to the Institute of Environmental Science and
Engineering in partial fulfilment of the requirement for the
degree of**

MASTER OF SCIENCE

In

ENVIRONMENTAL SCIENCE

Institute of Environmental Sciences and Engineering
School of Civil and Environmental Engineering
National University of Sciences and Technology
Sector H-12, Islamabad, Pakistan

APPROVAL CERTIFICATE


It is certified that the contents and form of the thesis entitled


“Monitoring the Temporal Variation of Formaldehyde Emissions Over Islamabad, Pakistan Using Mini MAX-DOAS, NASA Pandora Spectrometer, and Satellite Observations”


Submitted by


Abeer Salman

has been found satisfactory for partial fulfillment of the requirements of the degree of Master of Science in Environmental Sciences.


Supervisor:
Dr. Muhammad Fahim Khokhar
Professor
SCEE (IESE), NUST
Tenured Professor
Department of Environmental Sciences
IESE (SCEE) NUST Islamabad


Co-supervisor:
Dr. Salman Tariq
Assistant Professor
Department of Space Science, University
of the Punjab


GEC Member:
Dr. Muhammad Arshad
Professor
SCEE (IESE), NUST
Tenured Professor
IESE (SCEE) NUST Islamabad



GEC Member:
Dr. Muhammad Ansar Farooq
Associate Professor
SCEE (IESE), NUST
Associate Professor
SCEE (IESE), NUST

ACCEPTANCE CERTIFICATE

It is certified that the final copy of MS/MPhil Thesis written by Ms. Abeer Salman (Registration No: 00000361408) of IESE (SCEE) has been vetted by the undersigned, found complete in all respects as per NUST statutes/regulations, is free of plagiarism, errors, and mistakes, and is accepted as partial fulfillment for the award of MS/MPhil degree. It is further certified that necessary amendments as pointed out by GEC members of the scholar have also been incorporated in the said thesis.

Supervisor: 


Dr. Muhammad Fahim Khokhar
Dated: 05/10/23
Dr. Muhammad Fahim Khokhar
Tenured Professor
Environmental Sciences
IESE (SCEE) NUST Islamabad

Head of Department: 

Dr. Zeshan
Tenured Assoc Prof
Environmental Sciences
IESE (SCEE) NUST Islamabad
Dated: 06/10/2023

Associate Dean: 


Prof. Dr. Imran Hashmi
Associate Dean
IESE (SCEE) NUST Islamabad
Dated: 06-10-2023

Principal & Dean (SCEE): 
Prof. Dr. MUHAMMAD IRFAN
Principal & Dean

09 OCT 2023 SCEE, NUST
Dated:

DECLARATION CERTIFICATE

I declare that that this research work titled “Monitoring the Temporal Variation of Formaldehyde Emissions Over Islamabad, Pakistan Using Mini MAX-DOAS, NASA Pandora Spectrometer, and Satellite Observations” is my own work. The work has not been presented elsewhere for assessment. The material that has been used from other sources has been properly acknowledged/referred.


Signature of Student: 

Name of Student: Abeer Salman

Date: 05/10/2023

PLAGIARISM CERTIFICATE

This thesis has been checked for plagiarism. Turnitin endorsed by supervisor is attached.

Signature of Student: 

Signature of Supervisor: 

DEDICATION

Dedicated to my younger self, for having the stubborn bravery and foolish tenacity to see this through.

ACKNOWLEDGEMENTS

This research is a culmination of countless hours of hard work and dedication. While this journey was taxing, I am grateful for the invaluable contributions of numerous individuals who stood by my side, offering their wisdom, support, and encouragement.

My utmost gratitude goes to my supervisor, Dr. Muhammad Fahim Khokhar, whose expertise and mentorship were pivotal to the development of this research. His ability to both challenge and support, to ask the right questions and guide me towards finding the answers, has been instrumental in shaping this work. I would also like to thank Dr. Salman Tariq, Dr. Muhammad Arshad, and Dr. Muhammad Ansar Farooq for offering their guidance and invaluable feedback.

I am immensely grateful to my C-CARGO colleagues, especially Mr. Kashif Imran, Mr. Talha Saeed, and Ms. Rabia Majeed, for providing help whenever I needed it.

The emotional backbone provided by my family and friends was indispensable, turning moments of uncertainty into determination and giving me the strength to persevere. I would like to extend my heartfelt gratitude to those who stood beside me every step of the way, offering unwavering support and camaraderie. Noor, who has been a pillar of support throughout this journey, for consistently being a reassuring presence that I can always rely on. Azulfa and Mahnoor, for always offering a listening ear no matter the time. Iqran, for all the prayers.

I extend my deepest appreciation to Mahd, for his patience, understanding, and endless encouragement which made every challenge surmountable. For all the sacrifices and every gesture, both big and small, I am forever grateful.

Last but not least, I would like to thank my mother, for weaving pathways for me to walk on and teaching me how to live life with multitudes.

TABLE OF CONTENTS

TABLE OF CONTENTS	ix
LIST OF ABBREVIATIONS OR KEYWORDS	xii
LIST OF TABLES	xiii
LIST OF FIGURES	xiv
ABSTRACT	1
CHAPTER 1	2
INTRODUCTION	2
1.1. Background	2
1.2. Formaldehyde as an Air Pollutant.....	2
1.2.1. Sources of Formaldehyde	3
1.2.2. Sinks of Formaldehyde	5
1.3. Significance of the Study	6
1.4. Objectives of the Study	7
CHAPTER 2	8
LITERATURE REVIEW	8
2.1. Overview	8
2.2. HCHO Monitoring Studies in Pakistan.....	8
2.3. Temporal Variation of HCHO Emissions	10
2.4. Influence of Weather	12
2.4.1. Temperature	12
2.4.2. Relative Humidity	13
2.4.3. Wind Direction and Speed	13
2.4.4. Precipitation	14
2.5. Sources of HCHO.....	14
2.6. Instruments Used for HCHO Monitoring.....	15
2.6.1. Ground-Based Instruments	15
2.6.2. Satellite Instruments.....	16
2.6.3. Modelling Techniques	17
2.7. Research Gaps and Limitations.....	17
CHAPTER 3	19
MATERIALS AND METHODS	19

3.1. Understanding Formaldehyde Emissions in Islamabad	19
3.1.1. Study Area and Monitoring Period	19
3.2. Measurement Instruments	20
3.2.1. Mini MAX-DOAS	20
3.2.2. NASA Pandora Spectrometer	21
3.3. Software and Tools Used in the Study	24
3.3.1. Differential Optical Absorption Spectroscopy Intelligent System (DOASIS)	25
3.3.2. Windows Differential Optical Absorption Spectroscopy (WinDOAS)	26
3.3.2.1. Spectral calibration	26
3.3.2.2. Cross-section convolution.....	26
3.3.3. Quantitative Differential Optical Absorption Spectroscopy (QDOAS)	27
3.3.4. Analysis Through Microsoft Excel.....	30
3.3.4.1. dAMF calculation	31
3.3.4.2. Tropospheric VCD calculation.....	31
3.3.5. Validation of Ground-Based Data with Satellite Data.....	32
3.3.5.1. OMI.....	33
3.3.5.2. TROPOMI.....	34
3.3.6. RStudio	34
3.3.7. Meteorological Data.....	34
CHAPTER 4.....	35
RESULTS AND DISCUSSION	35
4.1. Ground-Based Monitoring at IESE, NUST.....	35
4.1.1. HCHO Time Series	35
4.1.2. HCHO Annual Diurnal Cycle at IESE, NUST	36
4.1.3. HCHO Seasonal Diurnal Cycle at IESE, NUST.....	38
4.1.4. HCHO Average Weekly Cycle at IESE, NUST	40
4.1.5. HCHO Average Monthly Cycle at IESE, NUST.....	41
4.1.6. HCHO Average Yearly Observations Over IESE, NUST.....	42
4.2. Satellite Observations.....	43
4.2.1. OMI.....	43
4.2.2. TROPOMI.....	44

4.3. Comparison of MAX-DOAS and NASA Pandora Spectrometer Measurements	48
4.4. Influence of Meteorological Parameters	50
4.4.1. Temperature	50
4.4.1.1. <i>Diurnal cycle</i>	50
4.4.1.2. <i>Monthly cycle</i>	53
4.4.1.3. <i>Yearly Cycle</i>	55
4.4.2. Global Horizontal Irradiance (GHI).....	55
4.4.3. Relative Humidity	58
4.3.4. Wind Speed	60
4.3.5. Meteorological Data Correlation Matrix	62
CHAPTER 5	64
CONCLUSIONS AND RECOMMENDATIONS.....	64
5.1. Conclusion.....	64
5.2. Recommendations	65
REFERENCES.....	67

LIST OF ABBREVIATIONS OR KEYWORDS

AMF	Air Mass Factor
BVOC	Biogenic Volatile Organic Compound
DOAS	Differential Optical Absorption Spectroscopy
GHI	Global Horizontal Irradiance
HAP	Hazardous Air Pollutants
IESE	Institute of Environmental Science and Engineering
MAX-DOAS	Multi-AXis Differential Optical Absorption Spectroscopy
NASA	National Aeronautics and Space Administration
NMVOC	Non-Methane Volatile Organic Compound
NUST	National University of Science and Technology
OMI	Ozone Monitoring Instrument
PGN	Pandonia Global Network
RH	Relative Humidity
SCD	Slant Column Density
SZA	Solar Zenith Angle
TROPOMI	Tropospheric Ozone Monitoring Instrument
VCD	Vertical Column Density
VOC	Volatile Organic Compound
WHO	World Health Organization

LIST OF TABLES

Table 3.1 – List of software and tools utilized for this study	24
Table 3.2 – Values used to obtain dark current and offset measurements	25
Table 3.3 – Comparison of the main features of OMI and TROPOMI	33
Table 4.1 – Categorization of Pakistan’s seasons according to months	38
Table 4.2 – Correlation values for the studied meteorological parameters	57

LIST OF FIGURES

Figure 3.1 – Mini MAX-DOAS installed at IESE, NUST	20
Figure 3.2 – NASA Pandora Spectrometer installed at IESE, NUST	21
Figure 3.3 – Interface of BlickO software used to operate NASA Pandora Spectrometer	22
Figure 3.4 – NASA Pandora Spectrometer main control box, containing spectrometer box, thermoelectric cooler, relay box, and computer	23
Figure 3.5 – QDOAS display tab	27
Figure 3.6 – QDOAS calibration tab	28
Figure 3.7 – QDOAS instrumental tab	28
Figure 3.8 – QDOAS output tab	29
Figure 3.9 – QDOAS HCHO analysis window properties	30
Figure 3.10 – QDOAS HCHO analysis window properties showing polynomial order	30
Figure 4.1 – MAX-DOAS HCHO time series (2015 – 2021)	35
Figure 4.2 – NASA Pandora Spectrometer HCHO time series (2022 – 2023)	35
Figure 4.3 – HCHO annual diurnal cycle measured by MAX-DOAS	36
Figure 4.4 – HCHO annual diurnal cycle measured by NASA Pandora Spectrometer	37
Figure 4.5 – Seasonal diurnal cycle of HCHO using MAX-DOAS observations	38
Figure 4.6 – HCHO average weekly cycle measured through MAX-DOAS	39
Figure 4.7 – HCHO average weekly cycle measured through NASA Pandora Spectrometer	40
Figure 4.8 – MAX-DOAS HCHO monthly cycle	41
Figure 4.9 – Pandora HCHO monthly cycle	41
Figure 4.10 – MAX-DOAS HCHO yearly cycle	42
Figure 4.11 – Validation of ground-based MAX-DOAS 12:00 – 14:00 measurements with OMI satellite measurements over IESE, NUST	43
Figure 4.12 – Correlation of HCHO VCDs of OMI vs. MAX-DOAS 12:00 – 14:00 average over IESE, NUST	43

Figure 4.13 – Validation of ground-based MAX-DOAS 12:00 – 14:00 measurements with TROPOMI satellite measurements over IESE, NUST	44
Figure 4.14 – Correlation of HCHO VCDs of TROPOMI vs. MAX-DOAS 12:00 – 14:00 average over IESE, NUST	44
Figure 4.15 – Validation of ground-based MAX-DOAS 06:00 – 18:00 measurements with TROPOMI satellite measurements over IESE, NUST	45
Figure 4.16 – Correlation of HCHO VCDs of TROPOMI vs. MAX-DOAS 06:00 – 18:00 average over IESE, NUST	45
Figure 4.17: – Validation of ground-based NASA Pandora Spectrometer 12:00 – 14:00 measurements with TROPOMI satellite measurements over IESE, NUST	46
Figure 4.18 – Correlation of HCHO VCDs of TROPOMI vs. Pandora 12:00 – 14:00 average over IESE, NUST	46
Figure 4.19 – Validation of ground-based NASA Pandora Spectrometer 06:00 – 18:00 measurements with TROPOMI satellite measurements over IESE, NUST	47
Figure 4.20 – Correlation of HCHO VCDs of TROPOMI vs. Pandora 06:00 – 18:00 average over IESE, NUST	47
Figure 4.21 – Comparison of MAX-DOAS and Pandora 12:00 – 14:00 average HCHO VCDs	48
Figure 4.22 – Comparison of MAX-DOAS and Pandora 06:00 – 18:00 average HCHO VCDs	48
Figure 4.23 – 24-hour temperature cycle over IESE, NUST	49
Figure 4.24 – Comparison of temperature with the diurnal cycle of MAX-DOAS HCHO VCDs	50
Figure 4.25 – Comparison of temperature with the diurnal cycle of NASA Pandora Spectrometer HCHO VCDs	50
Figure 4.26 – Comparison of temperature with the monthly cycle of MAX-DOAS HCHO VCDs	51
Figure 4.27 – Comparison of temperature with the monthly cycle of NASA Pandora Spectrometer HCHO VCDs	52
Figure 4.28 – Comparison of temperature with the yearly cycle of MAX-DOAS	53

HCHO VCDs	
Figure 4.29 – Comparison of GHI with the diurnal cycle of MAX-DOAS HCHO VCDs	54
Figure 4.30 – Comparison of GHI with the diurnal cycle of NASA Pandora Spectrometer HCHO VCDs	54
Figure 4.31 – Comparison of GHI with the monthly cycle of MAX-DOAS HCHO VCDs	55
Figure 4.32 – Comparison of GHI with the monthly cycle of Pandora HCHO VCDs	55
Figure 4.33 – Comparison of RH with the diurnal cycle of MAX-DOAS HCHO VCDs	56
Figure 4.34 – Comparison of RH with the diurnal cycle of NASA Pandora Spectrometer HCHO VCDs	56
Figure 4.35 – Comparison of wind speed with the diurnal cycle of MAX-DOAS HCHO VCDs	57
Figure 4.36 – Comparison of wind speed with the diurnal cycle of NASA Pandora Spectrometer HCHO VCDs	57
Figure 4.37 – Correlation matrix for MAX-DOAS and Pandora HCHO VCDs and meteorological parameters	59

ABSTRACT

The monitoring and analysis of formaldehyde (HCHO) column densities in urban environments is crucial due to adverse impacts of trace gases on human health and the environment. This study presents an in-depth investigation into the temporal variability of HCHO column densities in Islamabad, Pakistan from 2015-2023. Advanced ground-based instruments MAX-DOAS and NASA Pandora Spectrometer, as well as satellite observations from OMI and TROPOMI instruments were used. The study also presents a comprehensive analysis of meteorological parameters and their role in tropospheric HCHO levels. Diurnal measurements of HCHO showed highest levels during early morning and late evening hours due to the influence of temperature, low solar radiation, and absence of radicals involved in atmospheric chemical reactions. The seasonal cycle of HCHO showed higher levels during the summer months, reaching a peak in June due to higher temperatures and resultant biogenic emissions contributing to HCHO production. It was found to be the lowest in winter owing to lower solar irradiance and temperature. Both OMI and TROPOMI underestimated the ground-based HCHO observations due to their coarse spatial resolution. In comparison with OMI, TROPOMI had a higher correlation of 0.79 and 0.71 for MAX-DOAS and Pandora respectively for HCHO vertical column densities measured at the satellite overpass time. Comparisons between the two ground-based instruments revealed nuanced discrepancies in measurements, highlighting the need for rigorous intercomparison studies.

Keywords: HCHO, Temporal Variation, MAX-DOAS, NASA Pandora Spectrometer, Air Quality.

CHAPTER 1

INTRODUCTION

1.1. Background

Despite advancements in technology and continuous efforts to curb environmental degradation, air pollution remains a major concern in urban centers globally. Driven by rapid industrialization, urbanization and persistently increasing vehicular emissions, deterioration of air quality has grave impacts on the environment, human health, as well as the economy. According to a study by the Global Burden of Disease, exposure to air pollution contributed to increased risk of being affected by health issues such as cardiovascular diseases, respiratory infections, and neonatal disorders, and was responsible for an estimate of almost 7 million deaths in 2019 (Institute for Health Metrics and Evaluation, 2020). Additionally, the World Bank has estimated that the global cost of air pollution, mainly attributable to health impacts of degraded air quality, is about 8 trillion USD, which is equal to slightly over 6% of the global GDP (World Bank, 2022).

Though the effects of air pollution are felt throughout the world, the issue is much more severe in less developed countries. Rapidly developing nations like Pakistan face challenges such as unbridled economic growth, poor implementation of air quality laws and regulations, leniency regarding emissions standards, as well as dependence on non-renewable sources of energy (Anjum et al., 2021). In addition, developing nations are economically incapacitated to invest in alternative technologies to mitigate air pollution (UNEP, 2019). In 2022, Pakistan was found to be the country with the third most polluted air in the world, ranking higher than other South Asian countries like Bangladesh and India which were fifth and eighth respectively (IQAir, 2023). Currently, there is a severe lack of air quality monitoring systems in Pakistan, which contributes further to the challenge of assessing and mitigating air pollution in the country (Khan et al., 2023). Thus, the need to understand and address sources, distribution and temporal variation of air pollutants is critical.

1.2. Formaldehyde as an Air Pollutant

Formaldehyde (HCHO) is a reactive trace gas released into the atmosphere through

both natural and anthropogenic sources. It is classified as one of the 188 hazardous air pollutants (HAPs) by the United States Environmental Protection Agency (US EPA, 2022). HCHO has several adverse health impacts. Exposure to elevated concentrations can lead to acute health problems such as conjunctival, nasal, and pharyngeal irritation, allergic dermatitis, respiratory issues, as well as impacts on the nervous system causing symptoms like dizziness and headaches (Agency for Toxic Substances and Disease Registry, 2016; National Research Council (US) Committee on Toxicology, 1980; TURI, 2022). It also has several chronic effects. HCHO has been found to be a group 1 carcinogen (Protano et al., 2021; Zhu et al., 2017). Being subjected to an average level of approximately 0.7 parts per billion (ppb) of HCHO throughout an individual's lifespan can cause the development of lung and nasopharyngeal cancers in up to 13 individuals per million. This gas alone contributes to over half of the cumulative cancer risks associated with HAPs in the United States (Zhu et al., 2017). These adverse effects demonstrate the significant impact of HCHO on human health.

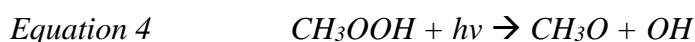
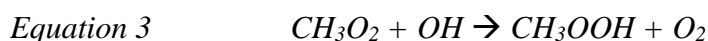
Apart from health risks, HCHO also exerts a substantial influence on air quality and atmospheric chemistry. It stands as the predominant atmospheric aldehyde across both urban and rural regions (Ho et al., 2006). Compounds containing carbonyl groups, such as aldehydes, are important precursors to products like ozone (O_3). Photolysis of HCHO causes a series of reactions which lead to the formation of strong oxidizing agents like hydroxyl (OH) and hydroperoxyl (HO_2) radicals, which then cause the production of tropospheric O_3 . Unlike beneficial O_3 found in the stratosphere, tropospheric O_3 is a greenhouse gas and a main component of photochemical smog. It causes cardiovascular and respiratory diseases, being responsible for about a million premature deaths per annum (Climate & Clean Air Coalition, 2022). It also affects the climate by increasing temperatures and influencing factors such as rate of evaporation and precipitation and impacts agricultural growth by decreasing crop productivity (Mahmood et al., 2020; Noreen et al., 2018).

1.2.1. Sources of Formaldehyde

While HCHO is a by-product of the oxidation of many hydrocarbons and VOCs (Gratsea et al., 2016; Razi et al., 2022), the main source of tropospheric HCHO is the

photooxidation of methane (CH₄) in oceanic regions and non-methane VOCs (NMVOCs) in continental regions (Khan et al., 2018; Khokhar et al., 2015; Y. Zhang et al., 2019).

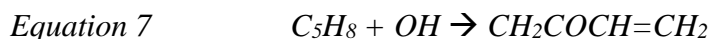
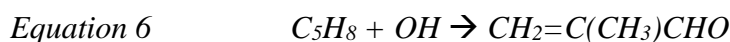
Methane is first converted to methyl radical (CH₃) followed by methyl peroxy radical (CH₃O₂). The methyl peroxy radical is then oxidized to acetic acid (CH₃OOH), which reacts with photons to form methoxide (CH₃O). Methoxide then reacts with molecular oxygen to form formaldehyde and water. The reactions through which CH₄ oxidizes into HCHO are represented by Equations 1 – 5 (Seinfeld & Pandis, 2016).



HCHO is a by-product of the oxidation of almost all VOCs and is commonly used as a marker for NMVOCs (Lok Chan et al., 2020). When looking at NMVOCs as sources of HCHO, it has been found that about 85% emissions are attributable to biogenic sources, 12% to anthropogenic sources, and 3% to pyrogenic sources (Freitas & Fornaro, 2022). The main biogenic source is isoprene (C₅H₈), which is the most abundant biogenic volatile organic compound (BVOC) found in the atmosphere. The annual global emissions of isoprene from vegetation are estimated at 600 teragrams, and this source consequently greatly affects atmospheric chemistry through the production of O₃ (Guenther et al., 2006). While isoprene emissions have an adverse impact on both the climate and human health, its residual lifetime is less than one hour (Pang et al., 2009), making it difficult to accurately measure emissions on a large scale. HCHO can be used as a proxy for the analysis of isoprene emissions. The lifetime of HCHO in the atmosphere is about 3 – 4 hours on average (Khan et al., 2018), making it easier to assess as it remains in proximity to its point of origin.

Isoprene produces HCHO through two main pathways. In the presence of OH

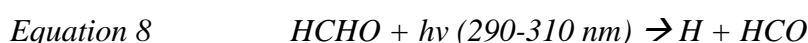
radicals, isoprene is converted to either methacrolein or methyl vinyl ketone. These products, in the presence of OH radicals reacting with molecular oxygen, then form HCHO. The reactions through which isoprene is converted into HCHO are represented by Equations 6 – 7.1 (Freitas & Fornaro, 2022).



Anthropogenic sources of HCHO include industrial processes, combustion of fossil fuels, vehicular emissions, while pyrogenic sources include agricultural stubble burning, garbage burning, and burning of biomass (C. Zhang et al., 2022; Fan et al., 2021; Hoque et al., 2018; Liu et al., 2023).

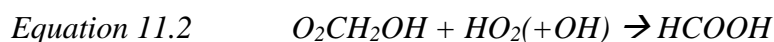
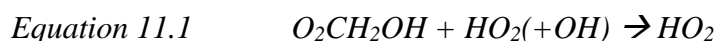
1.2.2. Sinks of Formaldehyde

HCHO is removed from the atmosphere mainly through photolysis, oxidation by OH and HO₂ radicals, as well as by wet deposition. Removal of HCHO by photolysis occurs at wavelengths lower than 400 nm, particularly at 290 – 310 nm and 320 – 350 nm (Freitas & Fornaro, 2022; Hoque et al., 2018). The photolysis reactions through which HCHO is removed from the atmosphere are shown in Equations 8 – 9 (Freitas & Fornaro, 2022).



Removal of HCHO through oxidation by OH and HO₂ radicals is represented by Equations 10 – 10.1 (Shoaib et al., 2020) and Equations 11 – 11.2 (Freitas & Fornaro, 2022).





Removal of HCHO by wet deposition is due to its pronounced electric dipole moment, which results in high water solubility (Seinfeld & Pandis, 2016). The reactions through which HCHO is removed by wet deposition are represented by Equations 12 – 12.2 (Freitas & Fornaro, 2022).



1.3. Significance of the Study

While it has been established that atmospheric trace gases contribute significantly to degrading air quality, Pakistan is lacking a comprehensive monitoring system to observe HCHO concentrations. Due to this, there is limited air quality baseline data available for the country. The significance of this study lies in several key aspects.

HCHO is a hazardous air pollutant which affects human health and the environment. Monitoring its temporal variation will help in better understanding the air quality in Islamabad. As climate change continues to amplify factors that exacerbate HCHO levels, this study provides valuable insights for policymakers, environmental agencies, urban planners, and other relevant authorities to make informed decisions regarding air quality management and mitigation strategies. It aims to equip them with insights into the present situation, as well as potential future trajectories of air quality in Pakistan. The identification of temporal patterns and trends in HCHO emissions can guide the formulation of targeted strategies to mitigate pollution, improve air quality, and safeguard public health in Islamabad.

This study uses novel monitoring techniques to monitor and analyze HCHO emissions. It pioneers the application of the inaugural NASA Pandora Spectrometer

instrument in South Asia, marking the first instance of HCHO measurement through this technology in Pakistan. This showcases the application of advanced technologies for air quality monitoring and contributes to the growing body of knowledge in the field of atmospheric sciences. The study also integrates ground-based measurements with satellite observations, which enhances the accuracy and reliability of the findings.

1.4. Objectives of the Study

This study was conducted to achieve the following objectives:

1. To retrieve atmospheric trace gas formaldehyde from MAX-DOAS and Pandora observations to determine its temporal variation.
2. To validate satellite-based data with MAX-DOAS and Pandora observations.
3. To examine the influence of meteorological parameters on the temporal variation of formaldehyde.

CHAPTER 2

LITERATURE REVIEW

2.1. Overview

Owing to a combination of factors such as increased industrial activities, population growth, and heavy reliance on non-renewable sources of energy, air pollution has emerged as a significant environmental predicament in Pakistan (Greenstone & Fan, 2019). Degraded air quality has severe effects on human health and the environment, and can gravely impact a country like Pakistan, which is already vulnerable to climate change. Though there is an abundance of research on prominent air pollutants such as carbon dioxide, nitrogen dioxide, and methane, gases like HCHO remain relatively less researched and warrant further investigation.

This literature review embarks on a comprehensive exploration of the interplay between the atmospheric trace gas HCHO and its complex interactions with the environment. By exploring an array of research studies, methodological approaches, and the evolving role of state-of-the-art technology, this review aims to provide an overview of the existing body of knowledge, whilst also pinpointing critical research gaps that need to be addressed. Through the review of literature, 6 main themes relevant to this study were identified and explored. These themes are discussed in the following subsections of this chapter.

2.2. HCHO Monitoring Studies in Pakistan

While other trace gases such as NO₂ and O₃ have been studied extensively, the evaluation of HCHO concentrations in Pakistan has only gained momentum in recent years. Notably, Khokhar et al. (2015) embarked on a comprehensive examination of spatiotemporal patterns of HCHO over Pakistan between 2003 and 2012 using satellite instruments like SCIAMACHY and GOME-2. This study identified elevated HCHO concentrations in urban centers, particularly within the province of Punjab, where cities exhibited the highest HCHO columns. Although Islamabad was also found to have significant concentrations of this trace gas, it did not rank among the cities with the highest column densities. Similarly, Zeb et al. (2019) investigated various atmospheric trace gases over Pakistan using satellite instruments including

OMI. This study also found Punjab to have the highest HCHO tropospheric columns.

Within this domain, Khan et al. (2018) focused on the twin cities of Islamabad and Rawalpindi. While this study was comparable to that of Khokhar et al. (2015), it incorporated ground-based measurements as well instead of relying solely on satellite data. The use of Mini MAX-DOAS instrument for stationary and mobile observations in tandem with OMI satellite data yielded insights into the HCHO scenario in the twin cities. Stationary monitoring was conducted in IESE, NUST while field campaigns were also conducted within the two cities. A prominent finding of this study was that HCHO concentrations surpassed WHO air quality guidelines on several occasions. Shoaib et al. (2020) adopted a similar methodology, concentrating only on stationary monitoring at IESE, NUST. This study also measured HCHO levels which exceeded WHO guidelines.

Expanding their research to encompass the broader South Asian region, Rana et al. (2019) and Baruah et al. (2022) investigated how HCHO emissions vary across different countries, including Pakistan. Both studies used OMI measurements, while Baruah et al. (2022) also employed the GEOS-Chem model in their study. Findings from both studies revealed that despite Pakistan having relatively lower tropospheric HCHO column densities, some of the highest concentrations were found in cities located in Punjab. Interestingly, Baruah et al. (2022) observed a downward annual trajectory for HCHO columns across South Asia.

However, Ali et al. (2022) established that the only significant decrease in this trace gas was over parts of China, Bangladesh, and India. This study offered an alternative approach of examining HCHO, focusing on observing changes in distribution of different pollutants over Asian countries during the COVID-19 pandemic. Although other countries showed either a strong positive or negative correlation between HCHO concentrations and active COVID-19 cases, Pakistan was the only country found to have an insignificant correlation. However, the reason behind this was not stated in the study. A study by Karim & Rappenglück (2023) also found that there was almost no reduction in HCHO during the COVID-19 lockdown.

2.3. Temporal Variation of HCHO Emissions

The temporal variation of a gas refers to how its concentration changes or fluctuates over a certain period. In the context of HCHO, it is important to look at its diurnal as well as seasonal pattern. This type of analysis helps in identifying trends, which can be valuable when understanding the dynamics of the trace gas in the atmosphere. The realm of HCHO monitoring studies in Pakistan remains relatively limited, so insights from research conducted in other regions has also been included. This provides a valuable lens through which the temporal variation of HCHO can be examined.

While investigating the diurnal variation of HCHO in Pakistan, Khan et al. (2018) found that column densities were at lowest during early morning hours, while they reached their maximum around noon. Conversely, Shoaib et al. (2020) highlighted that for the same study area, HCHO concentrations peaked during the early morning and late evening hours. This difference may be due to varying methodologies and the inclusion of field campaigns in the study by Khan et al. (2018), which may have resulted in higher concentrations during noontime due to emissions from traffic.

A study conducted by Tian et al. (2019) in Beijing found similar patterns as Khan et al. (2018), with HCHO concentrations being lowest in the morning and highest at noon, with peaks showing around 14:00. Comparable diurnal patterns were also noted in China by Liu et al. (2023) and Wang et al. (2017), as well as in South Korea by Spinei et al. (2018). These studies collectively pointed to HCHO concentrations increasing after sunrise, peaking in the afternoon, decreasing gradually in the evening, and reaching the lowest point at night. Moreover, Herman et al. (2018) explored HCHO in Korea using the Pandora spectrometer and found concentrations to be higher in the morning.

Park et al. (2017) established a contrasting diurnal trajectory in Seoul. It was observed that while HCHO vertical column densities peaked at noon, they were at their lowest at 14:00. This pattern remained consistent across all seasons. Meanwhile, although Hoque et al. (2018) observed higher HCHO concentrations during the early morning hours in Thailand, it did not find any significant diurnal variation patterns for HCHO.

A different insight into the diurnal pattern of HCHO was offered by Gratsea et al. (2016), who noted that it varies according to season. The study found that in Athens,

HCHO began to increase in concentration much earlier during the day in winter as compared to summers. This was attributed to anthropogenic sources such as central heating, which result in the production of HCHO. In the summer, a noon peak was observed, which was mainly attributed to photochemical reactions in the atmosphere. In both seasons, HCHO concentrations began to increase rapidly right after sunrise due to the oxidation of VOCs.

Khokhar et al. (2015) observed that HCHO had a notable seasonal variation in all provinces of Pakistan. Summer months saw the highest emissions while the lowest were during winter. This was predominantly driven by biogenic emissions of isoprene, which increase in warmer temperatures. Seasonal peaks observed in April, May and November aligned with crop residue burning activities during wheat harvesting and rice paddy clearing, and this finding was also supported by Zeb et al. (2019). Moreover, a study conducted in the Southern Hemisphere by Ryan et al. (2020) also recorded summer peaks in Australia and New Zealand, underpinned by biogenic emissions.

Hoque et al. (2018) identified enhanced HCHO levels during the dry season, mainly due to the burning of biomass. This contrasted with lower concentrations during the wet season, which was due to wet deposition.

While most literature concurred that HCHO emissions peak during the summer, Wang et al. (2017) unveiled a different perspective. It found that in Southern China, HCHO concentrations were highest in autumn, and lowest in spring. This was attributed to higher temperatures as well as secondary formation of HCHO in the autumn season. Y. Zhang et al. (2021) echoes these patterns in the Qinghai-Tibet Plateau region, where the autumn season saw an increasing trend of HCHO concentrations. However, the effect of natural factors such as temperature and precipitation resulted in these concentrations to decrease significantly, establishing summer as the season with the highest concentration of HCHO.

Freitas & Fornaro (2022) offer a completely different insight, concluding that summer and autumn had the lowest concentration of HCHO in Brazil while spring and winter had the highest. This was explained by thermal inversions occurring near the surface during winter, in addition to lower precipitation and weak winds resulting in

accumulation of the pollutant.

2.4. Influence of Weather

Having examined the seasonal patterns of HCHO concentrations, the focus now shifts towards the intricate relationship between these trends and a range of meteorological parameters that influence them. Sun et al. (2021) highlighted the role played by meteorological conditions in driving HCHO production. Apart from solar irradiance, factors such as ambient temperature, relative humidity, wind speed and direction, and precipitation have been identified as the primary drivers of variations in HCHO columns.

2.4.1. Temperature

Notably, temperature has been found to have a profound effect on the biogenic emissions of HCHO. This is because at higher temperatures, plants release more isoprene due to heat stress (Freitas & Fornaro, 2022; Khokhar et al., 2015). It has been estimated that a 5°C rise in temperature can cause isoprene emission rates to double (Stavrakou et al., 2018). This observation was corroborated by Ryan et al. (2023), who noted that HCHO emissions increase during heatwave periods. It must be noted that extended periods of heat waves can negatively impact HCHO production. This is because high temperatures tend to suppress fungal activity in plant roots, which causes stomatal channels to close, resulting in the inhibition of the production of isoprene (Fan et al., 2023).

Furthermore, the rate of photochemical reactions resulting in HCHO production also escalates at higher temperatures. These reactions are mainly the photooxidation of VOCs under the influence of intense solar radiation (Fan et al., 2023; Wang et al., 2017). A positive correlation between HCHO columns and ambient temperature was also reported by Y. Zhang et al. (2021), attributing it to temperature driven reactions of pollutants such as aerosols, particulate matter, and NO_x, which ultimately contribute to HCHO production.

In contrast, Hoque et al. (2018) observed that temperature did not exhibit a strong correlation with HCHO concentrations. This discrepancy was attributed to the relatively consistent temperature values across different seasons in the studied area, resulting in minimal variations in isoprene emissions as well.

2.4.2. Relative Humidity

Relative humidity, another important meteorological parameter, significantly influences HCHO production. This gauges the moisture content of air in relation to its capacity to hold moisture at a specific temperature (Patel et al., 2023). It is expressed as a percentage, with higher values indicating more humid air and lower values indicating drier air.

Similar to temperature, relative humidity also affects the photooxidation of VOCs, contributing to HCHO production. S. Zhang et al. (2021) documented a negative correlation between relative humidity and HCHO concentrations, noting that the highest HCHO levels were associated with low relative humidity and high temperatures. This aligns with Khokhar et al. (2015), who observed lower HCHO concentrations during high humidity instances in the coastal city of Karachi in Pakistan. Additionally, high humidity levels can prompt HCHO conversion to other pollutants through hydrolysis (Y. Zhang et al., 2021).

2.4.3. Wind Direction and Speed

Another pivotal factor impacting HCHO concentrations across regions is wind direction. The transport of air masses from polluted areas can introduce HCHO to downwind regions. Backward trajectory analyses conducted for the IESE, NUST monitoring site revealed elevated HCHO concentrations when the site was downwind from industrial zones in the twin cities. It was established that the study area did not have any prominent local source of HCHO and was mainly influenced by air masses traveling over polluted areas (Khan et al., 2018; Shoaib et al., 2020).

Transboundary transport of HCHO in Pakistan was also observed by Khokhar et al. (2015). Polluted winds from neighboring countries, especially India, were carried into Pakistan, resulting in higher HCHO columns in the country. Y. Zhang et al. (2021) had similar results, finding that monthly variations of HCHO concentrations were significantly influenced by the direction of wind. Adding to this, Tian et al. (2019) saw that on several instances, HCHO peak values were determined by wind direction, with highest values measured when air from polluted areas was carried towards the monitoring site.

Interestingly, S. Zhang et al. (2021) found primary emissions of HCHO to be less

reliant on wind direction as compared to secondary emissions, which were more closely associated with air masses from neighboring regions. It has also been noted that wind direction only has a minor impact on HCHO during the daytime, as photochemical processes dominate instead (Wang et al., 2017). Similarly, Gratsea et al. (2016) showed a weak relationship between wind direction and HCHO column amounts in urban areas. However, this study also observed that wind direction contributed to enhanced HCHO concentration in remote areas.

While wind speed, often coupled with wind direction, is an important factor (Khan et al., 2018; Shoaib et al., 2020), its exact influence on HCHO columns warrants further exploration due to the limited available information.

2.4.4. Precipitation

Precipitation also influences HCHO columns. With increased precipitation, the growth of vegetation is promoted. While isoprene emissions increase because of this, humidity and hydrolysis also increase, resulting in the conversion of HCHO into other products (Fan et al., 2023; Y. Zhang et al., 2021). Additionally, HCHO is removed by wet deposition, meaning that precipitation in the form of rainfall can have a scavenging impact on the trace gas.

2.5. Sources of HCHO

While investigating the temporal variation of HCHO, it is also important to examine the sources of the gas. There are two main sources of HCHO: anthropogenic and natural. Some of the major anthropogenic sources that were identified included burning of waste from agricultural activities, emissions from industrial processes, vehicular emissions, as well as the production and distribution of energy (Rana et al., 2019). Moreover, oil and gas processing facilities were identified as important sources of HCHO as well (Ali et al., 2022). C. Zhang et al. (2022) observed high HCHO concentrations in agricultural areas but found low emissions in industrial regions. Contrary to this, Nowlan et al. (2018) measured large HCHO columns near industrial facilities.

Moreover, Herman et al. (2018) noted that the transportation sector contributes minimally to HCHO production in urban areas with high population densities. It was found by Lok Chan et al. (2020) that there were lower levels of HCHO during the

weekend. Upon further investigation, reduced industrial activities and low traffic during weekends were identified as the main reason. Pyrogenic activities such as agricultural fires and open biomass burning are also responsible for HCHO emissions (C. Zhang et al., 2022; Sun et al., 2021).

Natural sources of HCHO mainly include biogenic emissions from isoprene oxidation. Y. Zhang et al. (2019) and Fan et al. (2021) stated that vegetation had one of the highest contributions towards HCHO. The vegetation type contributing most towards HCHO production was broadleaf forests, while other types such as coniferous trees and shrubs also contributed by emitting high amounts of isoprene (Fan et al., 2021; Millet et al., 2008). Natural pyrogenic sources such as forest fires also emit HCHO (Y. Zhang et al., 2019). Moreover, photochemical activities that occur in the atmosphere, such as oxidation of organic compounds, are major sources of tropospheric HCHO production (Ali et al., 2018; Herman et al., 2018).

2.6. Instruments Used for HCHO Monitoring

Research endeavors have utilized various instruments for HCHO monitoring. While some studies focus exclusively on using either ground-based measurements, satellite observations, or modeling, others incorporate a combination of these tools to achieve a comprehensive outlook on HCHO dynamics over different regions.

2.6.1. Ground-Based Instruments

The ground-based instruments commonly identified in this review were the MAX-DOAS and Pandora Spectrometer. The measurements taken from these instruments were compared with readings obtained from other tools. In a study by Ryan et al. (2020), MAX-DOAS measurements were validated against OMI observations, revealing that OMI was unable to accurately capture the seasonal variation of HCHO. It showed HCHO columns to be roughly 200% higher than those measured by MAX-DOAS. Similarly, Park et al. (2017) observed significantly higher HCHO VCDs from OMI in comparison to Pandora.

Conversely, Spinei et al. (2018) detected higher Pandora Spectrometer values for HCHO than those obtained from the Compact Atmospheric Multispecies Spectrometer (CAMS) onboard the NASA DC-8 aircraft. Yet, Nowland et al. (2018) noted a strong spatial and temporal correlation between HCHO columns derived from

Pandora Spectrometer and the GeoCAPE Airborne Simulator (GCAS) instrument onboard the King Air B-200 aircraft.

2.6.2. Satellite Instruments

Millet et al. (2008) observed a correlation between isoprene emission patterns and the spatial distribution of HCHO columns obtained from OMI. However, OMI appeared to be unable to identify anthropogenic emissions. Addressing this limitation, Marais et al. (2012) utilized OMI to filter out biomass burning and anthropogenic influences, isolating the biogenic factors. This technique holds promise for detecting HCHO emissions from anthropogenic sources as well.

In contrast, TROPOMI exhibits notably enhanced spatial resolution, estimated to be sixteen times superior to that of OMI (De Smedt et al., 2021). TROPOMI is built on algorithms akin to those developed for satellite instruments such as GOME, GOME-2, SCIAMACHY, and OMI. It is considered to be more advanced than OMI due to its capacity to reduce striping effects, enhanced precision which is comparable to COPERNICUS products, improved vertical column accuracy for HCHO, and a better signal-to-noise ratio (De Smedt et al., 2018, 2021).

Ryan et al. (2020) noted a marked improvement in the correlation between MAX-DOAS and TROPOMI values in comparison to those from OMI. However, Vigouroux et al. (2020) pointed out that while TROPOMI effectively captured the seasonal HCHO variations, it tended to overestimate concentrations during elevated levels of HCHO. It was suggested that accounting for aerosol effects could refine TROPOMI measurements.

According to De Smedt et al. (2021), both OMI and TROPOMI perform well for moderate to high HCHO levels, but OMI exhibits a higher bias for lower column densities. OMI tends to overestimate values for medium columns, whereas TROPOMI underestimates MAX-DOAS measurements for higher columns. This underestimation was also observed by Lok Chan et al. (2020), who found that MAX-DOAS readings were 30% higher than TROPOMI records. This discrepancy mainly results from TROPOMI's coarse spatial resolution.

2.6.3. Modelling Techniques

Other studies incorporated models to explore the temporal dynamics of HCHO. The Model of Emissions of Gases and Aerosols from Nature (MEGAN) was a prevalent choice for HCHO monitoring studies, enabling an understanding of the long-term HCHO column trends in relation to climatic changes. Stavrou et al. (2018) utilized MEGAN to compute biogenic isoprene emissions, shedding light on HCHO variations across diverse ecosystems and the response of biogenic HCHO sources to evolving climates. However, Kaiser et al. (2018) detected a bias in MEGAN result, indicating higher HCHO concentrations compared to OMI readings. Conversely, Millet et al. (2008) noted that OMI's measurements of isoprene emission were lower than MEGAN's estimations.

In addition to MEGAN, the CHIMERE model also proves valuable in assessing HCHO columns. Dufour et al. (2009) combined this model with SCIAMACHY observations and concluded that, on average, the discrepancy between the model and satellite instrument remained below 20%. Additionally, it was ascertained that SCIAMACHY could reduce errors in emission estimates by a factor of 2.

2.7. Research Gaps and Limitations

After reviewing relevant literature, several research gaps and limitations need to be acknowledged. There is limited spatial coverage as most HCHO monitoring studies concentrate on urban regions, leading to a lack of data from remote areas. This can result in an incomplete understanding of the distribution and sources of HCHO, especially in regions that have unique emission patterns. Some studies also have relatively short observation periods, because of which longer-term trends or rare events that may influence HCHO concentrations are not captured.

Instrumental differences also need to be addressed. Comparison of HCHO measurements obtained from different instruments or methods could lead to discrepancies due to varying sensitivities, measurement principles, and calibration approaches. Moreover, ensuring data consistency and cross-validation can be challenging.

Additionally, accurate estimation of HCHO concentrations relies on emission

inventories for precursor gases like isoprene and anthropogenic VOCs. Inaccuracies in these inventories can lead to inconsistent estimation of HCHO levels. The quantification of HCHO emissions from biogenic sources also remains a challenge. Incorporating accurate and region-specific emission factors for these sources can improve the accuracy of HCHO models.

Within Pakistan, limited ground-based data remains a challenge. Ground-based monitoring stations are limited and unevenly distributed, leading to spatial gaps in data coverage. This hinders the assessment of localized emission sources, as well as the validation of satellite measurements. Limited monitoring infrastructure in Pakistan also leads to difficulties in accurately validating HCHO measurements due to lack of comprehensive ground-truth data.

Addressing these research gaps and limitations is crucial for advancing the understanding of HCHO distribution, sources, and impacts on air quality and human health.

CHAPTER 3

MATERIALS AND METHODS

3.1. Understanding Formaldehyde Emissions in Islamabad

This study analyzed the temporal variation of HCHO emissions over the capital city of Islamabad, Pakistan using ground-based instruments as well as satellite data. Ground-based measurements were taken using the Mini Multi-Axis Differential Optical Absorption Spectroscopy (Mini MAX-DOAS) and NASA Pandora Spectrometer. The ground-based data was then validated by satellite data using the Ozone Monitoring Instrument (OMI) and Tropospheric Monitoring Instrument (TROPOMI). Additionally, the influence of meteorological parameters on HCHO levels was assessed.

3.1.1. Study Area and Monitoring Period

The selected study site for this research was IESE, NUST (33.6425 ° N, 72.9930 ° E), where stationary monitoring of HCHO was conducted. Both instruments used in this research are installed on the rooftop of the Institute of Environmental Sciences and Engineering (IESE) at the National University of Science and Technology (NUST) in Islamabad. The monitoring site is immediately surrounded by vegetation on one side, and a road on the other which sees regular transport activities. Furthermore, Islamabad's main highway, Srinagar Highway, is situated close to the site.

The Mini MAX-DOAS had a fixed schedule of monitoring with elevation viewing angles set at 2°, 4°, 5°, 10°, 15°, 30°, 45°, and 90° and data was obtained from 1st September 2015 till 17th September 2021. The instrument's frequent non-operational status rendered data collection unviable for several dates during this period, as well as from 2021 onwards. The Pandora Spectrometer was installed in IESE in October 2022, and therefore data was obtained from its installation on 25th October 2022 till 10th June 2023.

3.2. Measurement Instruments

3.2.1. Mini MAX-DOAS



Figure 3.1: Mini MAX-DOAS installed at IESE, NUST.

The Mini Multi-Axis Differential Optical Absorption Spectroscopy (MAX-DOAS) instrument was used in this research study. This instrument employs a remote sensing technique based on absorption spectroscopy in the ultraviolet (UV) and visible spectral range to measure atmospheric trace gases including HCHO. Absorption spectroscopy relies on the principles of Lambert-Beer's law, which in simple terms states that the concentration of a solution and path length are directly proportional to the absorbance of light (Wypych, 2015). In context of this study, this means that higher concentrations of the trace gas will cause the absorption of more light, whereas less light will be absorbed at lower concentrations. This law can be written as a formula as represented by Equation 13 (Bobrowski and Filsinger, 2005).

$$\text{Equation 13} \quad I(\lambda) = I_0(\lambda) \cdot e^{-L \cdot \sigma(\lambda) \cdot c}$$

Where $I(\lambda)$ is the radiation intensity of a beam of light, $I_0(\lambda)$ is the initial intensity of the beam, L is the length of the path in cm, $\sigma(\lambda)$ is the absorption cross section in $\text{cm}^2/\text{molecule}$, and c is the average trace gas concentration in $\text{molecules}/\text{cm}^3$. However, determining the accurate $I_0(\lambda)$ value from the atmosphere proves to be challenging, as this requires an atmosphere devoid of any absorbers. The Mini MAX-DOAS instrument employs the DOAS principle to address this issue, calculating the difference between absorption at two different wavelengths (Bobrowski and Filsinger, 2005). The DOAS technique can either be active or passive, depending on whether a synthetic or natural light source is used. In this study, the Mini MAX-DOAS was a

passive instrument as it measured HCHO only in the presence of sunlight.

The Mini MAX-DOAS instrument used in this study has dimensions of 13×19×14 cm. It has a front-mounted quartz lens with focal length of 40 mm used to collect and focus scattered sunlight, which is transmitted into an Ocean Optics USB2000+ spectrograph through quartz fiber. The instrument has a crossed Czerny-Turner spectrometer with a 0.7 nm spectral resolution, and the spectrometer maintains a stable temperature through a Peltier cooling system. A linear charge coupled device (CCD) detector is used to detect photons for the spectrograph, with a spectral range of 320 – 465 nm and 2048 pixels. The instrument also has a stepper motor on the outside of the box which is used to control the elevation viewing angles. The motor has a 0.1 degree/step precision and a frequency of 784 Hz. The instrument is connected to a computer system with Windows XP installed, where it can be operated through the DOAS Intelligent System (DOASIS) software.

3.2.2. NASA Pandora Spectrometer



Figure 3.2: NASA Pandora Spectrometer installed at IESE, NUST.

The second instrument used in this study is Pakistan's first NASA Pandora Spectrometer. This is a part of the Pandora Global Network (PGN) which allows researchers to remotely obtain data regarding atmospheric gases from over a hundred locations around the world. This instrument is used to measure atmospheric trace gas

columns. Similar to the MAX-DOAS instrument, Pandora Spectrometers also employ the DOAS technique to obtain measurements. The Pandora Spectrometer is highly accurate and can retrieve data with a temporal resolution of 80 seconds (NASA, n.d.). The instrument can be remotely accessed via TeamViewer or AnyDesk by the PGN Network Operators to resolve problems, update software, and ensure that the instrument is operating properly. The team also determines how frequently the instrument needs to be re-calibrated. The local operator is required to maintain a local log file, where all actions performed on the instrument are noted. This information is used by the PGN Network Operators for data quality control.

The Pandora Spectrometer is operated by the Blick Software Suite, which is written in Python language and consists of three software: BlickO, BlickF, and BlickP. BlickO is responsible for operating the instrument through functions such as moving the sun tracker, operating the camera, controlling temperature, taking measurements, etc. BlickF is the software responsible for monitoring BlickO (Figure 3.3) as well as transferring files from the local to a remote directory. BlickP converts Level 0 (L0) data to Level 1 (L1) data by applying instrumental corrections. Additionally, it is responsible for creating Level 2 (L2) data as well.

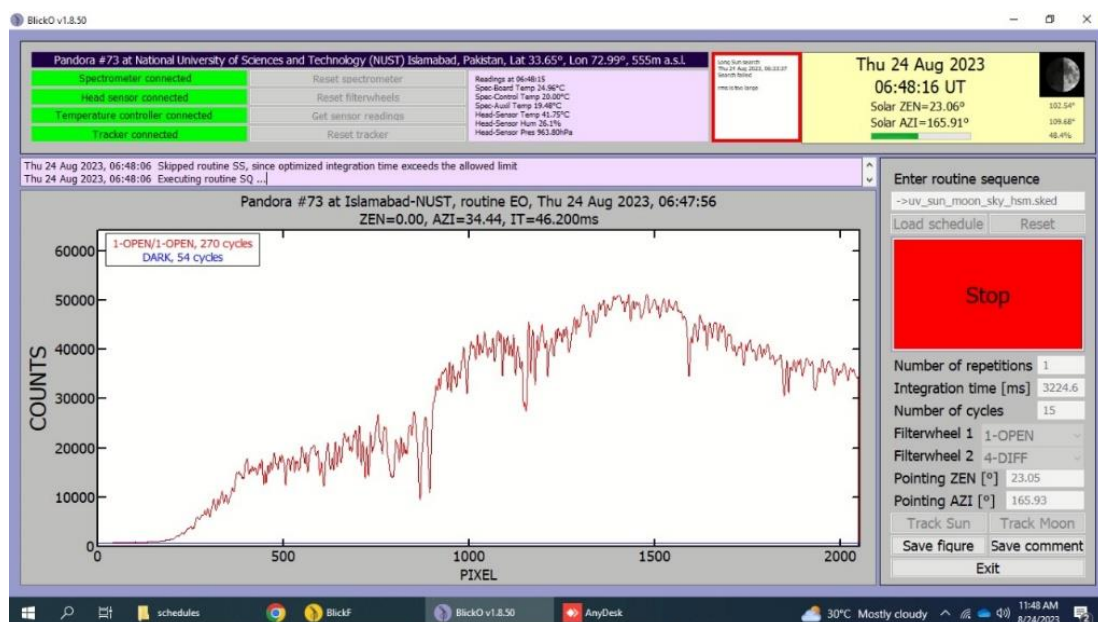


Figure 3.3: Interface of BlickO software used to operate NASA Pandora Spectrometer.

The Pandora instrument used in this study is the Pandora73s1, which has a 75×61 cm control box, and a 3 ft diameter base holding the spectrometer. The spectrometer is connected to an external computer running on Windows 11 and has three major components: the sensor head, control box and sun tracker. The sensor head has optical elements as well as a microcontroller. The optics manipulate light in a manner that facilitates a straightforward and precise analysis by the spectrometer, while the microcontroller governs the motors and conveys instructions from the PC to both the sun tracker and spectrometers.

The main control box (Figure 3.4) houses the spectrometers, which uphold a consistent temperature using a thermos-electric cooler. It also contains the relay box which administers power distribution and effective communication among different components, as well as a computer. The sun tracker's main role is to hold and maneuver the sensor head through the day, ensuring that it remains pointed at either the sun, moon, or any specific coordinated in the sky as directed by the routine mentioned in the operational software. In this study, the schedule file loaded was `uv_sun_moon_sky_hsm.sked`.



Figure 3.4: NASA Pandora Spectrometer main control box, containing spectrometer box, thermoelectric cooler, relay box, and computer.

All measured data can be remotely accessed from the Pandonia Global Network website through the index named Islamabad-NUST. For this study, L2 data for HCHO was used.

3.3. Software and Tools Used in the Study

The various software used to measure and analyze HCHO for this study are listed in Table 3.1 below.

Table 3.1: List of software and tools utilized for this study.

Sr. No.	Name of Software/Tool	Function/Purpose
1	Differential Optical Absorption Spectroscopy Intelligent System (DOASIS) v. 3.2.35	Software package used to run MAX-DOAS
2	Windows Differential Optical Absorption Spectroscopy (WinDOAS)	Wavelength calibration and convolution
3	QDOAS v. 2.112.1	Analysis of HCHO to obtain slant column densities
4	Microsoft Excel v. 2307	Mathematical calculations to determine vertical column densities and other statistical analyses
5	Giovanni (NASA Portal) v. 4.38	Level 3 tropospheric HCHO data from OMI
6	Google Earth Engine	Level 3 tropospheric HCHO data from TROPOMI
7	RStudio v. 2023.06.0	Data analysis
8	Blick Software Suite v. 1.8	Operating software for NASA Pandora Spectrometer

3.3.1. Differential Optical Absorption Spectroscopy Intelligent System (DOASIS)

DOASIS software is used to perform various functions while running the Mini MAX-DOAS instrument. Commands can be given using Jscript language, which can include changing elevation angles through the stepper motor, maintaining a stable temperature, acquiring spectra, etc. DOASIS was used to calculate the ring spectrum to filter out Raman scattering, as well as for measuring dark current and offset values for error reduction.

Photosensitive instruments like spectrometers have sensors to measure photons. Even when they are not exposed to light, these sensors can detect small amounts of electrical signals. In the context of the MAX-DOAS instrument, the dark current value refers to the small signal detected in darkness. This is akin to background noise, and therefore may impact the precision of measurements taken. Thus, it needs to be accounted for to get accurate data. Offset refers to a small, baseline value which is recorded by the detector in the absence of light. This can be due to inherent factors within the instrument's measurement system, such as imperfections in electronic components, sensor properties, etc. By correcting this offset value, measurement accuracy can be enhanced. The values used to obtain dark current and offset measurements are stated in Table 3.2.

Table 3.2: Values used to obtain dark current and offset measurements.

	Integration Time (milliseconds)	Number of Scans
Dark Current	10,000	1
Offset	100	1000

3.3.2. Windows Differential Optical Absorption Spectroscopy (WinDOAS)

WinDOAS software is used for the analysis of spectra recorded in the UV-visible range through DOAS technique. This software was used for two main steps: spectral calibration and cross-section convolution.

3.3.2.1. Spectral calibration

For spectral calibration, a measured spectrum was fitted to a convoluted solar spectrum. The wavelength of the reference solar spectrum was assigned to the detector's pixels, i.e., 2048. The wavelength range was split into 6 sub-windows to better analyze fits. During the calibration process, the shift and squeeze function was used to adjust the shift of measured and convoluted spectra. For each of the sub-windows, the Slit Function Parameter was employed. This function, which indicated a polynomial degree of 3, enabled the interpolation of missing data points, and helped obtain a comprehensive understanding of the data distribution.

The spectrum characterized by the lowest solar zenith angle (SZA) and highest concentration at a 90° angle at noon was chosen. The best spectrum was saved as an ascii file and used as a reference spectrum in the subsequent steps. This calibration fit is also referred to as the Kurucz-fit. This is because it usually involves obtaining a high-resolution spectrum from the Kurucz solar atlas to use as input. This spectrum is convoluted further according to the spatial resolution of the instrument being used – Mini MAX-DOAS in this case. The calibration procedure was repeated several times to minimize any discrepancies in the data.

3.3.2.2. Cross-section convolution

Employing the mathematical technique of convolution is integral for wavelength processing. The convolution/filtering tool in WinDOAS played a pivotal role in this step. The calibration file derived from the Kurucz-fit was used. A slit function type of Gaussian with a FWHM of 0.7 nm was chosen. The online convolution method was employed, where cross-sections of gases are automatically convoluted during the spectral analysis process.

3.3.3. Quantitative Differential Optical Absorption Spectroscopy (QDOAS)

For the analysis of HCHO, QDOAS software was used. The main settings applied in QDOAS for the analysis of HCHO in this study are shown in Figures 3.5 – 3.10. First, the date, time, SZA, and elevation viewing angle fields were selected in the display tab (Figure 3.5).

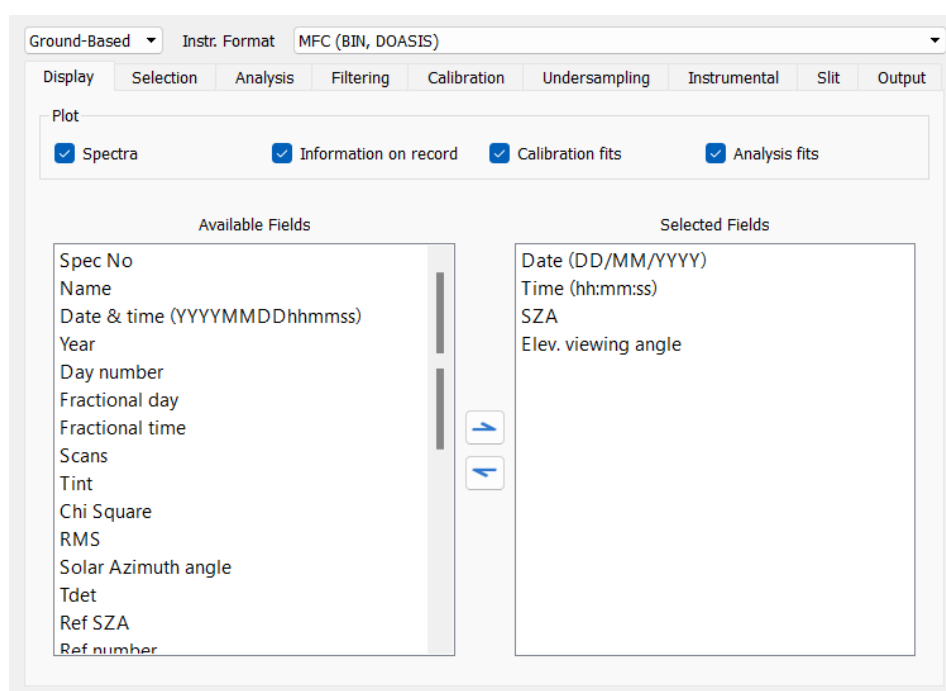


Figure 3.5: QDOAS display tab.

In the calibration tab, the solar reference file was added, and the calibration interval was set (Figure 3.6).

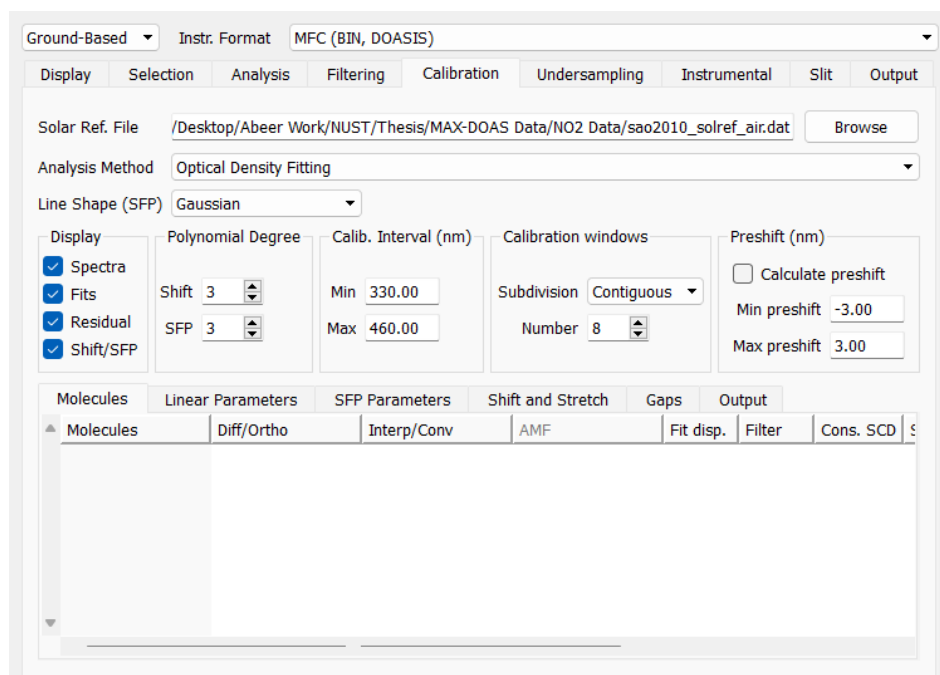


Figure 3.6: QDOAS calibration tab.

In the instrumental tab (Figure 3.7), the calibration file, and the dark current and offset files corresponding to the date of the loaded spectra were added. Additionally, the detector size of the Mini MAX-DOAS instrument, 2048, was entered.

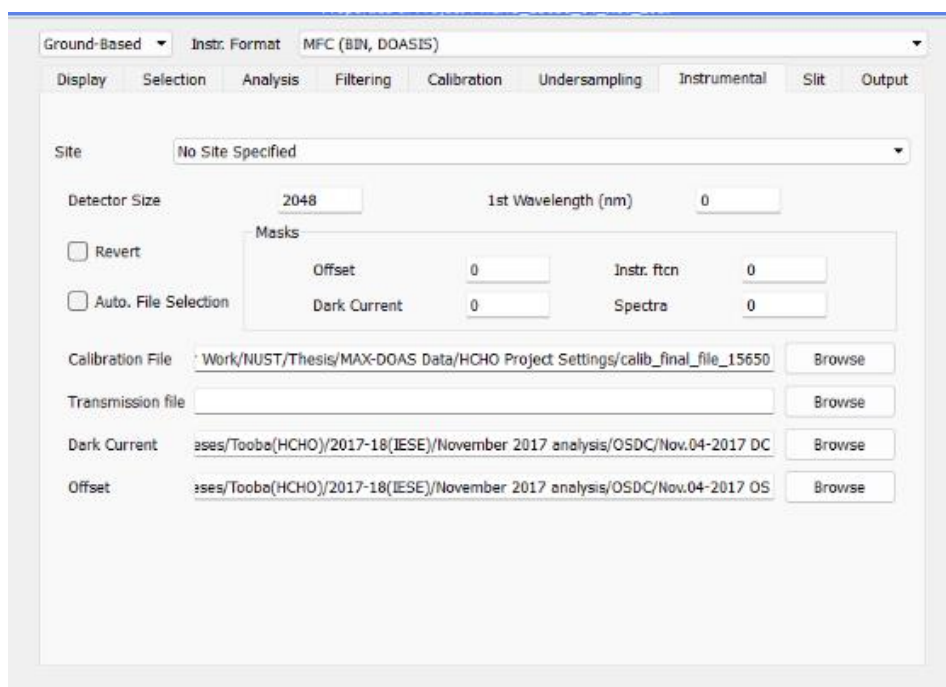


Figure 3.7: QDOAS instrumental tab.

Lastly, the output path was set and the date, time, time integration (T int), SZA, solar azimuth angle, azimuth viewing angle, and root mean square (RMS) fields were selected (Figure 3.8).

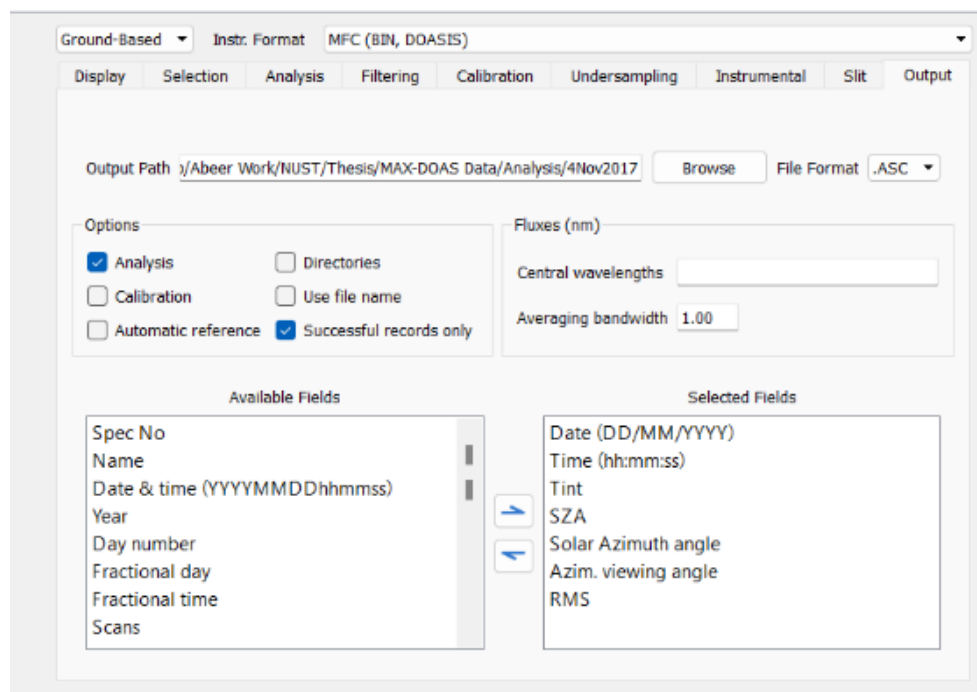


Figure 3.8: QDOAS output tab.

In the HCHO analysis window properties (Figure 3.9), the HCHO fitting interval was set at 336.5 – 359 nm in accordance with the results of DOAS fit with lowest residual errors, and the FWHM was set at 0.5 nm. The calibrated spectrum obtained from the previous steps was used as a reference spectrum. Cross-sections of gases were added, and their convolution settings were applied. Moreover, a polynomial order of 5 was selected (Figure 3.10).

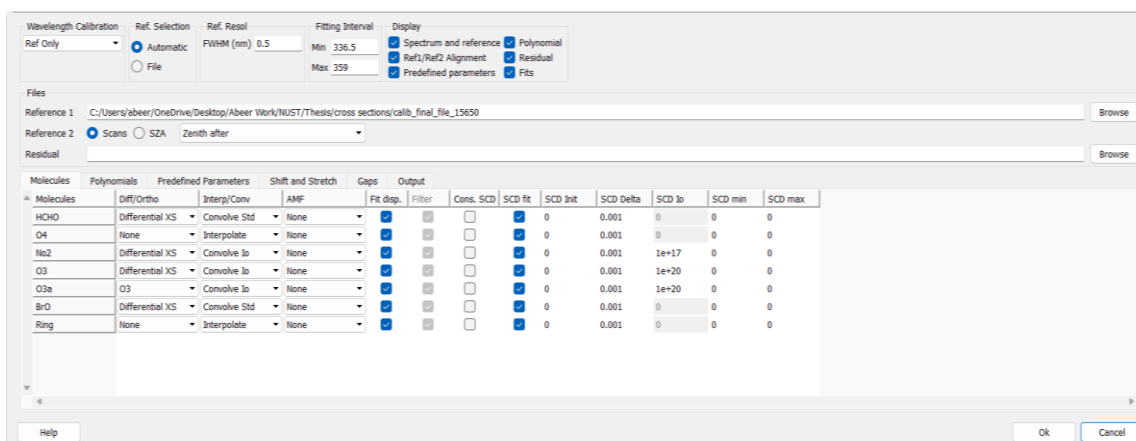


Figure 3.9: QDOAS HCHO analysis window properties.

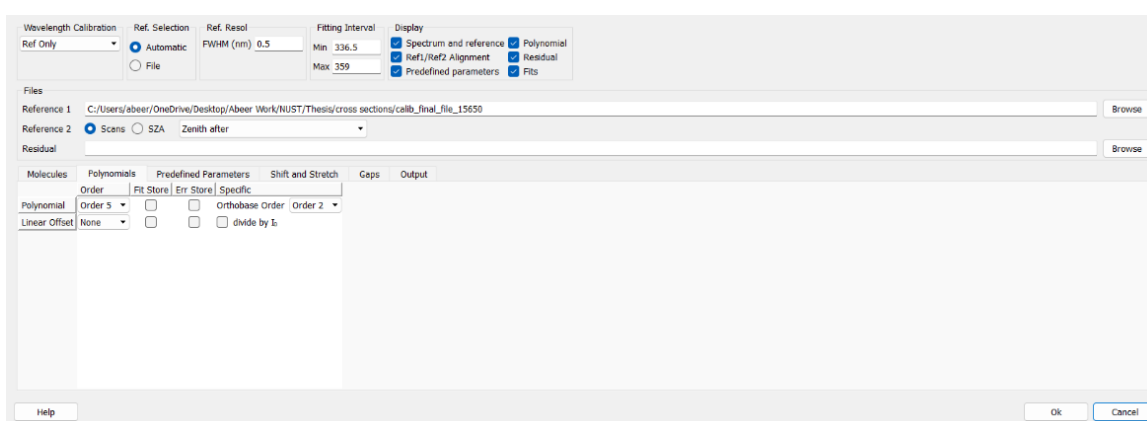


Figure 3.10: QDOAS HCHO analysis window properties showing polynomial order.

Analysis was run in QDOAS to obtain HCHO differential slant column densities (dSCDs), which represent the difference in column density of a specific trace gas along two different paths: one being the slant path from the instrument to a light source such as the sun, and the second being the vertical path through the atmosphere. The SCDs were saved in ascii file format and accessed using Microsoft Excel for further analysis.

3.3.4. Analysis Through Microsoft Excel

The ascii file was opened in Excel to perform further analysis, mainly to calculate the air mass factor (AMF) and using this to convert the SCDs into vertical column densities (VCDs). The AMF is a crucial parameter in atmospheric remote sensing, especially in techniques like DOAS. It is simply a ratio of the SCD and VCD. This

quantifies the influence of the vertical distribution of atmospheric trace gases like HCHO on the column density measurements from ground-based instruments like the Mini MAX-DOAS, or from space instruments like satellites. The AMF helps in accounting for how the concentration of trace gases changes with height, ensuring that measurements are correctly interpreted (Veefkind et al., 2006; Lorente et al., 2017).

A VCD represents the amount of a gas present in a vertical column of the Earth's atmosphere, directly above a specific location. This quantifies the concentration of the gas in a particular section of the atmosphere, from the ground to the top, helping in understanding the distribution of gases in the atmosphere (Royal Belgian Institute for Space Aeronomy, 2010). While converting SCDs to VCDs, it necessary to use the AMF as this acts as a correction factor by accounting for the complex interactions between light and the atmosphere thus accurately quantifying vertical distribution of atmospheric trace gases such as HCHO.

3.3.4.1. dAMF calculation

The differential air mass factor (dAMF) was used to determine the tropospheric VCD values. This, like dSCDs, is the difference between the AMF measured at a specific angle and the AMF measured at 90° (Liu et al., 2016). The formula used to calculate AMF in this study is stated in Equation 14.

$$\text{Equation 14} \quad AMF = \frac{1}{\sin\left(\frac{2 \times 3.14 \times \text{Elevation Viewing Angle}}{360}\right)}$$

3.3.4.2. Tropospheric VCD calculation

To calculate the tropospheric VCD, AMF and SCD values were used. The sequence of calculations required for this step are represented by Equations 15 – 20.

$$\text{Equation 15} \quad VCD = \frac{dSCD\alpha}{dAMF\alpha - AMF_{90^\circ}} \quad \text{where } \alpha \text{ is the elevation angle } \neq 90^\circ.$$

By using geometric approximation, AMF can be written as stated in Equation 16.

$$\text{Equation 16} \quad AMF = \frac{1}{\sin\alpha}$$

Thus, tropospheric VCDs can be calculated using the formula stated in Equation 17.

$$\text{Equation 17} \quad VCD_{trop} = \frac{dSCD\alpha}{\frac{1}{\sin\alpha} - 1}$$

In Microsoft Excel, the following formula was used to calculate VCDs:

$$\text{Equation 18} \quad VCD = \frac{SCD}{AMF-1}$$

3.3.5. Validation of Ground-Based Data with Satellite Data

To ensure the consistency and credibility of atmospheric datasets, it is important to compare and cross-reference measurements taken from ground-based instruments with satellite observations (Wu et al., 2019). For this study, the Ozone Monitoring Instrument (OMI) onboard NASA's Aura satellite and the Tropospheric Ozone Monitoring Instrument onboard the European Space Agency's Copernicus Sentinel-5 Precursor (S-5P) spacecraft were used for HCHO data validation. OMI was launched in 2004 and uses a wide field imaging spectrometer for daily global measurements (NASA, 2021). TROPOMI was launched in 2017 and uses a nadir-viewing wide field imaging spectrometer (ESA, 2023). The main features of both instruments are listed in Table 3.3 (ESA, 2023; NASA, 2021).

Table 3.3: Comparison of the main features of OMI and TROPOMI

Sr. No.	Parameters	OMI	TROPOMI
1	Spectral Bands	UV-Vis: 270-500 nm	UV-Vis: 270-500 nm Near IR: 675-775 nm Shortwave IR: 2305-2385 nm
2	Resolution	Spatial	13 km × 24 km ² 13 km × 48 km ² for Ozone profile
		Spectral	0.45 – 1.0 nm
3	Orbit Altitude	705 km	824 km
4	Swath Width	2600 km	2600 km

3.3.5.1. OMI

Level 3 (L3) HCHO data from OMI was obtained using Giovanni. A time-series, area-averaged map was plotted for HCHO column amount using OMHCHOdv003 at a daily temporal resolution and 0.1° spatial resolution. Data was acquired from 1st September 2015 until 17th September 2021 to correspond with MAX-DOAS measurement dates. IESE, NUST was selected as the region. The plot was downloaded in a CSV format and opened through Microsoft Excel.

OMI data for HCHO was available until June 2022, so validation with Pandora could not be possible.

3.3.5.2. TROPOMI

A code for L3 HCHO offline product was used to obtain TROPOMI data via Google Earth Engine. Data was acquired from 29th November 2018 till 17th September 2021 for MAX-DOAS, and 26th October 2022 till 10th June 2023 for Pandora. Plots were downloaded in a CSV format and opened through Microsoft Excel. For repeated dates, a pivot table was created to obtain daily averages.

3.3.6. RStudio

Once all data was obtained, RStudio was used for subsetting. This process helped in creating a file with MAX-DOAS/Pandora, OMI and TROPOMI measurements for the same dates.

3.3.7. Meteorological Data

Weather data was acquired from the U.S.-Pakistan Center for Advanced Studies in Energy, NUST. This included temperature, wind speed, global horizontal irradiance (GHI), and relative humidity (RH). Data was obtained from 1st September 2015 until 9th June 2021 for MAX-DOAS, and 25th October 2022 till 16th May 2023 for Pandora. Values for several dates were missing due to the weather station being non-operational for repair and maintenance purposes. Analysis was conducted using Microsoft Excel and RStudio.

CHAPTER 4

RESULTS AND DISCUSSION

4.1. Ground-Based Monitoring at IESE, NUST

4.1.1. HCHO Time Series

A time series graph for HCHO VCDs was plotted to show how the concentration of the trace gas changed over the period selected for this study. This was valuable for understanding the temporal variation of HCHO around IESE, NUST. Figure 4.1 shows the time series of HCHO VCDs as measured by MAX-DOAS, while Figure 4.2 represents HCHO VCDs as measured by Pandora Spectrometer. On average, HCHO values from both instruments are higher in summer months as compared to winter.

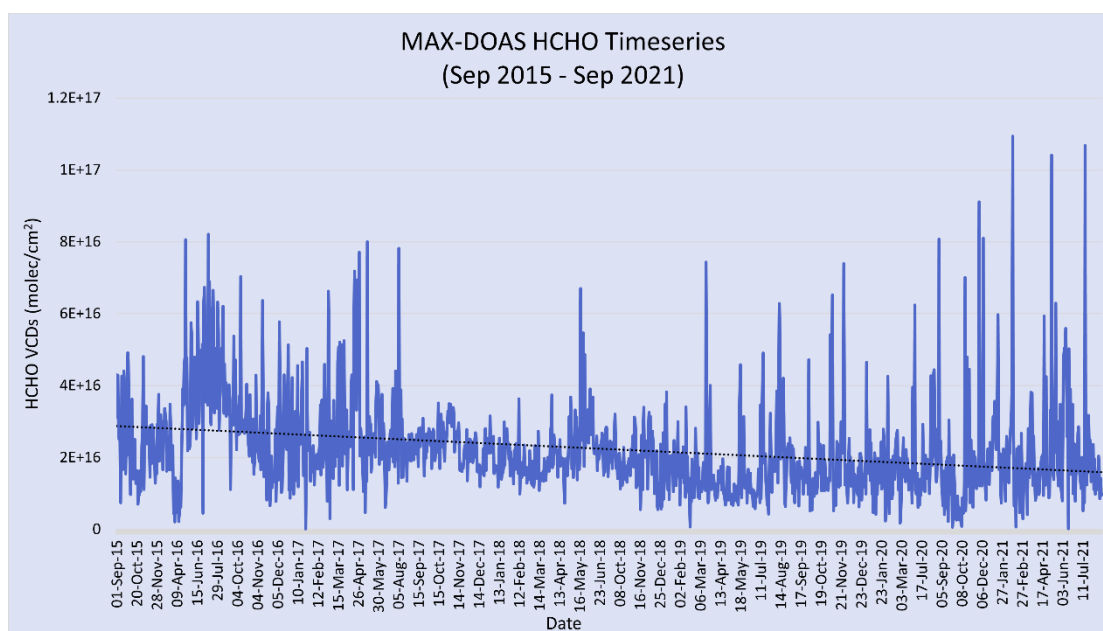


Figure 4.1: MAX-DOAS HCHO time series (2015 – 2021).

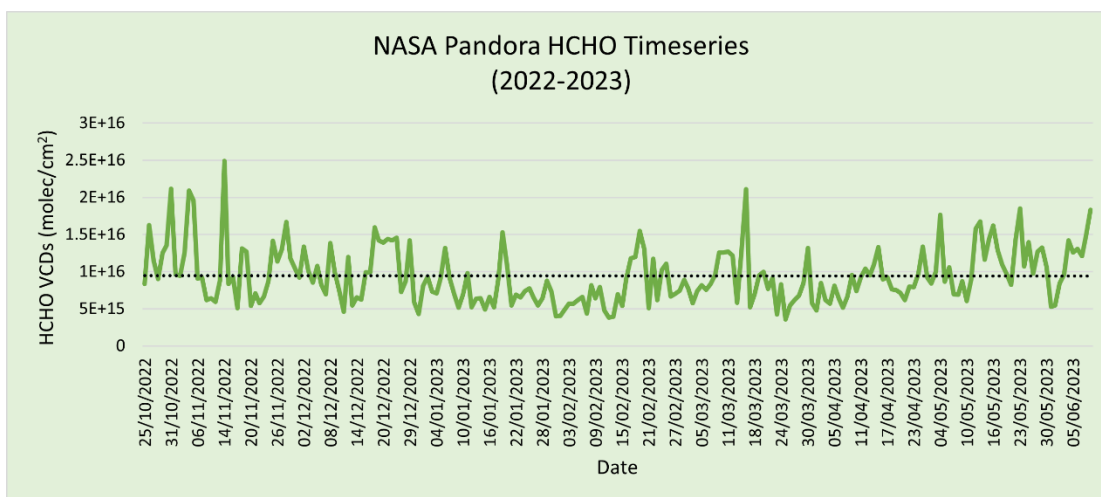


Figure 4.2: NASA Pandora Spectrometer HCHO time series (2022 – 2023).

4.1.2. HCHO Annual Diurnal Cycle at IESE, NUST

During the study period, the diurnal cycle of HCHO was investigated using hourly average of vertical column densities (VCDs). Specifically, a 12-hour window spanning from 06:00 to 18:00 in Pakistan Standard Time (PST) was chosen for analysis, aligning with the operational hours of the MAX-DOAS instrument. To ensure consistency and conduct a meaningful comparison, the same time range was applied to Pandora Spectrometer measurements as well.

Analyzing the annual diurnal cycle through MAX-DOAS measurements (Figure 4.3) revealed elevated HCHO concentrations during early morning and late evening hours. The lowest concentration was observed at 09:00, with a VCD of $2.48\text{E}+16$ molecules/cm², followed by a gradual increase throughout the day. Peak concentration of $4.79\text{E}+16$ molecules/cm² was reached at 18:00. These findings correspond with those reported by Shoaib et al. (2020). Morning concentrations were attributed to background concentrations and low solar irradiance, while increase in the afternoon solar intensity led to photolysis and other photochemical processes causing a decline in concentrations. This trend shifted as temperatures triggered biogenic emissions and subsequent VOC photooxidation, resulting in an evening increase.

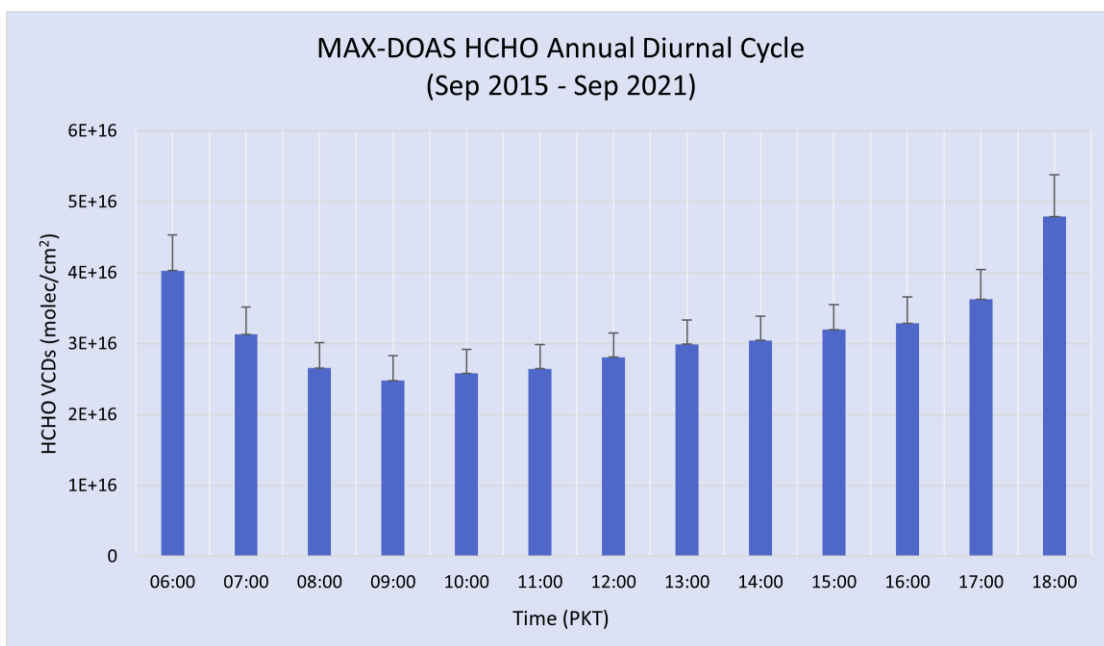


Figure 4.3: HCHO annual diurnal cycle measured by MAX-DOAS.

Examining the annual diurnal cycle using Pandora Spectrometer measurements (Figure 4.4) displayed a somewhat different pattern. While peak concentrations aligned with early morning and late evening periods, a noticeable rise in midday concentrations was evident. The lowest level occurred at 08:00, measuring $1.85\text{E}+16$ molecules/cm², then rising to $2.03\text{E}+16$ molecules/cm² by 11:00. Subsequently, concentrations of HCHO gradually decreased until 15:00, followed by a peak of $2.78\text{E}+16$ at 18:00. Discrepancies with MAX-DOAS values could stem from the relatively shorter observation window and potential data gaps in certain months when Pandora was not operational. To further understand the diurnal pattern of HCHO as measured by Pandora, other contributing factors will need to be examined.



Figure 4.4: HCHO annual diurnal cycle measured by NASA Pandora Spectrometer.

4.1.3. HCHO Seasonal Diurnal Cycle at IESE, NUST

To determine the difference in HCHO concentrations during different seasons, the seasonal diurnal cycle was also investigated. Seasonal categorization was established based on the climate profile for Pakistan as defined by the World Bank (2021). The specific categories are outlined in Table 4.1.

Table 4.1: Categorization of Pakistan's seasons according to months

Sr. No.	Season Name	Months
1	Pre-Monsoon / Spring	March – May
2	Monsoon / Summer	June – September
3	Post-Monsoon / Autumn	October – November
4	Winter	December – February

Figure 4.5 represents the seasonal diurnal cycle of HCHO based on MAX-DOAS observations. It is important to note that the seasonal diurnal cycle for HCHO was solely determined using VCDs obtained through the Mini MAX-DOAS instrument. This choice was necessitated by the fact that Pandora was installed at IESE in October 2022, resulting in incomplete data coverage across all seasons up to this study's conclusion in June 2023.

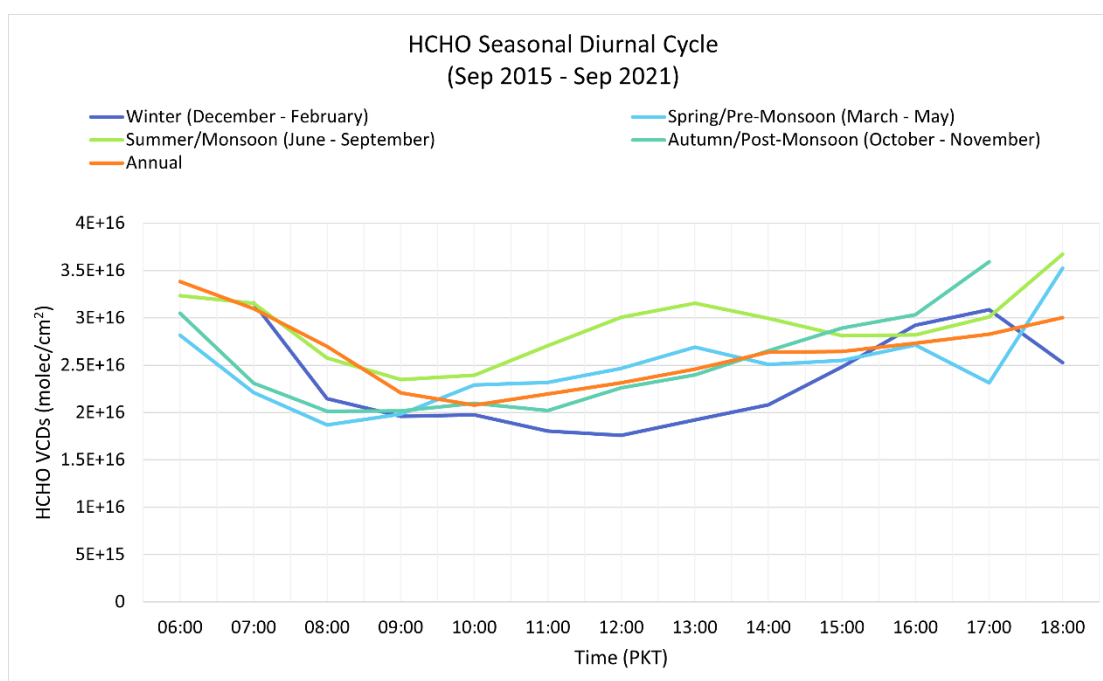


Figure 4.5: Seasonal diurnal cycle of HCHO using MAX-DOAS observations.

It can be seen in Figure 4.5 that the highest concentrations of HCHO were during the monsoon, or summer season, while winter months saw the lowest concentrations on average. This remains consistent with findings by Khokhar et al. (2015). Moreover, like Gratsea et al. (2016), this study also observed a summer afternoon peak. This is mainly as a result of photochemical reactions in the atmosphere which result in rapid HCHO production. During this time, winter season sees a dip in concentration. This can be because of lower solar intensity. Additionally, summer months see higher HCHO concentrations because of biogenic emissions of isoprene. During the winter, plants experience minimum heat stress, causing them to release lower levels of isoprene.

4.1.4. HCHO Average Weekly Cycle at IESE, NUST

The average weekly cycle for HCHO was examined to determine whether the days of the week have any influence on the concentration of the trace gas. As seen in Figures 4.6 – 4.7, the weekly cycle of HCHO as calculated using measurements from both MAX-DOAS and Pandora observations showed no pronounced differences over the course of the week (p -value > 0.05). This contradicts with the findings by Lok Chan et al. (2020), as there was no weekend effect observed in the results obtained for this study. It can therefore be assumed that anthropogenic activities were not a major source of HCHO at the IESE monitoring site.

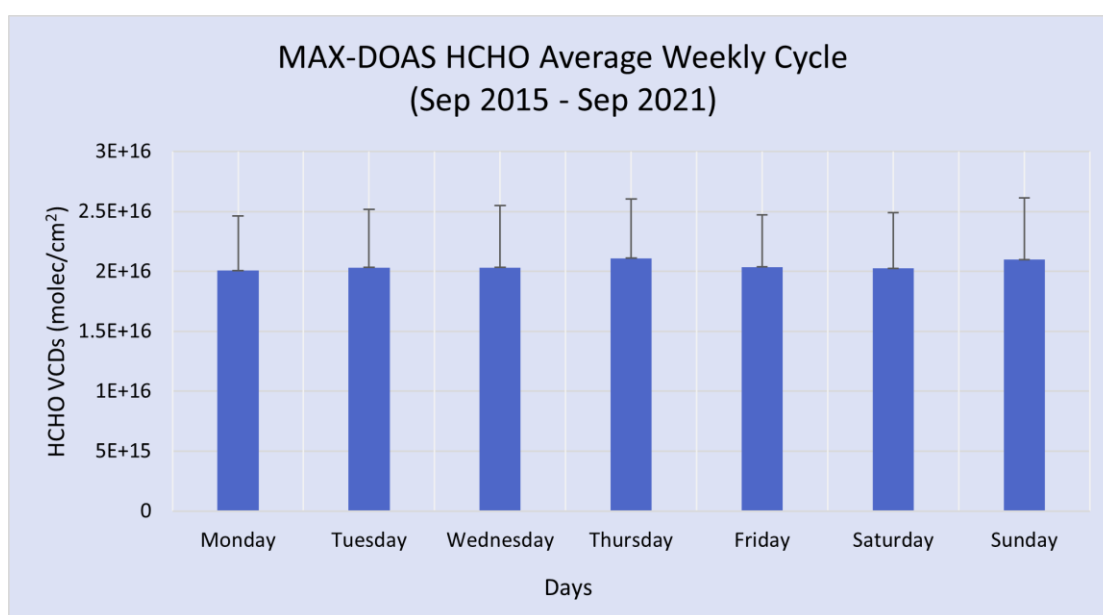


Figure 4.6: HCHO average weekly cycle measured through MAX-DOAS.

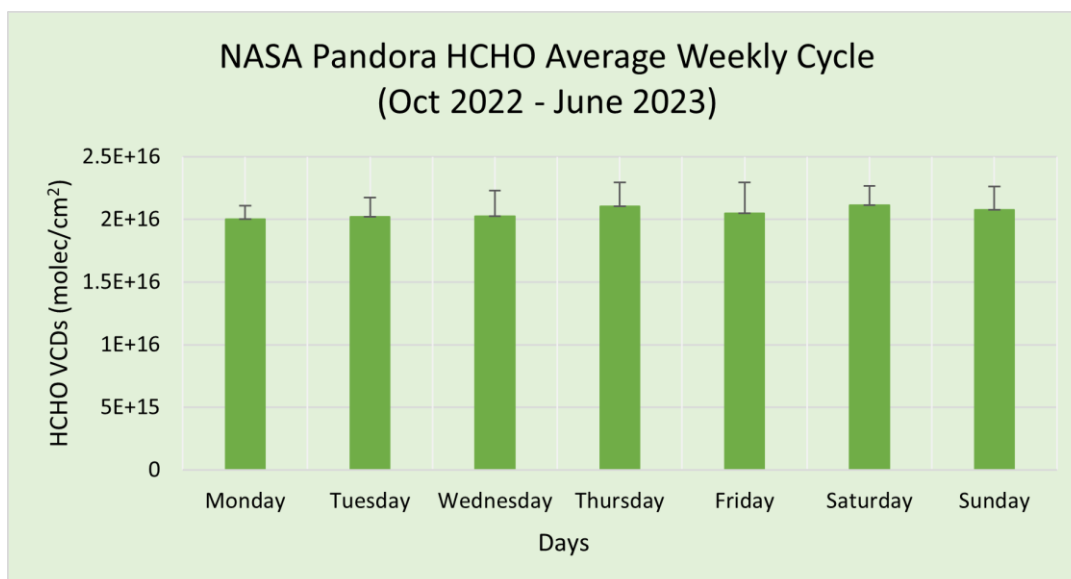


Figure 4.7: HCHO average weekly cycle measured through NASA Pandora Spectrometer.

4.1.5. HCHO Average Monthly Cycle at IESE, NUST

To assess the variation in HCHO concentrations over the course of the year, average monthly values were utilized. For MAX-DOAS measurements, HCHO concentrations were highest in summer months and lowest during the winter (Figure 4.8). For Pandora, the summer months from July to September were not available, so an accurate assessment could not be made. However, for the available months, Pandora also showed a similar trend of higher concentrations in summer and lower in winter (Figure 4.9). Measurements from both instruments showed a notable decrease in April.

Khokhar et al. (2015) and Zeb et al. (2019) observed seasonal peaks in April, May, and November due to crop residue burning activities occurring during that time in Pakistan. The increase of HCHO in March and May suggests the consequences of stubble burning following the harvesting of wheat. However, no peak can be observed in November. To further understand the decline in concentrations in April, meteorological parameters can be examined.

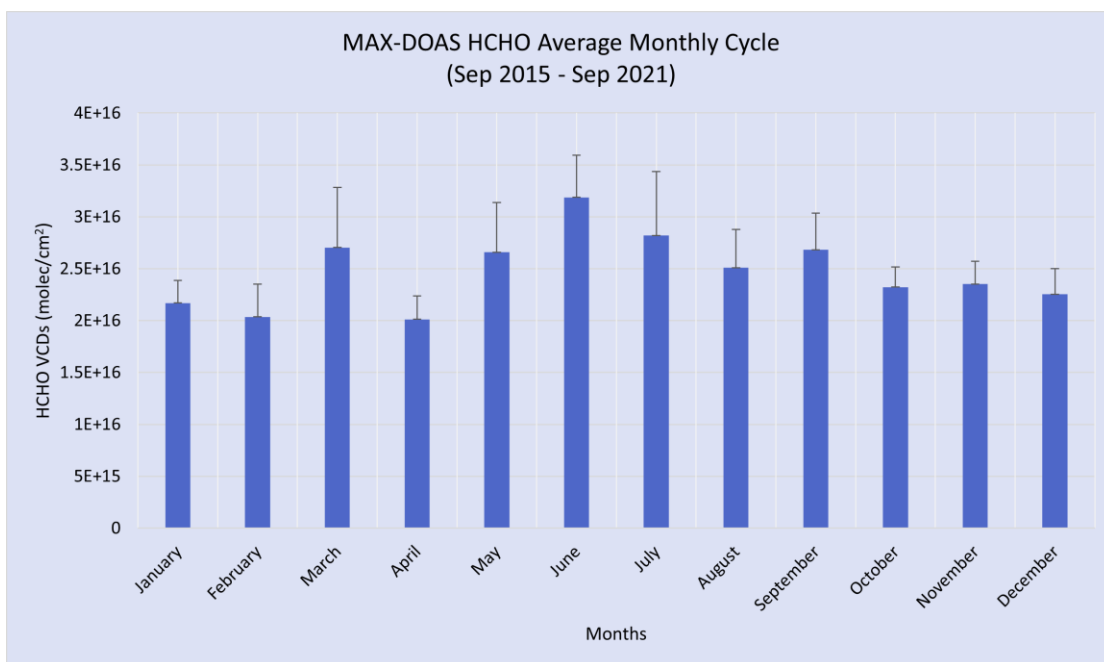


Figure 4.8: MAX-DOAS HCHO monthly cycle.

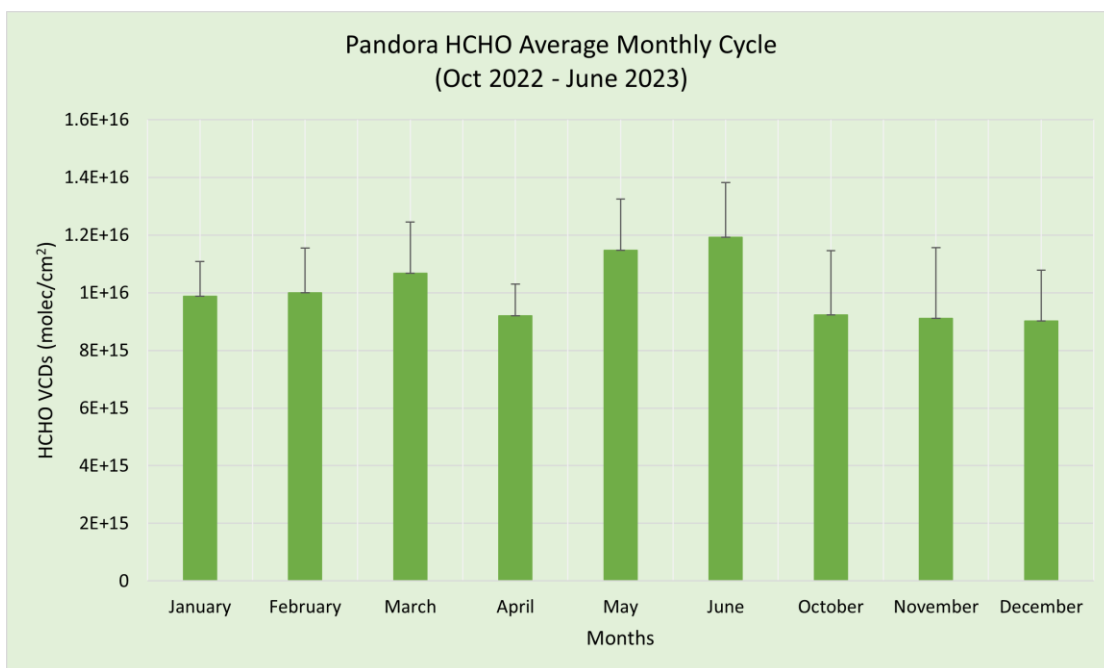


Figure 4.9: Pandora HCHO monthly cycle.

4.1.6. HCHO Average Yearly Observations Over IESE, NUST

To determine how HCHO levels varied throughout the monitoring period, yearly observations were analyzed. This analysis was only conducted for MAX-DOAS observations, as Pandora observations covered only nine months. As seen in Figure

4.10, the year 2016 had the highest HCHO VCDs, whereas 2020 had the lowest. Meteorological parameters were assessed to determine the cause of the increase in 2016. For 2020, it can be assumed that HCHO levels were low due to the COVID-19 pandemic resulting in lockdowns and consequently significantly reduced anthropogenic emissions from vehicles and industries.

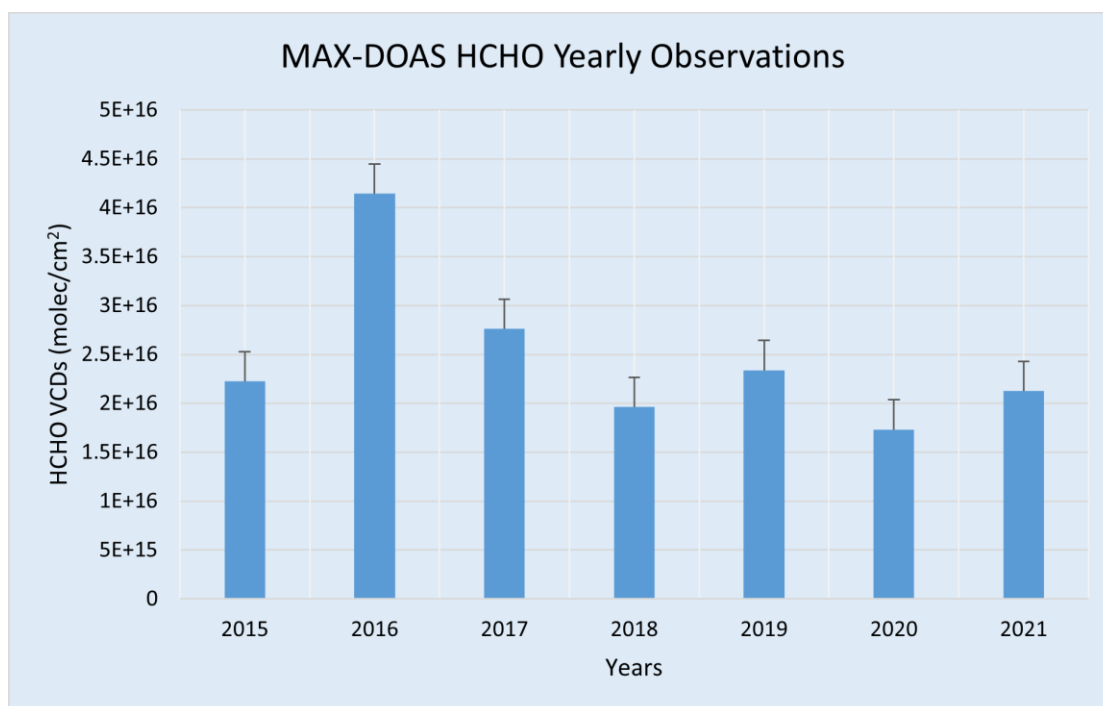


Figure 4.10: MAX-DOAS HCHO yearly cycle

4.2. Satellite Observations

4.2.1. OMI

The HCHO data received from MAX-DOAS instrument was validated against OMI data. For this purpose, MAX-DOAS VCDs were organized hourly, and measurements taken between 12 – 2 pm PST were extracted. This is to match with the overpass time for OMI, which is at approximately 1:30 pm local time. As seen in Figure 4.11, OMI significantly underestimated HCHO concentrations when compared with ground-based observations. This contrasts the findings of De Smedt et al. (2021), who noted an overestimation. OMI satellite data showed a correlation of 0.61 with MAX-DOAS measurements over IESE, NUST. Figure 4.12 depicts this correlation.

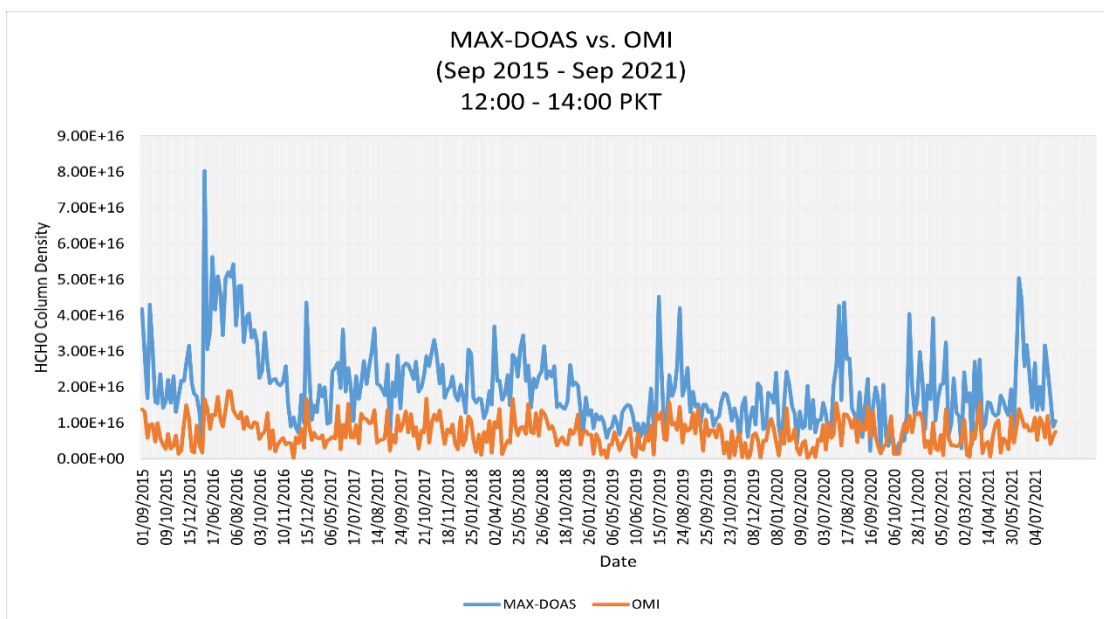


Figure 4.11: Validation of ground-based MAX-DOAS 12:00 – 14:00 measurements with OMI satellite measurements over IESE, NUST.

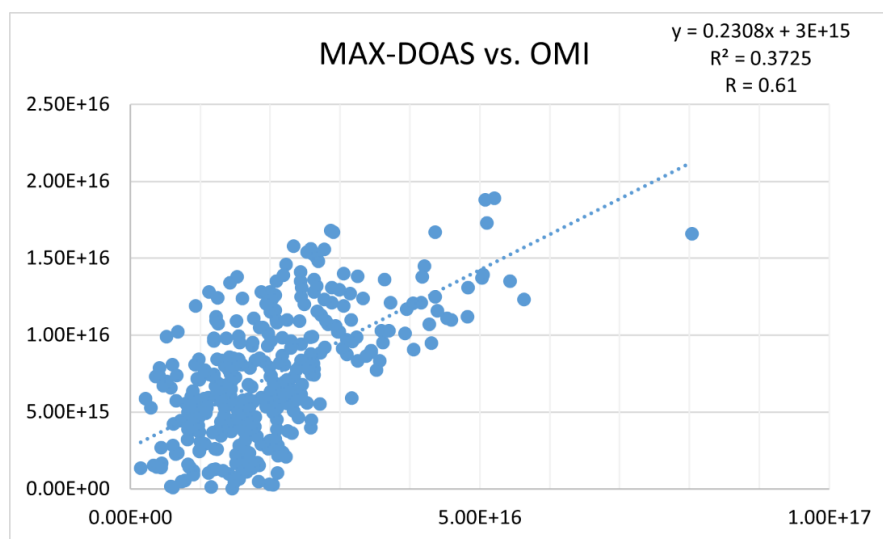


Figure 4.12: Correlation of HCHO VCDs of OMI vs. MAX-DOAS 12:00 – 14:00 average over IESE, NUST

As OMI data for HCHO was not available for the monitoring period of Pandora for this study, it was not included.

4.2.2. TROPOMI

Data from TROPOMI was compared with both MAX-DOAS and Pandora values. TROPOMI also underestimated the ground-based observations. This remains

consistent with the findings of De Smedt et al. (2021) and Lok Chan et al. (2020). While measurements between 12:00 – 14:00 PST (Figure 4.13) were used due to the satellite’s overpass time, measurements from 06:00 – 18:00 (Figure 4.15) were also assessed to compare diurnal cycle values from ground-based and satellite observations.

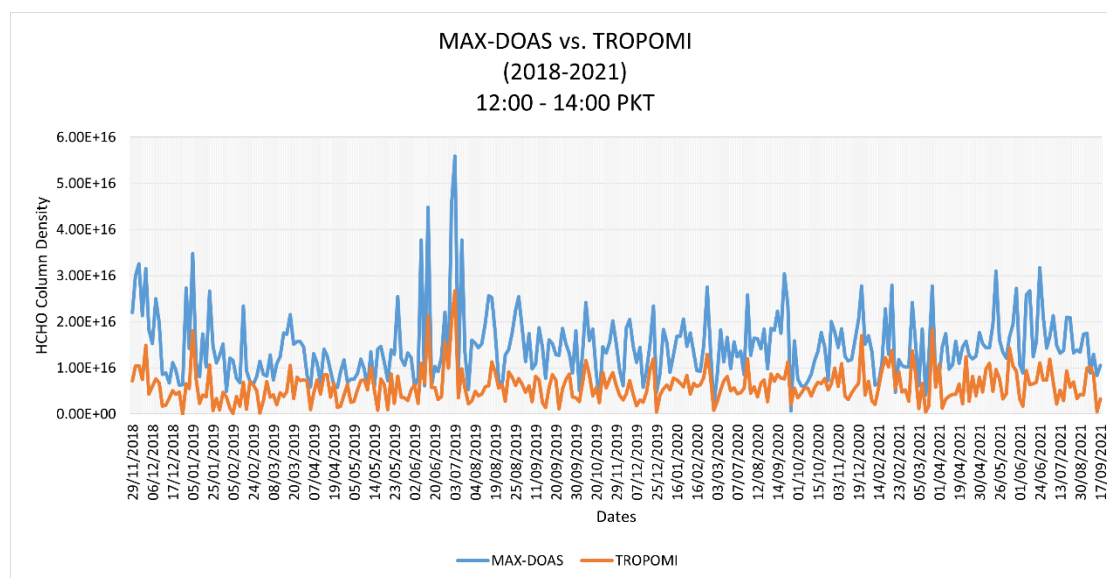


Figure 4.13: Validation of ground-based MAX-DOAS 12:00 – 14:00 measurements with TROPOMI satellite measurements over IESE, NUST.

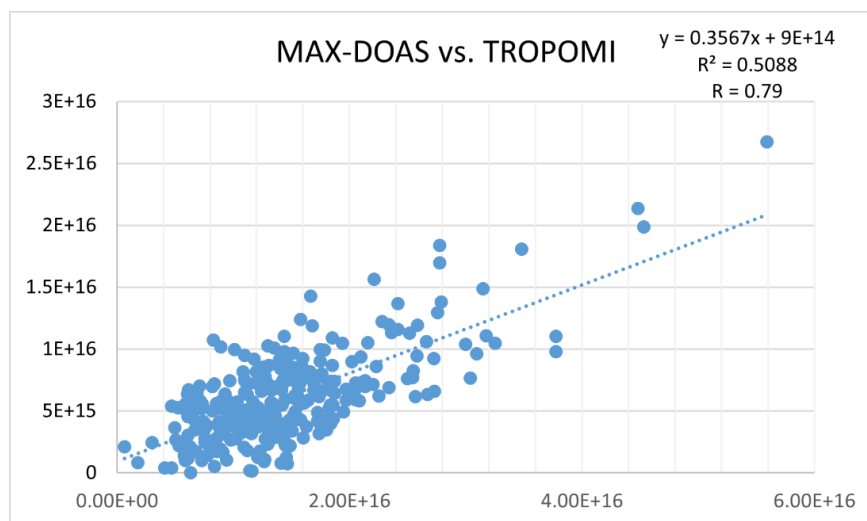


Figure 4.14: Correlation of HCHO VCDs of TROPOMI vs. MAX-DOAS 12:00 – 14:00 average over IESE, NUST.

HCHO VCDs obtained from MAX-DOAS showed a higher correlation with

TROPOMI for 12:00 – 14:00 (Figure 4.14) as compared to 06:00 – 18:00 (Figure 4.16). This is mainly due to the former matching with the satellite’s overpass time, giving more accurate results.

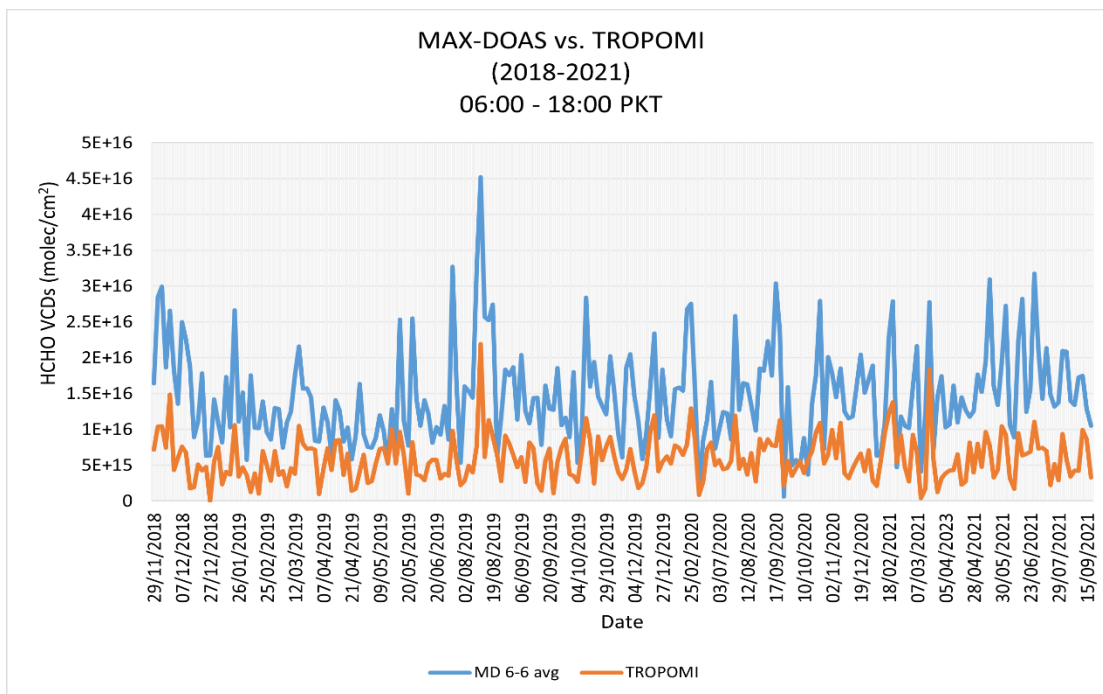


Figure 4.15: Validation of ground-based MAX-DOAS 06:00 – 18:00 measurements with TROPOMI satellite measurements over IESE, NUST.

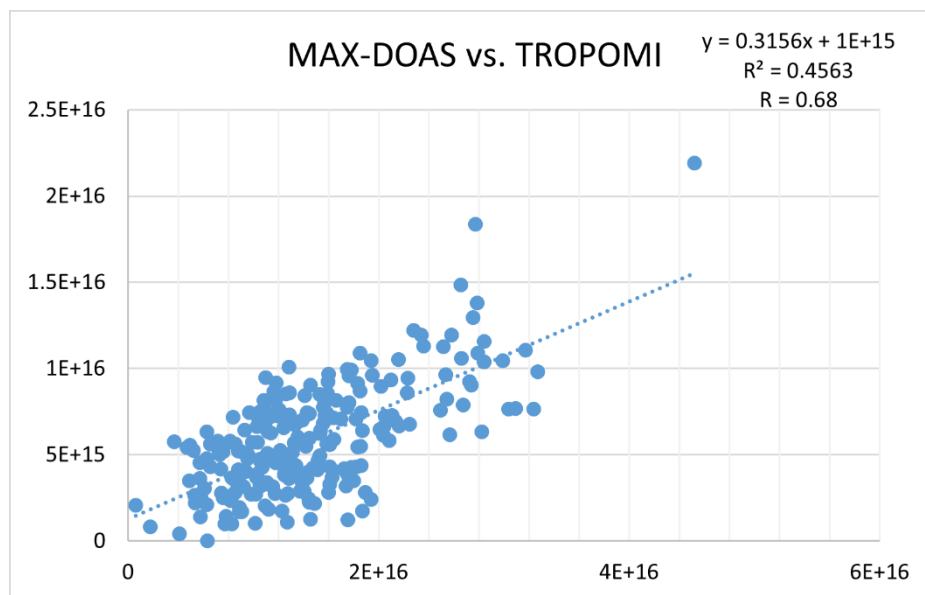


Figure 4.16: Correlation of HCHO VCDs of TROPOMI vs. MAX-DOAS 06:00 – 18:00 average over IESE, NUST.

The same data was examined using Pandora measurements (Figures 4.17 – 4.20). This also showed a similar trend as MAX-DOAS, with Pandora values also having a greater correlation with 12:00 – 14:00 values.

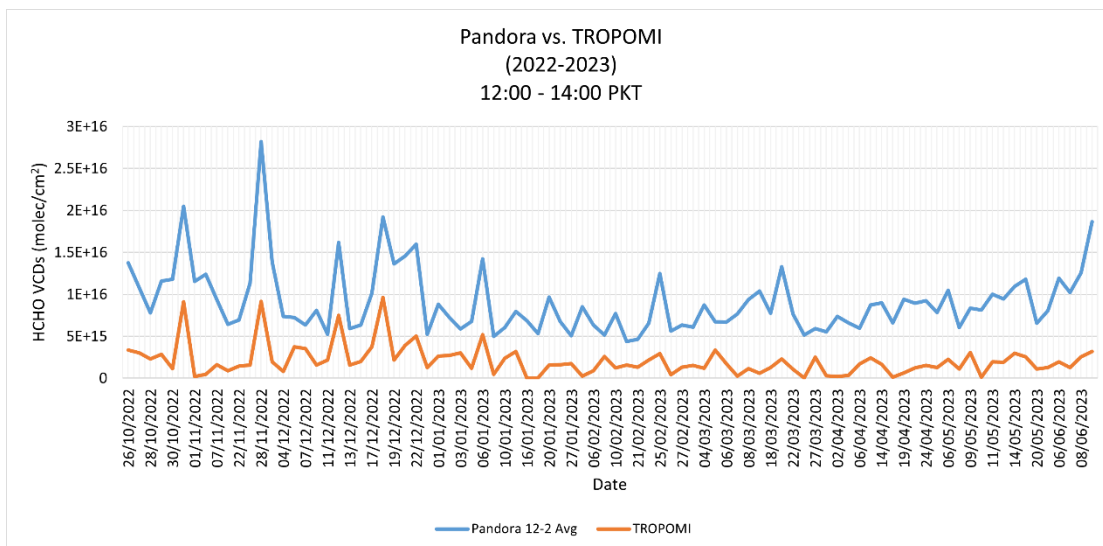


Figure 4.17: Validation of ground-based NASA Pandora Spectrometer 12:00 – 14:00 measurements with TROPOMI satellite measurements over IESE, NUST.

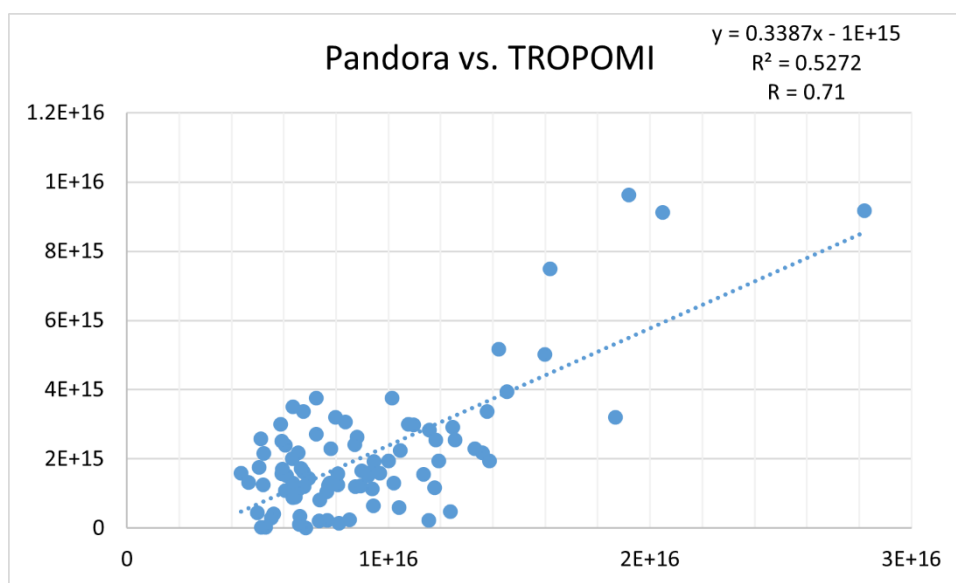


Figure 4.18: Correlation of HCHO VCDs of TROPOMI vs. Pandora 12:00 – 14:00 average over IESE, NUST.

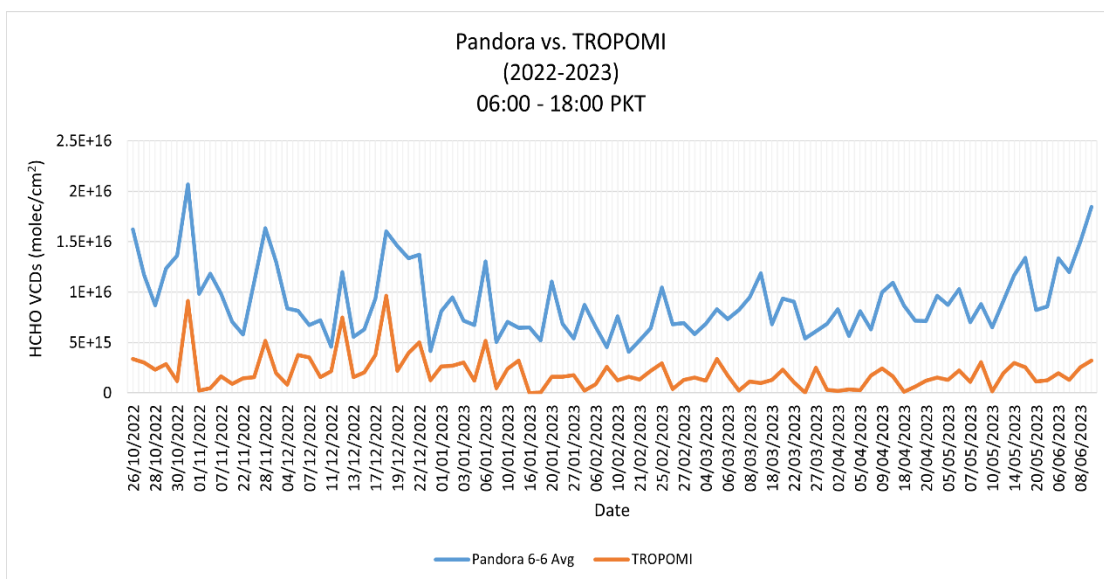


Figure 4.19: Validation of ground-based NASA Pandora Spectrometer 06:00 – 18:00 measurements with TROPOMI satellite measurements over IESE, NUST.

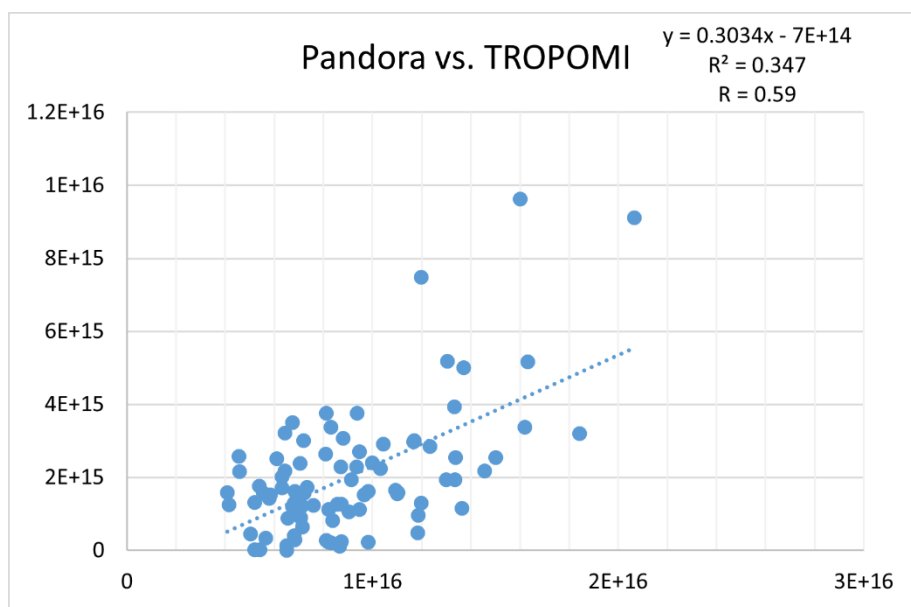


Figure 4.20: Correlation of HCHO VCDs of TROPOMI vs. Pandora 06:00 – 18:00 average over IESE, NUST.

4.3. Comparison of MAX-DOAS and NASA Pandora Spectrometer Measurements

To assess the difference in measurements by MAX-DOAS and Pandora, a comparison was made for the diurnal cycle of HCHO measured by both instruments. To ensure a valid comparison, MAX-DOAS observations were only taken for months from

October to June to match Pandora observations. Figure 4.21 shows that MAX-DOAS VCDs were higher than those measured by Pandora. One reason for this could be the significantly shorter study period for Pandora measurements as compared to MAX-DOAS. Additionally, the high vertical column densities of HCHO measured in 2016 also resulted in levels measured by MAX-DOAS being much higher than those measured by Pandora. As seen in Figure 4.22, when this year was excluded from the comparison, the values from both instruments were similar.

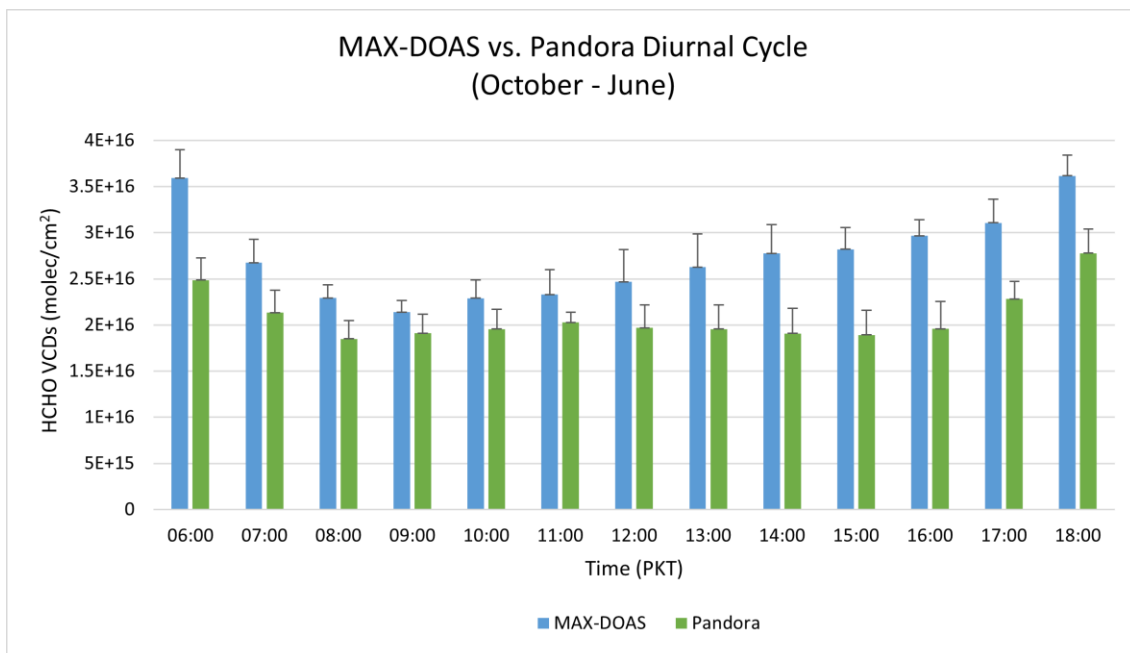


Figure 4.21: Comparison of MAX-DOAS and Pandora 06:00 – 18:00 average HCHO VCDs.

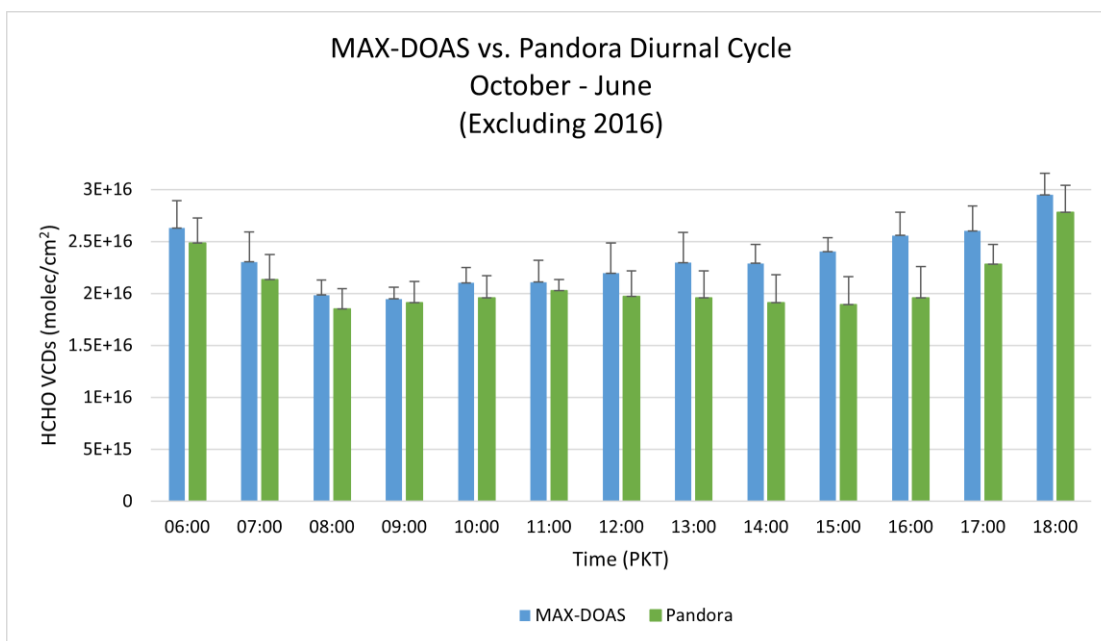


Figure 4.22: Comparison of MAX-DOAS and Pandora 06:00 – 18:00 average HCHO VCDs excluding the year 2016.

4.4. Influence of Meteorological Parameters

As established while reviewing literature, meteorological parameters have a notable influence on the production and removal of HCHO. For this reason, four main factors were analyzed in this study. These include temperature, global horizontal irradiance (GHI), relative humidity (RH), and wind speed.

4.4.1. Temperature

4.4.1.1. Diurnal cycle

Figure 4.23 shows the 24-hour cycle of temperature as observed in the study area from September 2015 till May 2023. It was observed that the temperature decreased after midnight, reaching a low at 06:00. It increased after sunrise, and then decreased again in the late evening hours.

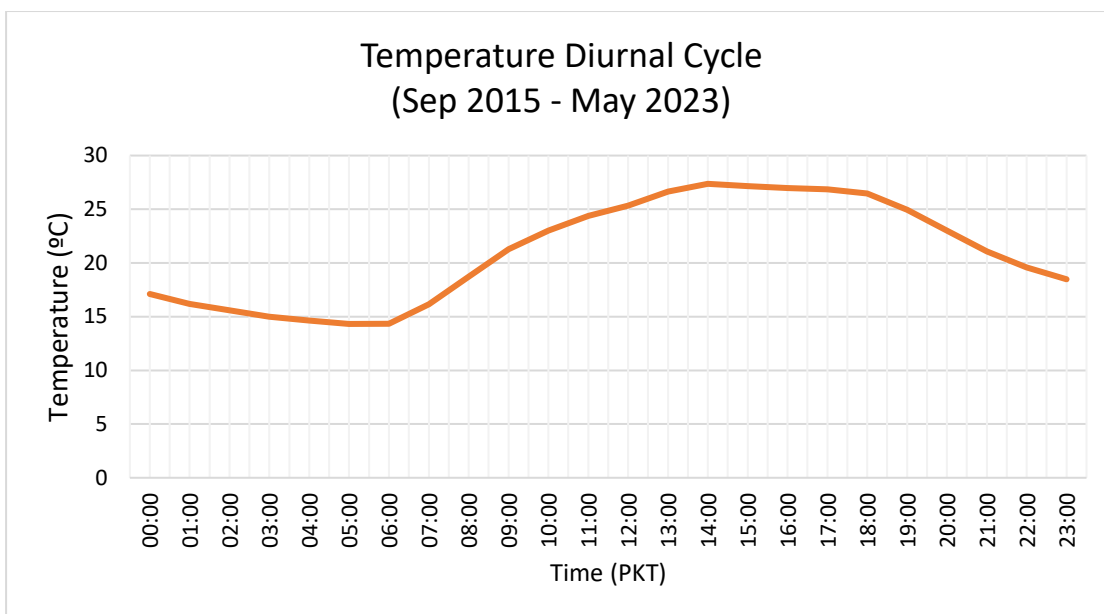


Figure 4.23: 24-hour temperature cycle over IESE, NUST.

As seen in Figure 4.24, temperature values align with MAX-DOAS HCHO VCDs, indicating a positive correlation. In the early morning hours, lower temperatures are observed which correspond with lower HCHO VCD values. However, as temperatures increase in the afternoon, VCD values do not increase significantly. This is because HCHO breaks down into other pollutants because of photolysis and other photochemical reactions (Freitas & Fornaro, 2022; Hoque et al., 2018). In the later hours of the day, solar intensity decreases while temperatures remain high, leading to increased production of HCHO. A maximum temperature of 26.7°C was recorded at 15:00.

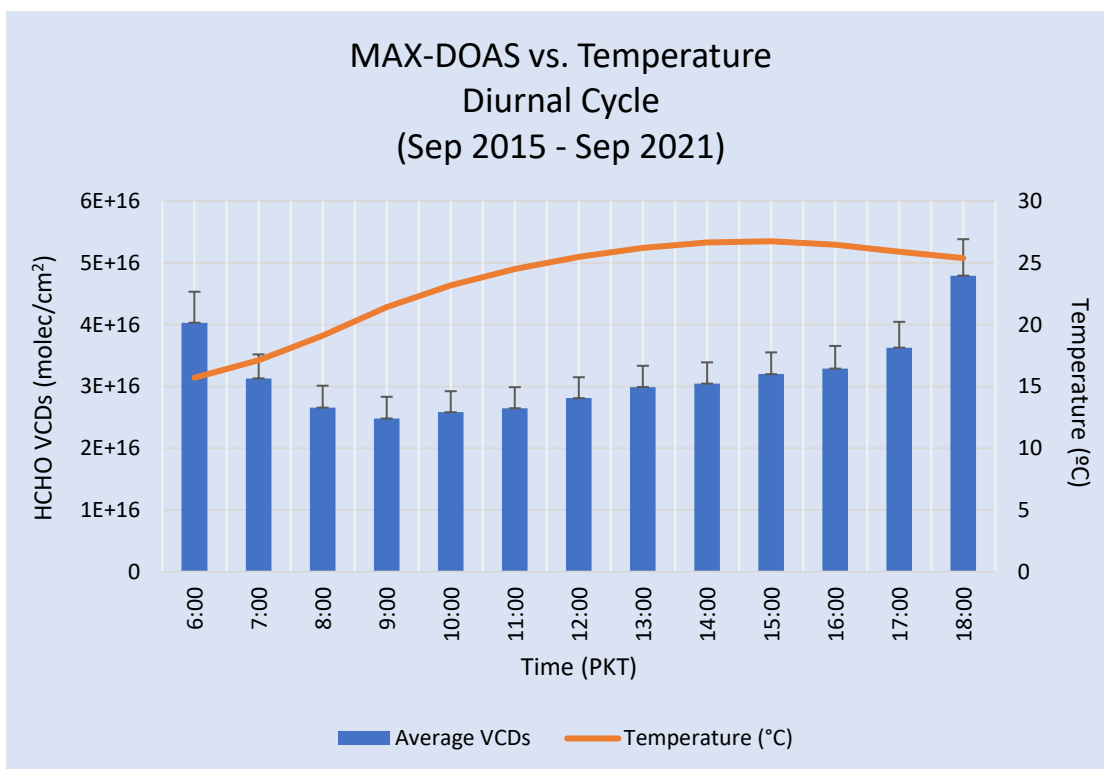


Figure 4.24: Comparison of temperature with the diurnal cycle of MAX-DOAS HCHO VCDs.

A similar trend is seen in Pandora measurements (Figure 4.25). A maximum temperature of 26.6°C was noted at 16:00.

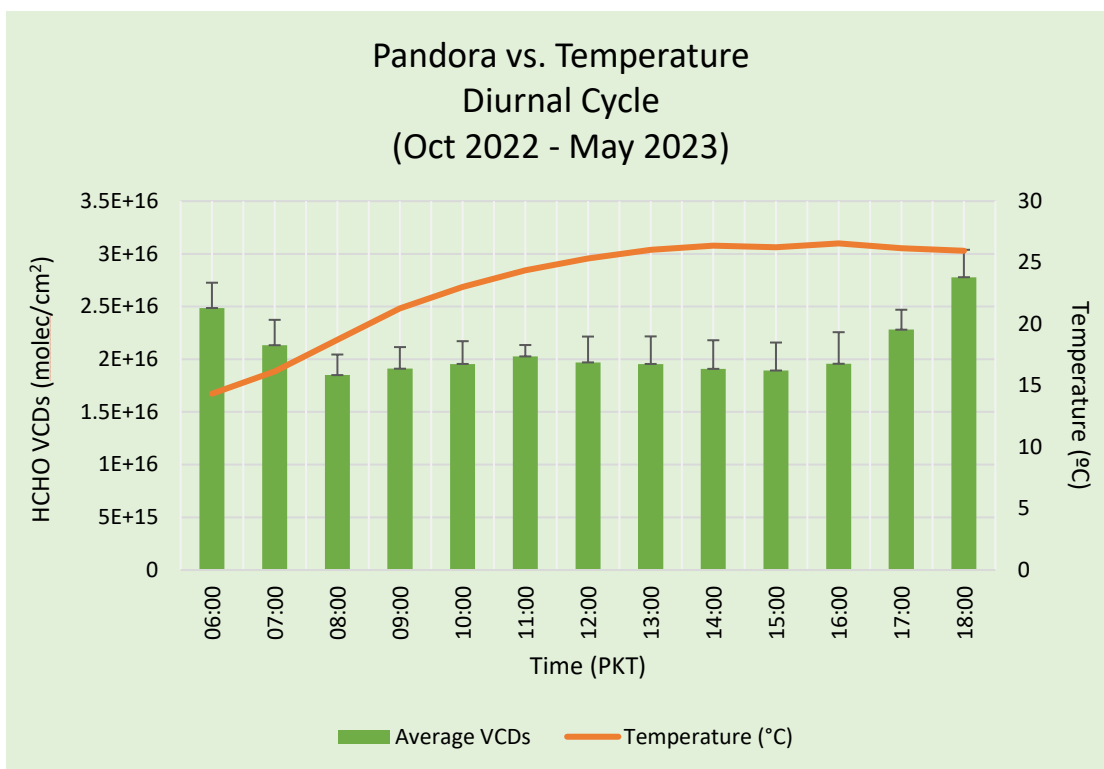


Figure 4.25: Comparison of temperature with the diurnal cycle of NASA Pandora Spectrometer HCHO VCDs

Upon further investigation, it was found that temperatures during the period when Pandora measurements were taken were much lower than those during the MAX-DOAS measurement period. While temperatures at 06:00 were 15.7°C for the MAX-DOAS period, they were 14.3°C for Pandora. This can explain the variation in HCHO VCD values between the two instruments as well.

4.4.1.2. Monthly cycle

When looking at temperature according to the months of the year, the decrease in VCDs in the month of April cannot be explained by ambient temperature (Figures 4.26 – 4.27). It can, however, be seen that the highest VCDs occurred in months with highest temperatures which indicates that biogenic emissions dominated during this period. Temperatures peaked in June for MAX-DOAS monitoring period, and May for Pandora monitoring period.

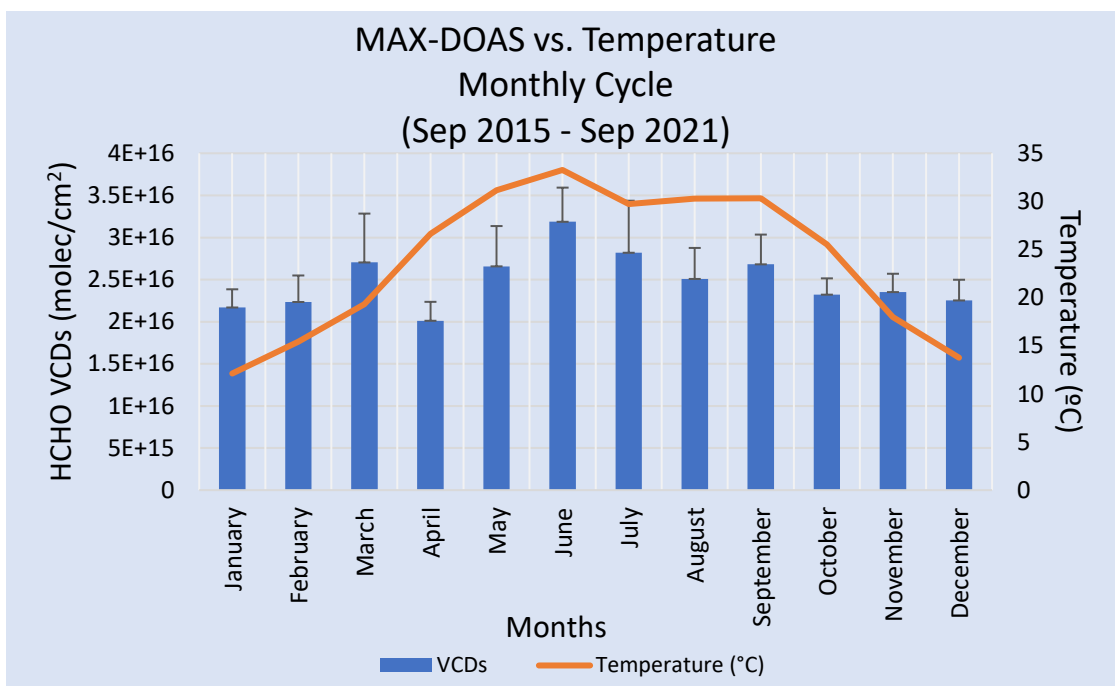


Figure 4.26: Comparison of temperature with the monthly cycle of MAX-DOAS HCHO VCDs.

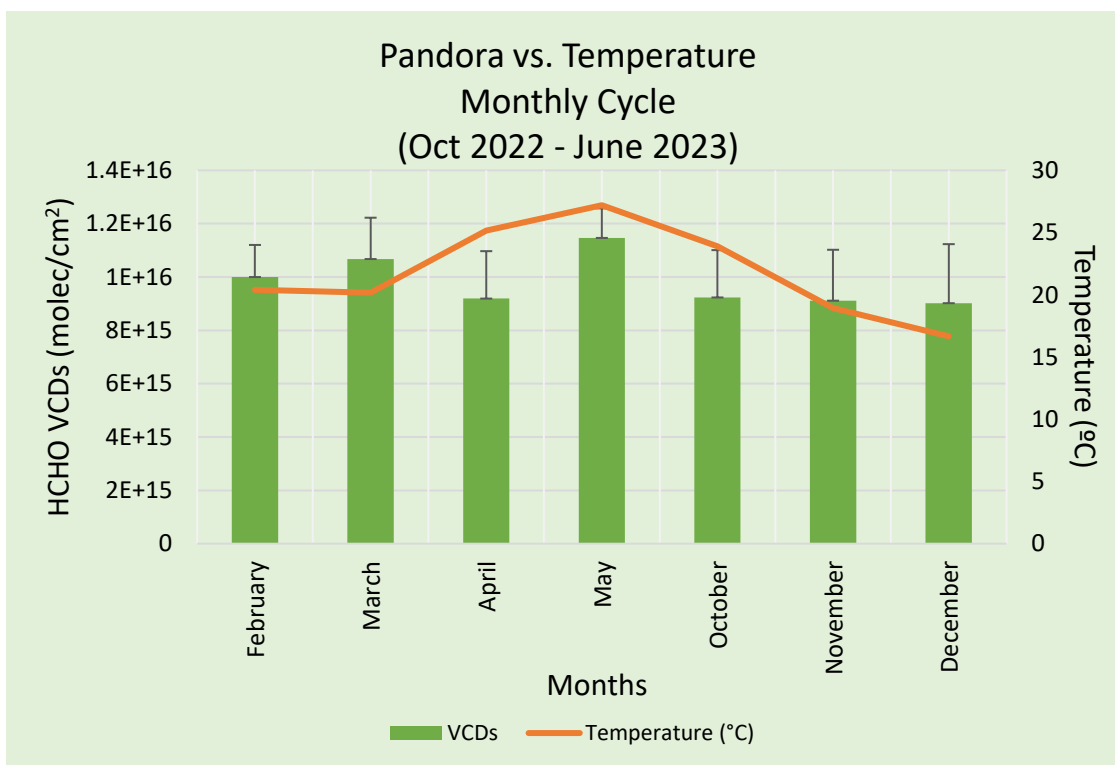


Figure 4.27: Comparison of temperature with the monthly cycle of NASA Pandora Spectrometer HCHO VCDs.

4.4.1.3. Yearly Cycle

When looking at the yearly cycle of MAX-DOAS VCDs in the context of temperature, it can be seen in Figure 4.28 that 2016 had the highest emissions whereas 2020 had the lowest. These values correspond with temperature, with 2016 having the highest average ambient temperature of 25.8°C compared to a low of 20.7°C in 2020. It can be concluded that due to COVID-19 and resultant lockdown situation in the country, there were minimum contribution of anthropogenic sources of HCHO in 2020.

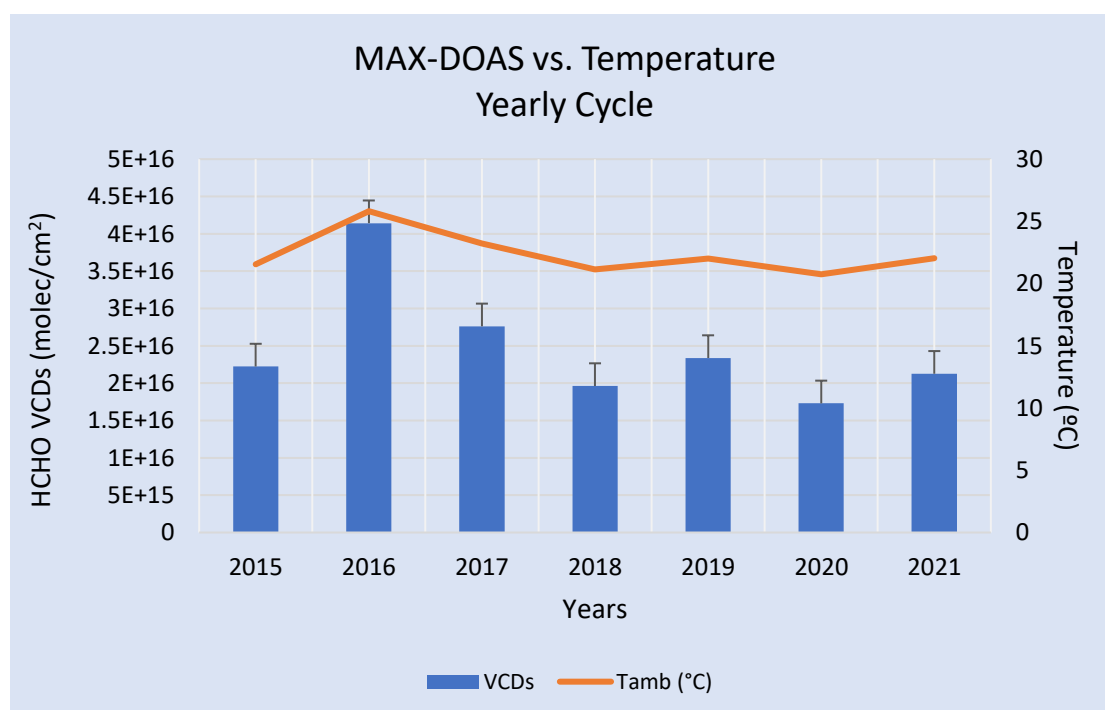


Figure 4.28: Comparison of temperature with the yearly cycle of MAX-DOAS HCHO VCDs.

4.4.2. Global Horizontal Irradiance (GHI)

GHI can be understood as the total solar radiation which reaches a horizontal surface on Earth. In other words, it measures the total solar energy received on a horizontal plane at a specific location (Khare et al., 2022). When looking at GHI in comparison to HCHO VCDs, an inverse relationship is observed. As GHI increases, HCHO levels decrease. This is due to increased photochemical reactions caused by intense solar radiation at higher GHI levels. It can be seen in Figures 4.29 and 4.30 that GHI is maximum during the afternoon, when the sun reaches its peak. Resultantly, a decrease

in HCHO concentrations can be observed as well.

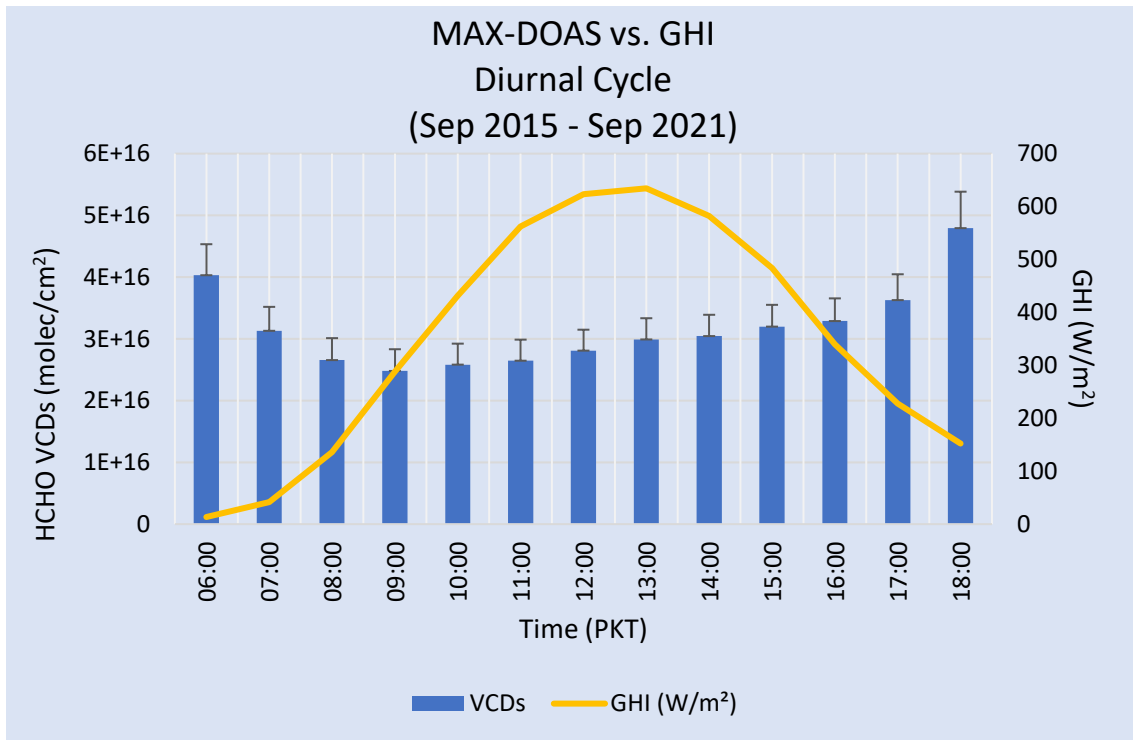


Figure 4.29: Comparison of GHI with the diurnal cycle of MAX-DOAS HCHO VCDs.

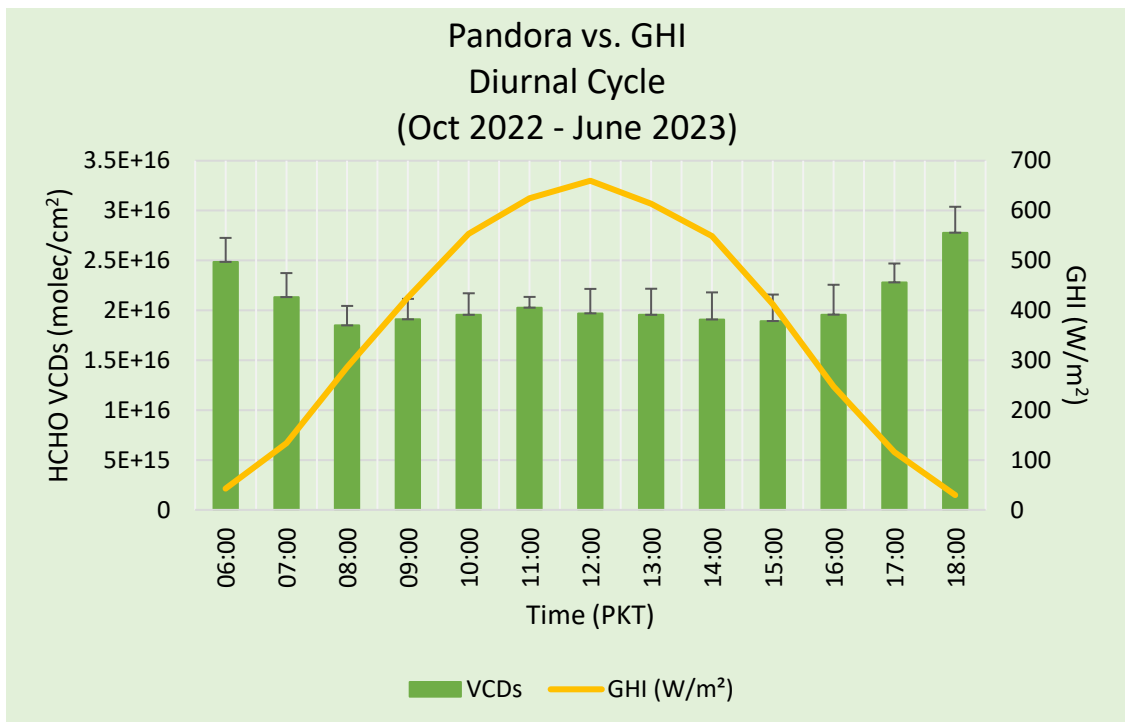


Figure 4.30: Comparison of GHI with the diurnal cycle of NASA Pandora Spectrometer HCHO VCDs.

The decrease in HCHO VCDs in the month of April can be explained by looking at the monthly cycle compared with GHI (Figures 4.31 and 4.32). A maximum GHI value of 571.4 W/m² and 452.0 W/m² was observed in April for MAX-DOAS and Pandora monitoring periods respectively, suggesting an increase in photochemical processes that led to the breakdown of HCHO in the atmosphere.

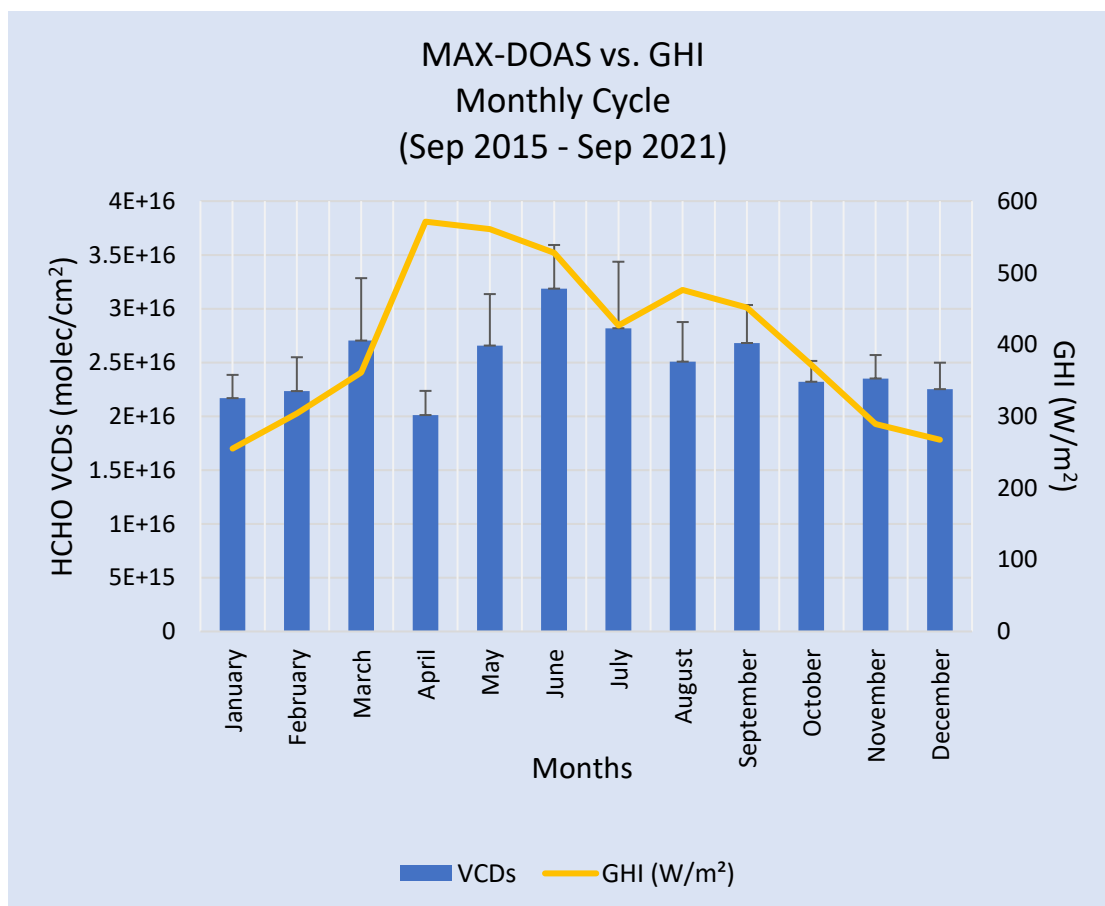


Figure 4.31: Comparison of GHI with the monthly cycle of MAX-DOAS HCHO VCDs.

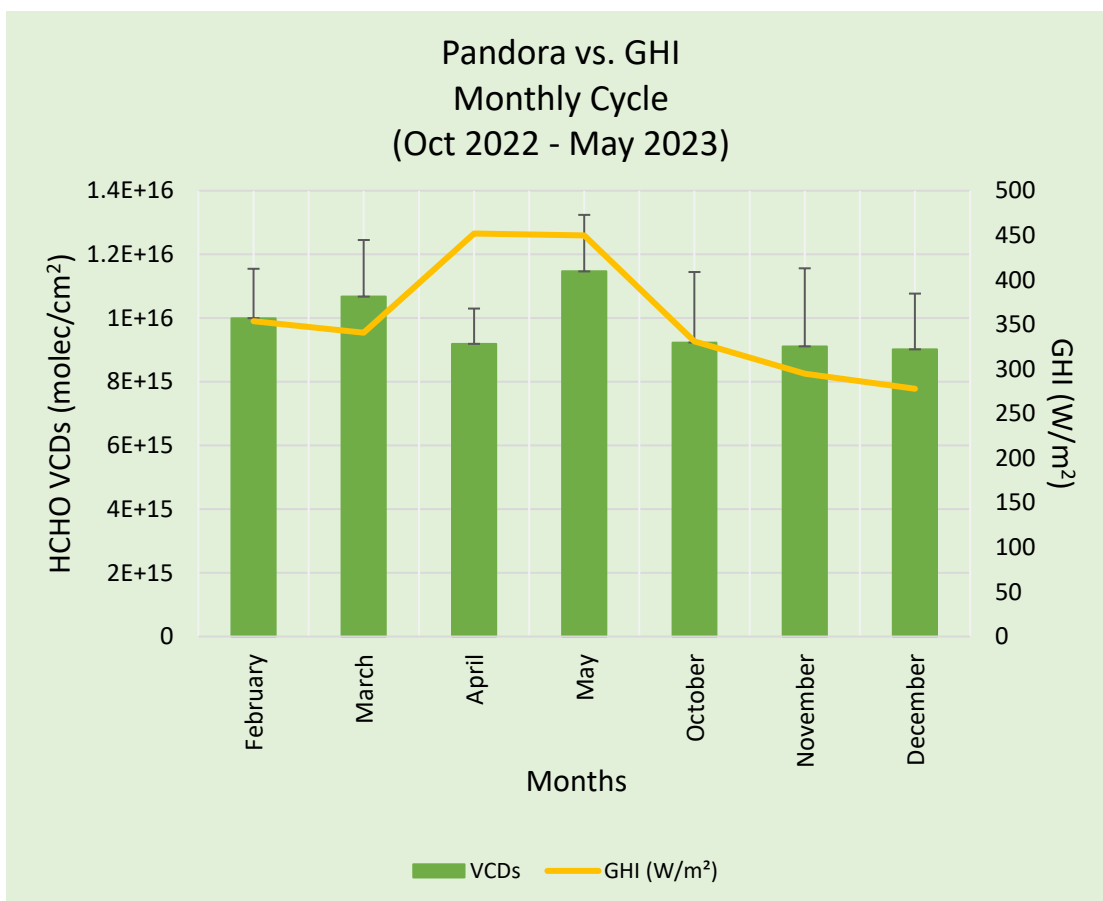


Figure 4.32: Comparison of GHI with the monthly cycle of Pandora HCHO VCDs.

4.4.3. Relative Humidity

As seen in Figure 4.33, relative humidity also had an inverse relationship with MAX-DOAS HCHO VCDs. Relative humidity is high during the early morning and decreases gradually over the course of the day. This is consistent with the findings of Khokhar et al. (2015), who found that there were lower HCHO concentrations during periods of high relative humidity. A maximum value of 71% relative humidity is observed at 06:00, with a low of 40% at 15:00. However, the 18:00 VCD value is much higher than that of 15:00. This is due to an increase in ambient temperature leading to higher biogenic emissions.

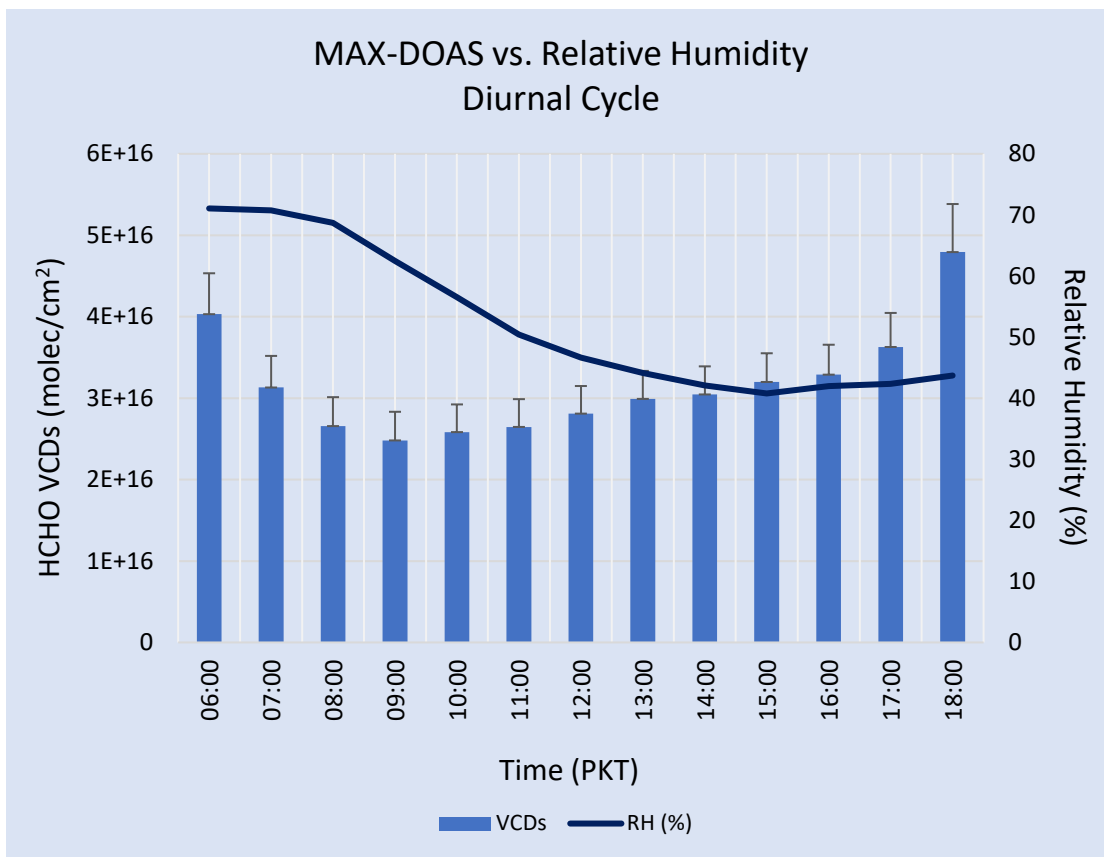


Figure 4.33: Comparison of RH with the diurnal cycle of MAX-DOAS HCHO VCDs.

Figure 4.34 shows a similar relative humidity trend with Pandora VCDs.

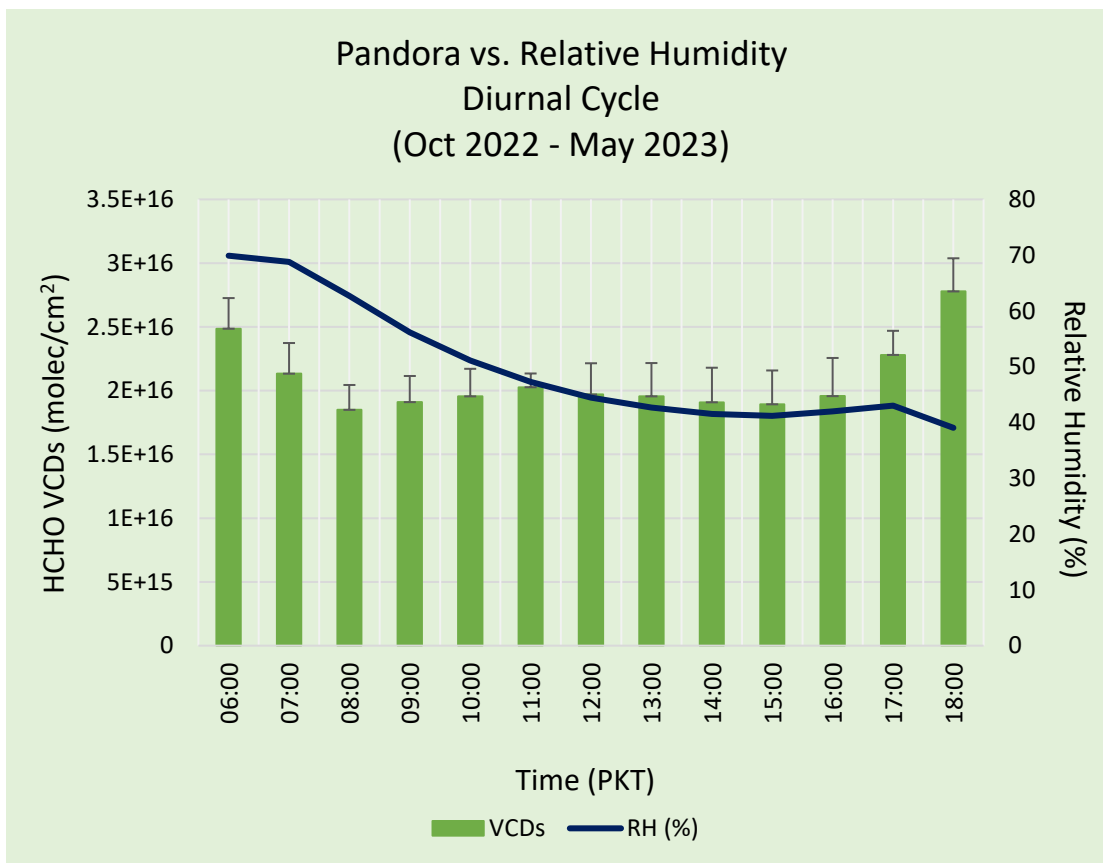


Figure 4.34: Comparison of RH with the diurnal cycle of NASA Pandora Spectrometer HCHO VCDs

4.3.4. Wind Speed

As there was a lack of information on the impact of wind speed on HCHO VCDs, this meteorological parameter was studied for this research. For MAX-DOAS measurements (Figure 4.35), a maximum wind speed of 2.85 m/s was observed for 15:00. For Pandora (Figure 4.36), the maximum was 2.75 m/s at 14:00. However, no clear relationship between HCHO VCDs and the speed of wind could be established.

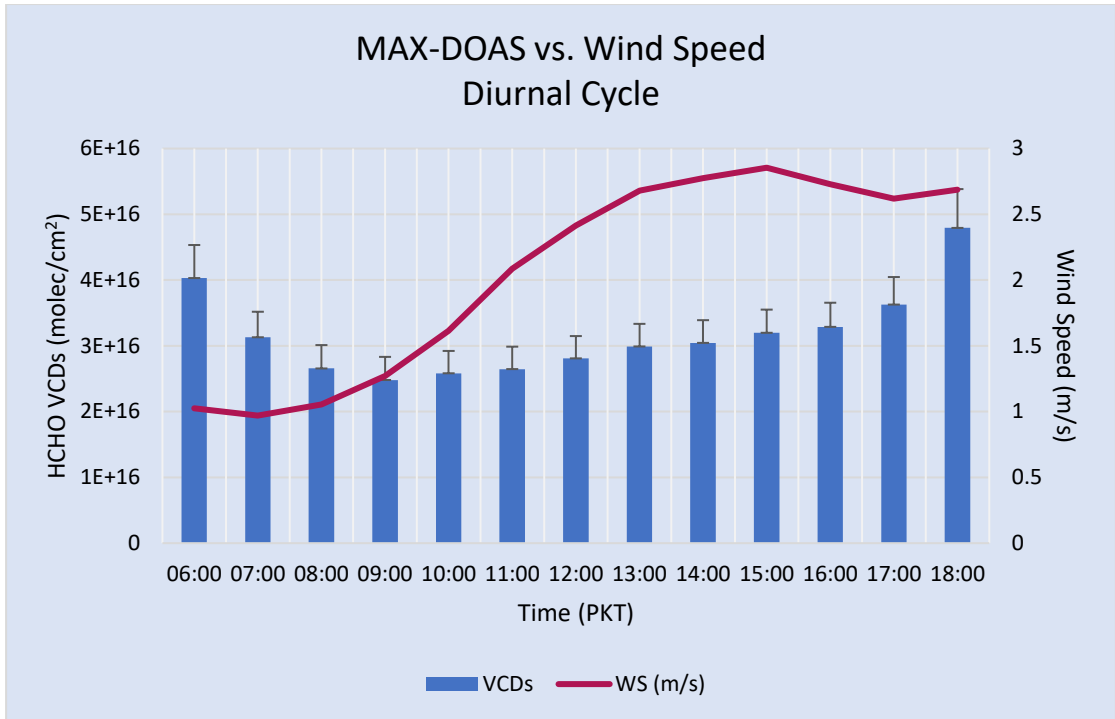


Figure 4.35: Comparison of wind speed with the diurnal cycle of MAX-DOAS HCHO VCDs.

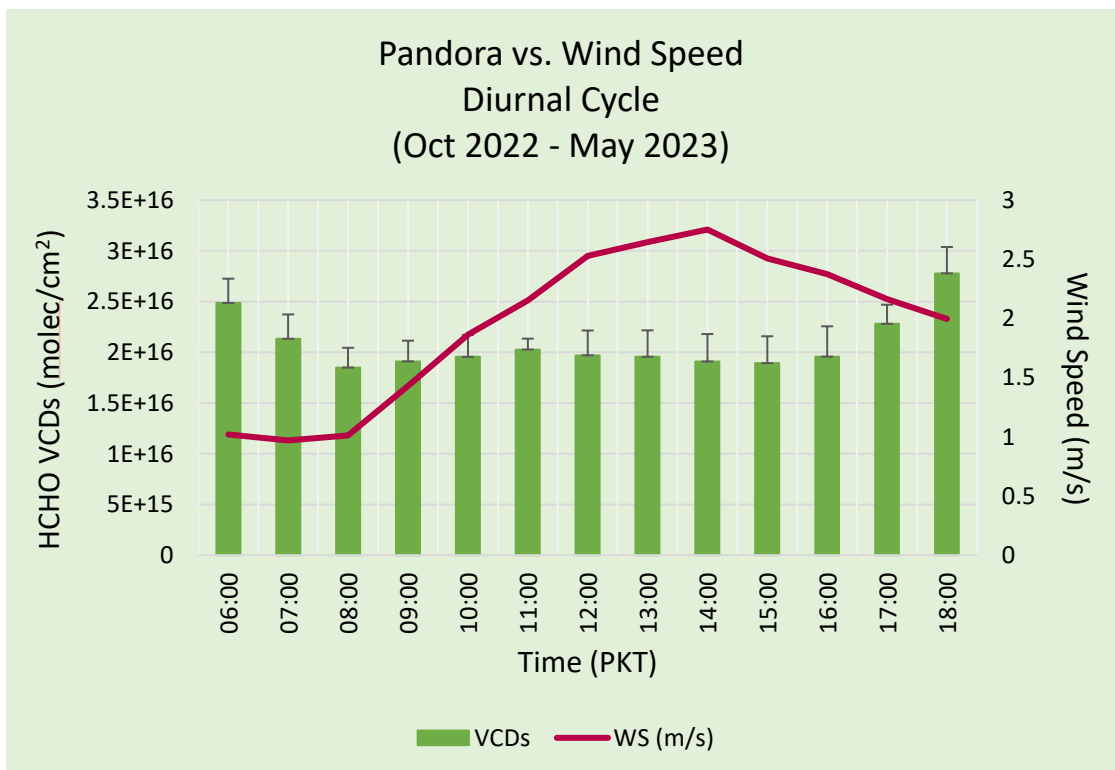


Figure 4.36: Comparison of wind speed with the diurnal cycle of NASA Pandora Spectrometer HCHO VCDs.

4.3.5. Meteorological Data Correlation Matrix

To better assess the relationship between different meteorological parameters and concentrations of HCHO, a correlation matrix was created using RStudio. The correlation matrix for MAX-DOAS and Pandora are shown in Figure 4.37. The correlation values for each parameter are also stated in Table 4.2 below.

Table 4.2: Correlation values for the studied meteorological parameters

Meteorological Parameter	Correlation value with MAX-DOAS HCHO VCDs	Correlation value with Pandora HCHO VCDs
Temperature	0.58	0.57
GHI	-0.43	-0.39
Wind Speed	0.02	0.01
Relative Humidity	-0.05	-0.08

Both MAX-DOAS and Pandora HCHO VCDs showed a strong positive correlation with temperature, a weak positive correlation with wind speed, a moderate negative correlation with GHI, and a weak negative correlation with relative humidity.

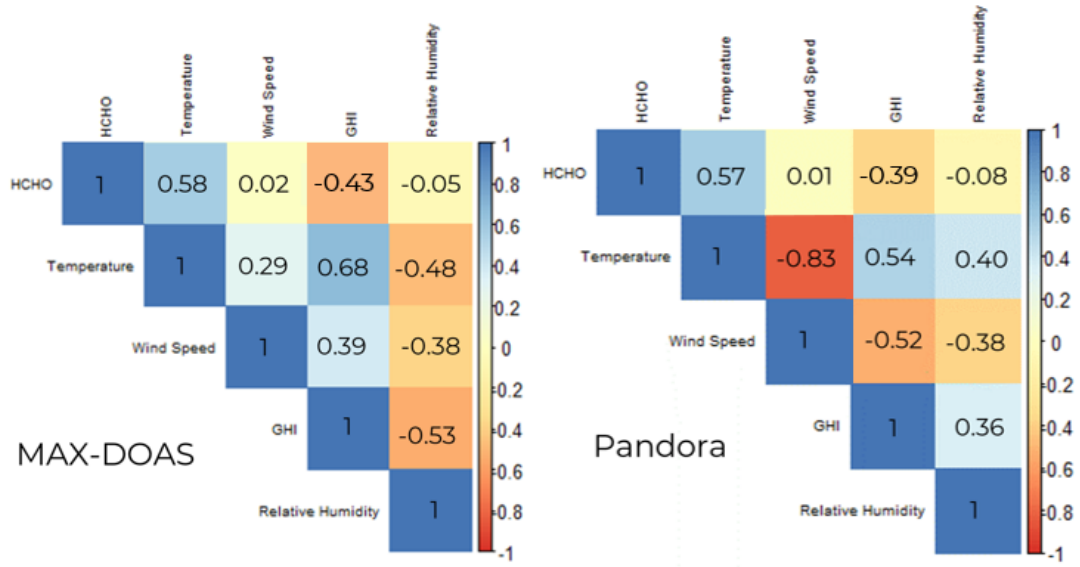


Figure 4.37: Correlation matrix for MAX-DOAS and Pandora HCHO VCDs and meteorological parameters

CHAPTER 5

CONCLUSIONS AND RECOMMENDATIONS

5.1. Conclusion

This study aimed to comprehensively investigate the temporal variation of HCHO levels in the urban environment of Islamabad, Pakistan, using ground-based MAX-DOAS and Pandora Spectrometer instruments in tandem with satellite observations from OMI and TROPOMI. Through the analysis of diurnal, seasonal, weekly, monthly, and yearly cycles, significant insights were gained in addition to the interplay between HCHO levels and the various meteorological parameters that influence them.

HCHO VCDs were found to be high during the early morning and evening hours due to background concentrations, low intensity of solar radiation, biogenic emissions, and oxidation of VOCs. During noon, photochemical reactions result in the removal of HCHO, causing levels to decline. Similarly, summer months exhibit higher HCHO levels due to increased temperature and resultant biogenic emissions, while winter months showed the lowest HCHO measurements due to low temperatures and solar radiation. Out of all four meteorological parameters assessed for this study, temperature had the greatest influence on HCHO VCD values, followed by GHI, relative humidity, and wind speed. This suggests that biogenic emissions of HCHO dominate over other sources in the IESE monitoring site.

Validation of ground-based instruments with satellite data showed an underestimation of HCHO concentrations by both OMI as well as with TROPOMI observations. However, TROPOMI proved to be slightly more in agreement with ground-based data as evident by higher correlation values for both MAX-DOAS as well as Pandora. However, a comparison of MAX-DOAS and Pandora Spectrometer showed that Pandora measured lower HCHO columns, which could be due to a shorter study period. This challenge limited the establishment of a clear rationale for the observed differences in measurements, which can be resolved through long-term analysis of HCHO using the NASA Pandora Spectrometer instrument.

In summary, this study contributes to the growing body of knowledge concerning

HCHO dynamics in an urban environment, emphasizing the need for further investigations into the synergistic relationships between HCHO and its sources. The findings underscore the importance of comprehensive monitoring approaches to capture the multifaceted nature of atmospheric trace gases and their interactions with other parameters. Ultimately, a deeper understanding of the temporal patterns of HCHO can inform air quality management strategies and provide insights into urban atmospheric chemistry.

5.2. Recommendations

Based on the findings of this study, the following recommendations are given to further improve HCHO monitoring studies:

1. Given the observed disparities between MAX-DOAS and Pandora Spectrometer measurements, it is recommended to conduct rigorous long-term intercomparison studies for these instruments.
2. Data collection should be continued for multiple years, ensuring complete coverage of all seasons. This would provide a more comprehensive dataset for future analysis and a more accurate representation of HCHO patterns.
3. The scope of this research can be extended by comparing these findings with other urban locations in Pakistan, as well as potentially with other countries that have similar climatic and urban characteristics. This would enable a broader understanding of HCHO behavior and help identify common trends and local anomalies.
4. Further investigation into the relationship between HCHO and meteorological parameters is recommended. There is currently a lack of data on the influence of wind speed on HCHO concentrations which needs to be explored.
5. Air quality modeling techniques can be used to simulate and predict HCHO concentrations under various scenarios, especially in the context of climate change for Pakistan. This could help forecast potential air quality challenges that could be faced in the foreseeable future, and support policy decisions.
6. The influence of urban design, such as road layout, green spaces, infrastructure, etc. on HCHO concentrations can be studied to understand how urban morphology influences the dispersion of trace gases. Examining the

impact of the urban heat island on HCHO could also provide insights for sustainable urban planning.

7. A long-term monitoring network needs to be established for continuous HCHO measurements across Pakistan. This would facilitate the monitoring of trends, enable early detection of pollution episodes, and help in the timely development of intervention measures.
8. Public awareness regarding the risks associated with elevated HCHO levels needs to be raised amongst local communities, authorities, and policymakers.
9. Relevant governmental and environmental agencies need to collaborate to develop and implement air quality management policies. This research can provide valuable insights for formulating effective strategies to mitigate the impact of HCHO emissions on public health and the environment.

REFERENCES

- Agency for Toxic Substances and Disease Registry. (2016, February 10). *Formaldehyde and your health*. Agency for Toxic Substances and Disease Registry. <https://www.atsdr.cdc.gov/formaldehyde/>
- Ali, A., Farhan, S. bin, Zhang, Y., Nasir, J., Farhan, H., Zamir, U. bin, & Gao, H. (2022). Changes in temporal pattern and spatial distribution of environmental pollutants in 8 Asian countries owing to COVID-19 pandemic. *Chemosphere*, 308. <https://doi.org/10.1016/j.chemosphere.2022.136075>
- Anjum, M. S., Ali, S. M., Imad-ud-din, M., Subhani, M. A., Anwar, M. N., Nizami, A.-S., Ashraf, U., & Khokhar, M. F. (2021). An Emerged Challenge of Air Pollution and Ever-Increasing Particulate Matter in Pakistan; A Critical Review. *Journal of Hazardous Materials*, 402, 123943. <https://doi.org/10.1016/j.jhazmat.2020.123943>
- Baruah, U. D., Robeson, S. M., Saikia, A., Mili, N., Sung, K., & Chand, P. (2022). Spatio-temporal characterization of tropospheric ozone and its precursor pollutants NO₂ and HCHO over South Asia. *Science of the Total Environment*, 809. <https://doi.org/10.1016/j.scitotenv.2021.151135>
- Bobrowski, N., & Filsinger, F. (2005). *Mini MAX-DOAS – an Introduction*. University of Heidelberg.
- Chen, C.-H., Chen, T.-F., Huang, S.-P., & Chang, K.-H. (2021). Comparison of the RADM2 and RACM chemical mechanisms in O₃ simulations: effect of the photolysis rate constant. *Scientific Reports*, 11(1). <https://doi.org/10.1038/s41598-021-84629-4>
- Climate & Clean Air Coalition. (2022). *Tropospheric ozone*. Tropospheric ozone | Climate & Clean Air Coalition. <https://www.ccacoalition.org/short-lived-climate-pollutants/tropospheric-ozone>

- de Smedt, I., Theys, N., Yu, H., Danckaert, T., Lerot, C., Compernelle, S., van Roozendael, M., Richter, A., Hilboll, A., Peters, E., Pedernana, M., Loyola, D., Beirle, S., Wagner, T., Eskes, H., van Geffen, J., Folkert Boersma, K., & Veefkind, P. (2018). Algorithm theoretical baseline for formaldehyde retrievals from S5P TROPOMI and from the QA4ECV project. *Atmospheric Measurement Techniques*, 11(4), 2395–2426. <https://doi.org/10.5194/amt-11-2395-2018>
- de Smedt, I., Pinardi, G., Vigouroux, C., Compernelle, S., Bais, A., Benavent, N., Boersma, F., Chan, K. L., Donner, S., Eichmann, K. U., Hedelt, P., Hendrick, F., Irie, H., Kumar, V., Lambert, J. C., Langerock, B., Lerot, C., Liu, C., Loyola, D., ... van Roozendael, M. (2021). Comparative assessment of TROPOMI and OMI formaldehyde observations and validation against MAX-DOAS network column measurements. *Atmospheric Chemistry and Physics*, 21(16), 12561–12593. <https://doi.org/10.5194/acp-21-12561-2021>
- Dufour, G., Wittrock, F., Camredon, M., Beekmann, M., Richter, A., Aumont, B., & Burrows, J. P. (2009). Atmospheric Chemistry and Physics SCIAMACHY formaldehyde observations: constraint for isoprene emission estimates over Europe? In *Atmos. Chem. Phys.* (Vol. 9). www.atmos-chem-phys.net/9/1647/2009/
- ESA. (2023). *Tropospheric Monitoring Instrument*. TROPOMI. <https://www.tropomi.eu/>
- Fan, J., Ju, T., Wang, Q., Gao, H., Huang, R., & Duan, J. (2021). Spatiotemporal variations and potential sources of tropospheric formaldehyde over eastern China based on OMI satellite data. *Atmospheric Pollution Research*, 12(1), 272–285. <https://doi.org/10.1016/j.apr.2020.09.011>
- Fan, J., Wang, T., Wang, Q., Ma, D., Li, Y., Zhou, M., & Wang, T. (2023). Assessment of HCHO in Beijing during 2009 to 2020 using satellite observation and numerical model: Spatial characteristic and impact factor. *Science of The*

- Freitas, A. D., & Fornaro, A. (2022). Atmospheric Formaldehyde Monitored by TROPOMI Satellite Instrument throughout 2020 over São Paulo State, Brazil. *Remote Sensing*, 14(13). <https://doi.org/10.3390/rs14133032>
- Gratsea, M., Vrekoussis, M., Richter, A., Wittrock, F., Schönhardt, A., Burrows, J., Kazadzis, S., Mihalopoulos, N., & Gerasopoulos, E. (2016). Slant column MAX-DOAS measurements of nitrogen dioxide, formaldehyde, glyoxal and oxygen dimer in the urban environment of Athens. *Atmospheric Environment*, 135, 118–131. <https://doi.org/10.1016/j.atmosenv.2016.03.048>
- Greenstone, M., & Fan, Q. (2019). (rep.). *Pakistan's Air Pollution Challenge & Potential for Longer Lives* (Ser. Air Quality Life Index). Chicago, Illinois.
- Guenther, A., Karl, T., Harley, P., Wiedinmyer, C., Palmer, P. I., & Geron, C. (2006). Estimates of global terrestrial isoprene emissions using MEGAN (Model of Emissions of Gases and Aerosols from Nature). *Atmospheric Chemistry and Physics*, 6(11), 3181–3210. <https://doi.org/10.5194/acp-6-3181-2006>
- Herman, J., Spinei, E., Fried, A., Kim, J., Kim, J., Kim, W., Cede, A., Abuhassan, N., & Segal-Rozenhaimer, M. (2018). NO₂ and HCHO measurements in Korea from 2012 to 2016 from Pandora spectrometer instruments compared with OMI retrievals and with aircraft measurements during the KORUS-AQ campaign. *Atmospheric Measurement Techniques*, 11(8), 4583–4603. <https://doi.org/10.5194/amt-11-4583-2018>
- Ho, K., Lee, S., & Tsai, W. (2006). Carbonyl compounds in the roadside environment of Hong Kong. *Journal of Hazardous Materials*, 133(1–3), 24–29. <https://doi.org/10.1016/j.jhazmat.2005.09.054>
- Hoque, H. M. S., Irie, H., & Damiani, A. (2018). First MAX-DOAS Observations of Formaldehyde and Glyoxal in Phimai, Thailand. *Journal of Geophysical*

Research: Atmospheres, 123(17), 9957–9975.
<https://doi.org/10.1029/2018JD028480>

Institute For Health Metrics and Evaluation. (2020). (rep.). *Air Pollution - Level 2 Risk* (Vol. 393, Ser. Disease, injury, and risk factsheets).

IQAir. (2023). *World's Most Polluted Countries*. IQAir.
<https://www.iqair.com/world-most-polluted-countries>

Kaiser, J., Jacob, D. J., Zhu, L., Travis, K. R., Fisher, J. A., González Abad, G., Zhang, L., Zhang, X., Fried, A., Crouse, J. D., Clair, J. M. S., & Wisthaler, A. (2018). High-resolution inversion of OMI formaldehyde columns to quantify isoprene emission on ecosystem-relevant scales: Application to the southeast US. *Atmospheric Chemistry and Physics, 18(8), 5483–5497.*
<https://doi.org/10.5194/acp-18-5483-2018>

Karim, I., & Rappenglück, B. (2023). Impact of Covid-19 lockdown regulations on PM_{2.5} and trace gases (NO₂, SO₂, CH₄, HCHO, C₂H₂O₂ and O₃) over Lahore, Pakistan. *Atmospheric Environment, 303.*
<https://doi.org/10.1016/j.atmosenv.2023.119746>

Khan, W. A., Khokhar, M. F., Shoaib, A., & Nawaz, R. (2018). Monitoring and analysis of formaldehyde columns over Rawalpindi-Islamabad, Pakistan using MAX-DOAS and satellite observation. *Atmospheric Pollution Research, 9(5), 840–848.* <https://doi.org/10.1016/j.apr.2017.12.008>

Khan, W., Sharif, F., Khokhar, M. F., Shahzad, L., Ehsan, N., & Jahanzaib, M. (2023). Monitoring of Ambient Air Quality Patterns and Assessment of Air Pollutants' Correlation and Effects on Ambient Air Quality of Lahore, Pakistan. *Atmosphere, 14(8), 1257–1257.*
<https://doi.org/10.3390/atmos14081257>

Khare, V., Khare, C., Nema, S., & Baredar, P. (2022). Chapter 8 - Case study: Solar–wind hybrid renewable energy system. In *Decision Science and Operations Management of Solar Energy Systems* (pp. 273–322). essay, Academic Press.

- Khokhar, M. F., Khalid, T., Yasmin, N., & de Smedt, I. (2015). Spatio-temporal analyses of formaldehyde over Pakistan by using SCIAMACHY and GOME-2 observations. *Aerosol and Air Quality Research*, *15*(5), 1760–1773. <https://doi.org/10.4209/aaqr.2014.12.0339>
- Liu, H., Liu, C., Xie, Z., Li, Y., Huang, X., Wang, S., Xu, J., & Xie, P. (2016). A paradox for air pollution controlling in China revealed by “Apec blue” and “Parade blue.” *Scientific Reports*, *6*(1), 1–13. <https://doi.org/10.1038/srep34408>
- Liu, T., Lin, Y., Chen, J., Chen, G., Yang, C., Xu, L., Li, M., Fan, X., Zhang, F., & Hong, Y. (2023). Pollution mechanisms and photochemical effects of atmospheric HCHO in a coastal city of southeast China. *Science of the Total Environment*, *859*. <https://doi.org/10.1016/j.scitotenv.2022.160210>
- Lok Chan, K., Wiegner, M., van Geffen, J., de Smedt, I., Alberti, C., Cheng, Z., Ye, S., & Wenig, M. (2020). MAX-DOAS measurements of tropospheric NO₂ and HCHO in Munich and the comparison to OMI and TROPOMI satellite observations. *Atmospheric Measurement Techniques*, *13*(8), 4499–4520. <https://doi.org/10.5194/amt-13-4499-2020>
- Lorente, A., Folkert Boersma, K., Yu, H., Dörner, S., Hilboll, A., Richter, A., Liu, M., Lamsal, L. N., Barkley, M., De Smedt, I., Van Roozendael, M., Wang, Y., Wagner, T., Beirle, S., Lin, J.-T., Krotkov, N., Stammes, P., Wang, P., Eskes, H. J., & Krol, M. (2017). Structural uncertainty in air mass factor calculation for NO₂ and HCHO satellite retrievals. *Atmospheric Measurement Techniques*, *10*(3), 759–782. <https://doi.org/10.5194/amt-10-759-2017>
- Mahmood, F., Khokhar, M. F., & Mahmood, Z. (2020). Examining the relationship of tropospheric ozone and climate change on crop productivity using the multivariate panel data techniques. *Journal of Environmental Management*, *272*, 111024. <https://doi.org/10.1016/j.jenvman.2020.111024>
- Marais, E. A., Jacob, D. J., Kurosu, T. P., Chance, K., Murphy, J. G., Reeves, C., Mills, G., Casadio, S., Millet, D. B., Barkley, M. P., Paulot, F., & Mao, J. (2012). Isoprene emissions in Africa inferred from OMI observations of

formaldehyde columns. *Atmospheric Chemistry and Physics*, 12(14), 6219–6235. <https://doi.org/10.5194/acp-12-6219-2012>

Millet, D. B., Jacob, D. J., Boersma, K. F., Fu, T. M., Kurosu, T. P., Chance, K., Heald, C. L., & Guenther, A. (2008). Spatial distribution of isoprene emissions from North America derived from formaldehyde column measurements by the OMI satellite sensor. *Journal of Geophysical Research Atmospheres*, 113(2). <https://doi.org/10.1029/2007JD008950>

NASA. (2021). *The aura mission*. NASA. <https://aura.gsfc.nasa.gov/omi.html>

NASA. (n.d.). *NASA pandora project*. NASA. <https://pandora.gsfc.nasa.gov/Instrument/>

National Research Council (US) Committee on Toxicology. (1980). Effects on Humans. In *Formaldehyde - An Assessment of Its Health Effects*. essay, National Academies Press (US).

Noreen, A., Khokhar, M. F., Zeb, N., Yasmin, N., & Hakeem, K. R. (2018). Spatio-temporal assessment and seasonal variation of tropospheric ozone in Pakistan during the last decade. *Environmental Science and Pollution Research*, 25(9), 8441–8454. <https://doi.org/10.1007/s11356-017-1010-2>

Nowlan, C. R., Liu, X., Janz, S. J., Kowalewski, M. G., Chance, K., Follette-Cook, M. B., Fried, A., González Abad, G., Herman, J. R., Judd, L. M., Kwon, H. A., Loughner, C. P., Pickering, K. E., Richter, D., Spinei, E., Walega, J., Weibring, P., & Weinheimer, A. J. (2018). Nitrogen dioxide and formaldehyde measurements from the GEOstationary Coastal and Air Pollution Events (GEOCAPE) Airborne Simulator over Houston, Texas. *Atmospheric Measurement Techniques*, 11(11), 5941–5964. <https://doi.org/10.5194/amt-11-5941-2018>

Pang, X., Mu, Y., Zhang, Y., Lee, X., & Yuan, J. (2009). Contribution of isoprene to formaldehyde and ozone formation based on its oxidation products measurement in Beijing, China. *Atmospheric Environment*, 43(13), 2142–2147. <https://doi.org/10.1016/j.atmosenv.2009.01.022>

- Park, J., Lee, H., Kim, J., Herman, J., & Kim, D. (2017). HCHO column density retrieval using Pandora measurements in Seoul, Korea: Temporal characteristics and comparison with OMI measurement. In *Geophysical Research Abstracts* (Vol. 19).
- Patel, G., Prudhvi, P. V. V. P., Patra, A., Pathak, S. S., Sonawane, A. D., & Shirkole, S. S. (2023). Different parameters affecting the efficiency of dryers. In S. M. Jafari & N. Malekjani (Eds.), *Drying Technology in Food Processing: Unit Operations and Processing Equipment in the Food Industry* (pp. 705–742). essay, Woodhead Publishing.
- Protano, C., Buomprisco, G., Cammalleri, V., Pocino, R. N., Marotta, D., Simonazzi, S., Cardoni, F., Petyx, M., Iavicoli, S., & Vitali, M. (2021). The carcinogenic effects of formaldehyde occupational exposure: A systematic review. *Cancers (Basel)*, *14*(1), 165. <https://doi.org/10.3390/cancers14010165>
- Rana, A. D., Parvez, S., Ul-Haq, Z., Batool, S. A., Chaudhary, M. N., Mahmood, K., & Tariq, S. (2019). Anthropogenic, biogenic and pyrogenic emission sources and atmospheric formaldehyde (HCHO) and nitrogen dioxide (NO₂) columns over different landuse/landcovers of South Asia. *Applied Ecology and Environmental Research*, *17*(5), 10989–11015. https://doi.org/10.15666/aeer/1705_1098911015
- Razi, M., Dörner, S., Donner, S., Ahmad, N., Khokhar, M. F., & Wagner, T. (2022). Study of the interrelationships between NO₂, SO₂, HCHO and CHOCHO vertical column densities derived by car MAX-DOAS observations in and around the megacity of Lahore, Pakistan. *EGU General Assembly 2022*. <https://doi.org/10.5194/egusphere-egu22-10254>
- Royal Belgian Institute for Space Aeronomy. (2010, December 9). *Slant Column and Vertical Column Densities. SCD vs. VCD*. <https://sacs.aeronomie.be/info/scdvcd.php>
- Ryan, R. G., Silver, J. D., Querel, R., Smale, D., Rhodes, S., Tully, M., Jones, N., & Schofield, R. (2020). Comparison of formaldehyde tropospheric columns in

- Australia and New Zealand using MAX-DOAS, FTIR and TROPOMI. *Atmospheric Measurement Techniques*, 13(12), 6501–6519. <https://doi.org/10.5194/amt-13-6501-2020>
- Ryan, R. G., Marais, E. A., Gershenson-Smith, E., Ramsay, R., Muller, J.-P., Tirpitz, J.-L., & Frieß, U. (2023). Measurement report: MAX-DOAS measurements characterise Central London ozone pollution episodes during 2022 heatwaves. *Atmospheric Chemistry and Physics*, 23(12), 7121–7139. <https://doi.org/10.5194/acp-23-7121-2023>
- Seinfeld, J. H., & Pandis, S. N. (2016). *Atmospheric Chemistry and physics: From air pollution to climate change*. John Wiley & Sons.
- Shoib, A., Khokhar, M. F., & Sandhu, O. (2020). Investigating the temporal variation of formaldehyde using MAX-DOAS and satellite observations over Islamabad, Pakistan. *Atmospheric Pollution Research*, 11(1), 193–204. <https://doi.org/10.1016/j.apr.2019.10.008>
- Spinei, E., Whitehill, A., Fried, A., Tiefengraber, M., Herman, J. R., Knepp, T. N., Herndon, S., Müller, M., Abuhassan, N., Cede, A., Richter, D., Walega, J., Crawford, J., Szykman, J., Valin, L., Williams, D. J., Long, R., Swap, R. J., Lee, Y., ... Poche, B. (2018). The First Evaluation of Formaldehyde Column Observations by Pandora Spectrometers during the KORUS-AQ Field Study The first evaluation of formaldehyde column observations by improved Pandora spectrometers during the KORUS-AQ field study. *Atmos. Meas. Tech*, 11, 4943–4961. <https://doi.org/10.5194/amt-2018-57>
- Stavroukou, T., Müller, J. F., Bauwens, M., de Smedt, I., van Roozendaal, M., & Guenther, A. (2018). Impact of Short-Term Climate Variability on Volatile Organic Compounds Emissions Assessed Using OMI Satellite Formaldehyde Observations. *Geophysical Research Letters*, 45(16), 8681–8689. <https://doi.org/10.1029/2018GL078676>
- Sun, W., Zhu, L., de Smedt, I., Bai, B., Pu, D., Chen, Y., Shu, L., Wang, D., Fu, T. M., Wang, X., & Yang, X. (2021). Global Significant Changes in Formaldehyde

- (HCHO) Columns Observed from Space at the Early Stage of the COVID-19 Pandemic. In *Geophysical Research Letters* (Vol. 48, Issue 4). Blackwell Publishing Ltd. <https://doi.org/10.1029/2020GL091265>
- Tian, X., Xie, P., Xu, J., Wang, Y., Li, A., Wu, F., Hu, Z., Liu, C., & Zhang, Q. (2019). Ground-based MAX-DOAS observations of tropospheric formaldehyde VCDs and comparisons with the CAMS model at a rural site near Beijing during APEC 2014. *Atmospheric Chemistry and Physics*, 19(5), 3375–3393. <https://doi.org/10.5194/acp-19-3375-2019>
- TURI. (2022, January 14). *Health and Environment*. Toxic Use Reduction Institute. https://www.turi.org/TURI_Publications/TURI_Chemical_Fact_Sheets/Formaldehyde_Fact_Sheet/Formaldehyde_Facts/Health_and_Environment
- UNEP (2019, May 9). *Air pollution hurts the poorest most*. UN Environment Program. Retrieved July 29, 2023, from <https://www.unep.org/news-and-stories/story/air-pollution-hurts-poorest-most>
- US EPA. (2022, January 5). *Initial List of Hazardous Air Pollutants with Modifications*. EPA. <https://www.epa.gov/haps/initial-list-hazardous-air-pollutants-modifications>
- Vigouroux, C., Langerock, B., Augusto Bauer Aquino, C., Blumenstock, T., Cheng, Z., de Mazière, M., de Smedt, I., Grutter, M., Hannigan, J. W., Jones, N., Kivi, R., Loyola, Di., Lutsch, E., Mahieu, E., Makarova, M., Metzger, J. M., Morino, I., Murata, I., Nagahama, T., ... Winkler, H. (2020). TROPOMI-Sentinel-5 Precursor formaldehyde validation using an extensive network of ground-based Fourier-transform infrared stations. *Atmospheric Measurement Techniques*, 13(7), 3751–3767. <https://doi.org/10.5194/amt-13-3751-2020>
- Veefkind, J. P., de Haan, J. F., Brinksma, E. J., Kroon, M., & Levelt, P. F. (2006). Total ozone from the Ozone Monitoring Instrument (OMI) using the DOAS technique. *IEEE Transactions on Geoscience and Remote Sensing*, 44(5), 1239–1244. <https://doi.org/10.1109/tgrs.2006.871204>

- Wang, C., Huang, X. F., Han, Y., Zhu, B., & He, L. Y. (2017). Sources and Potential Photochemical Roles of Formaldehyde in an Urban Atmosphere in South China. *Journal of Geophysical Research: Atmospheres*, 122(21), 11,934-11,947. <https://doi.org/10.1002/2017JD027266>
- World Bank. (2021). *Pakistan*. Climate Change Knowledge Portal. <https://climateknowledgeportal.worldbank.org/country/pakistan/climate-data-historical>
- World Bank. (2022). (rep.). *The Global Health Cost of PM2.5 Air Pollution: A Case for Action Beyond 2021*. World Bank.
- Wu, X., Xiao, Q., Wen, J., You, D., & Hueni, A. (2019). Advances in quantitative remote sensing product validation: Overview and current status. *Earth-Science Reviews*, 196, 102875. <https://doi.org/10.1016/j.earscirev.2019.102875>
- Wypych, G. (Ed.). (2015). *Handbook of UV Degradation and Stabilization*. ChemTec Publishing.
- Zanis, P., Monks, P. S., Schuepbach, E., & Penkett, S. A. (2000). The Role of In Situ Photochemistry in the Control of Ozone during Spring at the Jungfraujoeh (3,580 m asl) – Comparison of Model Results with Measurements. *Journal of Atmospheric Chemistry*, 37(1), 1–27. <https://doi.org/10.1023/a:1006349926926>
- Zeb, N., Khokhar, M. F., Pozzer, A., & Khan, S. A. (2019). Exploring the temporal trends and seasonal behaviour of tropospheric trace gases over Pakistan by exploiting satellite observations. *Atmospheric Environment*, 198, 279–290. <https://doi.org/10.1016/j.atmosenv.2018.10.053>
- Zhang, S., Wang, S., Zhang, R., Guo, Y., Yan, Y., Ding, Z., & Zhou, B. (2021). Investigating the Sources of Formaldehyde and Corresponding Photochemical Indications at a Suburb Site in Shanghai from MAX-DOAS Measurements. *Journal of Geophysical Research: Atmospheres*, 126(6). <https://doi.org/10.1029/2020JD033351>

- Zhang, Y., Li, R., Min, Q., Bo, H., Fu, Y., Wang, Y., & Gao, Z. (2019). The Controlling Factors of Atmospheric Formaldehyde (HCHO) in Amazon as Seen from Satellite. *Earth and Space Science*, 6(6), 959–971. <https://doi.org/10.1029/2019EA000627>
- Zhang, Y., Ju, T., Shi, Y., Wang, Q., Li, F., & Zhang, G. (2021). *Analysis of spatiotemporal variation of formaldehyde column concentration in Qinghai-Tibet Plateau and its influencing factors*. <https://doi.org/10.1007/s11356-021-14719-3/Published>
- Zhang, C., Li, J., Zhao, W., Yao, Q., Wang, H., & Wang, B. (2022). Open biomass burning emissions and their contribution to ambient formaldehyde in Guangdong province, China. *Science of the Total Environment*, 838. <https://doi.org/10.1016/j.scitotenv.2022.155904>
- Zhu, L., Jacob, D. J., Keutsch, F. N., Mickley, L. J., Scheffe, R., Strum, M., González Abad, G., Chance, K., Yang, K., Rappenglück, B., Millet, D. B., Baasandorj, M., Jaeglé, L., & Shah, V. (2017). Formaldehyde (HCHO) as a hazardous air pollutant: Mapping surface air concentrations from satellite and inferring cancer risks in the United States. *Environmental Science & Technology*, 51(10), 5650–5657. <https://doi.org/10.1021/acs.est.7b01356>

Abeer

by Dr. Usman Ahmad

Submission date: 05-Oct-2023 01:49PM (UTC+0500)

Submission ID: 2186305598

File name: 172_Dr._Usman_Ahmad_Abeer_80_1863535573.docx (6.35M)

Word count: 13902

Character count: 77592

Abeer

ORIGINALITY REPORT

10%

SIMILARITY INDEX

8%

INTERNET SOURCES

5%

PUBLICATIONS

4%

STUDENT PAPERS

PRIMARY SOURCES

1	Submitted to Higher Education Commission Pakistan Student Paper	2%
2	www.hedensted.dk Internet Source	1%
3	Ahmad Iqbal, Naveed Ahmad, Hassan Mohyud Din, Michel Van Roozendaal et al. "Retrieval of NO ₂ Columns by Exploiting MAX-DOAS Observations and Comparison with OMI and TROPOMI Data during the Time Period of 2015–2019", Aerosol and Air Quality Research, 2022 Publication	1%
4	archiv.ub.uni-heidelberg.de Internet Source	1%
5	etd.aau.edu.et Internet Source	<1%
6	Submitted to Eastlake High School Student Paper	<1%
7	hdl.handle.net	

Internet Source

<1 %

8

www.coursehero.com

Internet Source

<1 %

9

acp.copernicus.org

Internet Source

<1 %

10

etheses.bham.ac.uk

Internet Source

<1 %

11

gcris.iyte.edu.tr

Internet Source

<1 %

12

www.researchgate.net

Internet Source

<1 %

13

Arthur Philip Cracknell, Costas Varotsos.
"Remote Sensing and Atmospheric Ozone",
Springer Science and Business Media LLC,
2012

Publication

<1 %

14

eprints.usm.my

Internet Source

<1 %

15

Muhammad Shehzaib Anjum, Syeda Mahnoor Ali, Muhammad Imad-ud-din, Muhammad Ahmed Subhani et al. "An Emerged Challenge of Air Pollution and Ever-Increasing Particulate Matter in Pakistan; A Critical Review", Journal of Hazardous Materials, 2021

<1 %

16 aiep.pl <1 %
Internet Source

17 A. J. M. PETERS, K. F. BOERSMA, M. KROON, J. C. HAINS ET AL. "The Cabauw Intercomparison campaign for Nitrogen Dioxide measuring Instruments (CINDI): design, execution, and early results", Copernicus GmbH, 2011 <1 %
Publication

18 Submitted to University of Edinburgh <1 %
Student Paper

19 Maria Mathisen, Tor A Strand, Biswa N Sharma, Ram K Chandyo et al. "RNA viruses in community-acquired childhood pneumonia in semi-urban Nepal; a cross-sectional study", BMC Medicine, 2009 <1 %
Publication

20 Qianqian Hong, Cheng Liu, Ka Lok Chan, Qihou Hu, Zhouqing Xie, Haoran Liu, Fuqi Si, Jianguo Liu. "Ship-based MAX-DOAS measurements of tropospheric NO₂, SO₂, and HCHO distribution along the Yangtze River", Atmospheric Chemistry and Physics, 2018 <1 %
Publication

21 www.gov.uk <1 %
Internet Source

22 Submitted to The Hong Kong Polytechnic University
Student Paper <1 %

23 Submitted to University of Baghdad
Student Paper <1 %

24 repositorio.ufmg.br
Internet Source <1 %

25 unesdoc.unesco.org
Internet Source <1 %

26 repository.sustech.edu
Internet Source <1 %

27 digital.library.unt.edu
Internet Source <1 %

28 eo4society.esa.int
Internet Source <1 %

29 oarep.usim.edu.my
Internet Source <1 %

30 www.arb.ca.gov
Internet Source <1 %

31 www.mdpi.com
Internet Source <1 %

32 www.scielo.br
Internet Source <1 %

33 mymedr.afpm.org.my

<1 %

34

Ruijun Dang, Daniel J. Jacob, Viral Shah, Sebastian D. Eastham et al. " Background nitrogen dioxide (NO₂) over the United States and its implications for satellite observations and trends: effects of nitrate photolysis, aircraft, and open fires ", Atmospheric Chemistry and Physics, 2023

Publication

<1 %

35

icacgp-igac2018.org

Internet Source

<1 %

36

link.springer.com

Internet Source

<1 %

37

mettisglobal.news

Internet Source

<1 %

38

worldwidescience.org

Internet Source

<1 %

39

www.atmos-chem-phys.net

Internet Source

<1 %

40

www.ncbi.nlm.nih.gov

Internet Source

<1 %

41

Bao Chuong. "Measurements of the kinetics of the OH-initiated oxidation of methyl vinyl ketone and methacrolein", International Journal of Chemical Kinetics, 2004

<1 %

42

Submitted to University of Exeter

Student Paper

<1 %

43

digitalarchive.boun.edu.tr

Internet Source

<1 %

44

dspace.unza.zm

Internet Source

<1 %

45

erepository.uonbi.ac.ke

Internet Source

<1 %

46

www.bchydro.com

Internet Source

<1 %

47

"Sensors Set", Wiley, 1995

Publication

<1 %

48

Emeka A. Ugboma, Iwona S. Stachlewska, Philipp Schneider, Kerstin Stebel. "Satellite observations showed a negligible reduction in NO₂ pollution due to COVID-19 lockdown over Poland", Frontiers in Environmental Science, 2023

Publication

<1 %

49

Submitted to GRIPS National Graduate Institute for Policy Studies

Student Paper

<1 %

50

Paolo Pettinari, Antonio Donateo, Enzo Papandrea, Daniele Bortoli, Gianluca Pappaccogli, Elisa Castelli. "Analysis of NO₂

<1 %

and O3 Total Columns from DOAS Zenith-Sky Measurements in South Italy", Remote Sensing, 2022

Publication

51

cmascenter.org

Internet Source

<1 %

52

digital.maag.ysu.edu:8080

Internet Source

<1 %

53

eos.org

Internet Source

<1 %

54

univendspace.univen.ac.za

Internet Source

<1 %

55

Data Assimilation for Atmospheric Oceanic and Hydrologic Applications (Vol II), 2013.

Publication

<1 %

56

William Lahoz. "Research Satellites", Data Assimilation, 2010

Publication

<1 %

57

d-nb.info

Internet Source

<1 %

58

d-scholarship.pitt.edu

Internet Source

<1 %

59

doi.org

Internet Source

<1 %

60

pr.hec.gov.pk

Internet Source

<1 %

61

www.apsi.tech

Internet Source

<1 %

62

www.bfs.de

Internet Source

<1 %

63

www.eafit.edu.co

Internet Source

<1 %

64

www.globalcarbonproject.org

Internet Source

<1 %

65

www.repositorio.ieo.es

Internet Source

<1 %

66

www.science.gov

Internet Source

<1 %

67

www.yumpu.com

Internet Source

<1 %

68

Jake P. Rowe, Kyle J. Zarzana, Natalie Kille, Tobias Borsdorff et al. "Carbon Monoxide in Optically Thick Wildfire Smoke: Evaluating TROPOMI Using CU Airborne SOF Column Observations", ACS Earth and Space Chemistry, 2022

Publication

<1 %

69

Wenhao Wang, Xiong Liu, Jianzhao Bi, Yang Liu. "A machine learning model to estimate

<1 %

ground-level ozone concentrations in California using TROPOMI data and high-resolution meteorology", Environment International, 2022

Publication

70

Can Li, Joanna Joiner, Nickolay A. Krotkov, Laura Dunlap. "A new method for global retrievals of HCHO total columns from the Suomi National Polar-orbiting Partnership Ozone Mapping and Profiler Suite", Geophysical Research Letters, 2015

Publication

<1 %

71

Mary Angelique G. Demetillo, Aracely Navarro, Katherine K. Knowles, Kimberly P. Fields et al. "Observing Nitrogen Dioxide Air Pollution Inequality Using High-Spatial-Resolution Remote Sensing Measurements in Houston, Texas", Environmental Science & Technology, 2020

Publication

<1 %

Exclude quotes Off

Exclude matches Off

Exclude bibliography Off